UNIVERSITY OF LEEDS

This is a repository copy of *Controls on amorphous organic matter type and sulphurization in a Mississippian black shale*.

White Rose Research Online URL for this paper:
http://eprints.whiterose.ac.uk/144609/

Version: Accepted Version

Article:
Emmings, JF, Hennissen, JAI, Stephenson, MH et al. (6 more authors) (2019) Controls on amorphous organic matter type and sulphurization in a Mississippian black shale. Review of Palaeobotany and Palynology, 268. pp. 1-18. ISSN 0034-6667

https://doi.org/10.1016/j.revpalbo.2019.04.004

Reuse
This article is distributed under the terms of the Creative Commons Attribution-NonCommercial-NoDerivs (CC BY-NC-ND) licence. This licence only allows you to download this work and share it with others as long as you credit the authors, but you can't change the article in any way or use it commercially. More information and the full terms of the licence here: https://creativecommons.org/licenses/

Takedown
If you consider content in White Rose Research Online to be in breach of UK law, please notify us by emailing eprints@whiterose.ac.uk including the URL of the record and the reason for the withdrawal request.

White Rose university consortium
Universities of Leeds, Sheffield & York

eprints@whiterose.ac.uk
https://eprints.whiterose.ac.uk/

Manuscript Details

Manuscript number	PALBO_2018_204_R1
Title	Controls on Amorphous Organic Matter Type and Sulphurization in a Mississippian Black Shale
Article type	Research paper

Abstract

Palaeoredox proxies (Fe speciation, trace element and δ34Spy) integrated with sedimentological and palynological observations link the distribution and type of particulate organic matter (OM) preserved to hydrocarbon source rock potential. In the Mississippian Bowland Shale Formation (Lancashire, UK), particulate OM is dominated by 'heterogeneous' amorphous OM (AOM), primarily 'sharp-edged, pellet-like' (AOMpel) and 'heterogeneous, granular' (AOMgr) types. AOMpel is abundant in muds deposited under anoxic and moderately to highly sulphidic conditions and most likely represents the faecal minipellets of zooplankton and/or pellets of macro-zooplankters. We recognise two intervals, 'A' and 'B', which exhibit Sorg/TOC > 0.04, suggesting a bulk Type II-S kerogen composition. The Interval A palynofacies is typified by pyritised AOMpel (AOMpyr) particles that contain high-relief organic spheres surrounding individual pyrite framboids, within each AOMpyr particle. These textures are interpreted as sulphurized OM local to pyrite framboids (Sorg-PF). Sorg-PF is rarely observed in Interval B, and absent in all other samples. Redox oscillation between ferruginous and euxinic conditions during early diagenesis of Interval A likely promoted S cycling in microenvironments surrounding pyrite framboids, which generated reactive S species and reactive OM required for sulphurization. Early diagenetic redox oscillation processes were apparently triggered by relative sea level fall, associated with an increased supply of FeHR from adjacent shelves into the basin. Interval B represents deposition during the late stages of basin infill and transition from anoxic to (sub)oxic bottom waters, where AOMpel is replaced by AOMgr as the dominant type of AOM. A large particle diameter at the limit of the mesh size (500 μm), sheet-like, fragmented character, and presence of candidate organic sheaths suggests AOMgr at least partially represent fragments of benthic microbial mats, probably as sulphide-oxidisers. A ternary plot of AOMpel + AOMpyr versus AOMgr versus spores + phytoclasts links the observed palynofacies to bottom and pore water redox conditions, water column productivity and proximity to fluvial (deltaic) supply of spores and phytoclasts. These variables were moderated by changing basin accommodation, driven primarily by eustatic sea level fluctuation. A sequence-stratigraphic control on AOM type and sulphurization is important for understanding the link between source rock heterogeneity and the timing of hydrocarbon generation and expulsion from this source rock.

Keywords	mudstone; amorphous organic matter; sulphur; redox
Manuscript category	Phytoliths, Multidisciplinary Stratigraphic Studies Involving Palynology

Corresponding Author	Joe Emmings
Corresponding Author's Institution	British Geological Survey
Order of Authors	Joe Emmings, Jan Hennissen, Michael Stephenson, Simon Poulton, Christopher Vane, Sarah Davies, Melanie Leng, Angela Lamb, Vicky Moss-Hayes
Suggested reviewers	Nicolas Tribovillard, Muriel Pacton, Andrew Aplin, John Marshall

Highlights

- The Bowland Shale palynofacies is dominated by amorphous organic matter (AOM)
- AOM includes ‘pellet-like’ (AOMpel) and ‘granular’ (AOMgr) types
- AOMpel may represent faecal pellets sourced from a productive water column
- AOMgr may represent fragments of chemosynthetic microbial mats
- The distribution of organic S is linked to redox and sea level change

Abstract

Palaeoredox proxies (Fe speciation, trace element and $\delta^{34}S_{py}$) integrated with sedimentological and palynological observations link the distribution and type of particulate organic matter (OM) preserved to hydrocarbon source rock potential. In the Mississippian Bowland Shale Formation (Lancashire, UK), particulate OM is dominated by 'heterogeneous' amorphous OM (AOM), primarily 'sharp-edged, pellet-like' (AOMpel) and 'heterogeneous, granular' (AOMgr) types. AOMpel is abundant in muds deposited under anoxic and moderately to highly sulphidic conditions and most likely represents the faecal minipellets of zooplankton and/or pellets of macro-zooplankters. We recognise two intervals, 'A' and 'B', which exhibit $S_{org}/TOC > 0.04$, suggesting a bulk Type II-S kerogen composition. The Interval A palynofacies is typified by pyritised AOMpel (AOMpyr) particles that contain high-relief organic spheres surrounding individual pyrite framboids, within each AOMpyr particle. These textures are interpreted as sulphurized OM local to pyrite framboids ($S_{org\text{-}PF}$). $S_{org\text{-}PF}$ is rarely observed in Interval B, and absent in all other samples. Redox oscillation between ferruginous and euxinic conditions during early diagenesis of Interval A likely promoted S cycling in microenvironments surrounding pyrite framboids, which generated reactive S species and reactive OM required for sulphurization. Early diagenetic redox oscillation processes were apparently triggered by relative sea level fall, associated with an increased supply of Fe_{HR} from adjacent shelves into the basin. Interval B represents deposition during the late stages of basin infill and transition from anoxic to (sub)oxic bottom waters, where AOMpel is replaced by AOMgr as the dominant type of AOM. A large particle diameter at the limit of the mesh size (500 μm), sheet-like, fragmented character, and presence of candidate organic sheaths suggests AOMgr at least partially represent fragments of benthic

microbial mats, probably as sulphide-oxidisers. A ternary plot of AOMpel + AOMpyr versus AOMgr versus spores + phytoclasts links the observed palynofacies to bottom and pore water redox conditions, water column productivity and proximity to fluvial (deltaic) supply of spores and phytoclasts. These variables were moderated by changing basin accommodation, driven primarily by eustatic sea level fluctuation. A sequence-stratigraphic control on AOM type and sulphurization is important for understanding the link between source rock heterogeneity and the timing of hydrocarbon generation and expulsion from this source rock.

Controls on Amorphous Organic Matter Type and Sulphurization in a Mississippian Black Shale

Joseph F. Emmings[a,b]*, Jan A. I. Hennissen[a], Michael H. Stephenson[a], Simon W. Poulton[c], Christopher H. Vane[a], Sarah Davies[b], Melanie J. Leng[d,e], Angela Lamb[d], Vicky Moss-Hayes[a]

[a]British Geological Survey, Keyworth, Nottingham, NG12 5GG, UK.

[b]School of Geography, Geology and the Environment, University of Leicester, Leicester, LE1 7RH, UK.

[c]School of Earth and Environment, University of Leeds, Leeds, LS2 9JT, UK.

[d]NERC Isotopes Geosciences Facilities, British Geological Survey, Keyworth, Nottingham NG12 5GG, UK.

[e]Centre for Environmental Geochemistry, Sutton Bonington Campus, University of Nottingham, Sutton Bonington, Leicestershire, LE12 5RD, UK

*Corresponding author email address: josmin65@bgs.ac.uk

Abstract

Palaeoredox proxies (Fe speciation, trace element and $\delta^{34}S_{py}$) integrated with sedimentological and palynological observations link the distribution and type of particulate organic matter (OM) preserved to hydrocarbon source rock potential. In the Mississippian Bowland Shale Formation (Lancashire, UK), particulate OM is dominated by 'heterogeneous' amorphous OM (AOM), primarily 'sharp-edged, pellet-like' (AOMpel) and 'heterogeneous, granular' (AOMgr) types. AOMpel is abundant in muds deposited under anoxic and moderately to highly sulphidic conditions and most likely represents the faecal minipellets of zooplankton and/or pellets of macro-zooplankters. We recognise two intervals, 'A' and 'B', which exhibit $S_{org}/TOC > 0.04$, suggesting a bulk Type II-S kerogen composition. The Interval A palynofacies is

typified by pyritised AOMpel (AOMpyr) particles that contain high-relief organic spheres surrounding individual pyrite framboids, within each AOMpyr particle. These textures are interpreted as sulphurized OM local to pyrite framboids ($S_{org\text{-}PF}$). $S_{org\text{-}PF}$ is rarely observed in Interval B, and absent in all other samples. Redox oscillation between ferruginous and euxinic conditions during early diagenesis of Interval A likely promoted S cycling in microenvironments surrounding pyrite framboids, which generated reactive S species and reactive OM required for sulphurization. Early diagenetic redox oscillation processes were apparently triggered by relative sea level fall, associated with an increased supply of Fe_{HR} from adjacent shelves into the basin. Interval B represents deposition during the late stages of basin infill and transition from anoxic to (sub)oxic bottom waters, where AOMpel is replaced by AOMgr as the dominant type of AOM. A large particle diameter at the limit of the mesh size (500 μm), sheet-like, fragmented character, and presence of candidate organic sheaths suggests AOMgr at least partially represent fragments of benthic microbial mats, probably as sulphide-oxidisers. A ternary plot of AOMpel + AOMpyr versus AOMgr versus spores + phytoclasts links the observed palynofacies to bottom and pore water redox conditions, water column productivity and proximity to fluvial (deltaic) supply of spores and phytoclasts. These variables were moderated by changing basin accommodation, driven primarily by eustatic sea level fluctuation. A sequence-stratigraphic control on AOM type and sulphurization is important for understanding the link between source rock heterogeneity and the timing of hydrocarbon generation and expulsion from this source rock.

Keywords: mudstone, amorphous organic matter, sulphur, redox

1. Introduction

The upper unit of the Mississippian Bowland Shale Formation (Upper Bowland Shale; herein 'Bowland Shale') is a potential target for unconventional hydrocarbon exploration and an important conventional hydrocarbon source rock in the UK (e.g., Andrews et al. 2013; Clarke et al., 2018) and time-equivalent units across Europe (Kerschke and Schulz, 2013; Nyhuis et al., 2015). The spatial and temporal distribution and type of organic matter (OM) in organic-rich mudstones, such as the Bowland Shale, is an important control on hydrocarbon prospectivity (e.g., Jarvie et al., 2012). Palynological assessment of particulate OM type yields important data relating to hydrocarbon source rock generative potential, particularly when supplemented with organic geochemical analyses such as RockEval pyrolysis (e.g., Espitalie et al., 1977). Palynofacies analysis can be used to quantify the proportions of highly aliphatic ('Type I'), moderately aliphatic ('Type II'), humic ('Type III') and refractory ('Type IV') palynofacies components (e.g., Tyson, 1995). Since sulphur (S) radicals associated with organic S (S_{org}) catalyse hydrocarbon maturation (Lewan, 1998), the recognition of S-rich (sulphurized) OM ('Type II-S') is also important with respect to understanding hydrocarbon source rock prospectivity (e.g., Orr, 1986; Dembicki, 2009).

In Mississippian organic-rich mudstones, in particular, the extracted palynological OM fraction (e.g., Wood et al., 1996) is dominated by amorphous OM (AOM; e.g., Könitzer et al., 2016; Hennissen et al., 2017). This is especially typical of Mississippian source rocks, given the lack of recognisable marine palynomorphs during the 'Phytoplankton Blackout' (Pitrat, 1970; Riegel, 1996; Riegel, 2008; Servais et al., 2016; Tappan, 1970). This 100-Myr phenomenon is possibly explained by high

nutrient availability, and therefore high rates of primary productivity, in the palaeo-Rheic-Tethys seaway (Servais et al., 2016). These productive (low stress) conditions potentially supported phytoplankton which did not produce cysts, considered marine palynomorphs with relatively high preservation potential, because encystment was unnecessary (Servais et al., 2016).

AOM is usually described under transmitted and fluorescent light by eye (e.g., Tyson, 1995), and is often subdivided into 'homogenous' and 'heterogeneous' types (e.g., Hennissen et al., 2017). 'Homogenous' AOM includes gellified humic material, and is therefore often interpreted as Type III OM (Tyson, 1995). 'Heterogeneous' AOM is subdivided into "diffuse-edged" (also termed "granular") and "sharp-edged" AOM (Tyson, 1995). The former is typically interpreted as bacterial or highly degraded plant material and defined as Type III OM. "Sharp-edged" AOM is usually interpreted as 'well-preserved' Type I or II OM, particularly if this is highly fluorescent under ultra-violet light (Tyson, 1995). Where AOM exhibits a distinctive orange colour under transmitted light, this is usually a proxy for S-rich compounds (e.g., Tribovillard et al., 2001). Under suitable conditions, S may be incorporated into OM during syngenesis or early diagenesis, a process that is termed sulphurization (e.g., Sinninghe Damsté and de Leeuw, 1990; Amrani, 2014).

In order to understand controls on the types and distribution of AOM and mechanisms for sulphurization, geochemical and palynological data were integrated through three sections of the Mississippian Upper Bowland Shale in the Craven Basin (Lancashire, UK), a basin with ongoing hydrocarbon exploration (Clarke et al., 2018). Palynofacies abundance data were integrated with syngenetic and early

diagenetic palaeoredox proxies including Fe-speciation, redox-sensitive trace element and $\delta^{34}S_{py}$ analyses.

2. Geological Setting

The Bowland Shale was deposited in a series of epicontinental basins within the Rheic-palaeo-Tethys palaeoequatorial seaway, spanning from present-day North America to Poland (e.g., Davies et al., 1999). This seaway developed in response to oblique collision between Gondwana and Laurussia (Warr, 2000), including phases of extension (e.g., active rifting), thermal subsidence, strike-slip and compression tectonism. Mississippian extension (Leeder, 1982) generated a series of graben and half-graben structures, separated by platform 'blocks' and 'highs' (e.g., Waters and Davies, 2006) (Fig. 1a). Transition from active rifting to thermal subsidence broadly aligns with subdivision of the Bowland Shale Formation into lower and upper units coincident with the Visean-Serpukhovian boundary (Bisat, 1923; Davydov et al., 2012; Earp, 1961; Menning et al., 2006; Waters et al., 2009). The Upper Bowland Shale was deposited from the early to late Pendleian (~330-330.7 Ma; Gastaldo et al., 2009; Waters and Condon, 2012) in the Craven Basin (Fig. 1c).

The switch from rift to thermal sag, coupled with the advance of Pendle fluviodeltaic systems across and around the Askrigg Block, produced an interdigitating succession of hemipelagic and siliciclastic facies in the Craven Basin, as the mixed-to-siliciclastic Upper Bowland Shale (e.g., Brandon et al., 1998). Sedimentary facies include hemipelagites, turbidites, hybrid event beds and lenticular mudstones (Emmings et al., 2019) and the Hind Sandstone Member (Aitkenhead et al., 1992; Moseley, 1952; Moseley, 1962), which is an injectite (Kane, 2010). Craven Basin

125 water depth likely ranged from ~100 to 200 m (Davies, 2008; Holdsworth and
126 Collinson, 1988) through to several hundred metres (Davies et al., 1993).
127
128 Hemipelagic sediments in the Bowland Shale include discrete, macrofauna-bearing,
129 calcareous sedimentary packages ('marine bands'; e.g., Ramsbottom, 1977; Fig. 1c)
130 that are typically linked to starved siliciclastic input during the maximum rate of
131 transgression (Posamentier et al., 1988) and/or at maximum marine flooding
132 (Martinsen et al., 1995). Marine band cyclicity was likely a response to far-field ice-
133 sheet volume on Gondwana (Veevers and Powell, 1987).
134
135 The macrofaunal body fossils present, particularly ammonoids, form the basis of a
136 high-resolution biostratigraphic framework (Ramsbottom and Saunders, 1985). The
137 ammonoid biozones E_{1a1}, E_{1b1}, E_{1b2} and E_{1c1} are recognised in the Upper Bowland
138 Shale (e.g., Brandon et al., 1998) (Fig. 1c), with an average periodicity of 111 ka
139 (Waters and Condon, 2012). Multiple flooding surfaces are recognised for E_{1a1} (a, b
140 and c) and E_{1b2} (a and b) marine bands (Fig. 1c), which may represent sub-100 ka
141 precession or obliquity forcing (Waters and Condon, 2012).
142
143 The Bowland Shale was followed by deposition of delta-top facies on the Askrigg
144 Block and a submarine turbidite fan complex in the basin (Fraser and Gawthorpe,
145 1990; Kirby et al., 2000), as the Pendleton Formation (Waters et al., 2007) (Fig. 1c).
146 Variscan inversion of the Craven Basin resulted in the development of a set of north-
147 east south-west trending folds, thrust-folds and monoclines, collectively defined as
148 the Ribblesdale Fold Belt (Arthurton, 1984; Gawthorpe, 1987) (Fig. 1b).
149

3. Materials and Methods

Outcrop locality Hind Clough (grid ref: 364430 453210, British National Grid projection) exposes the Upper Bowland Shale as a ~124 m thick stream-cut and weathered slope section (e.g., Moseley, 1962; Brandon et al., 1998; Emmings et al., 2019) on the north-west edge of the Ribblesdale Fold Belt (Arthurton, 1984; Gawthorpe, 1987). Together the sections at Hind Clough and in nearby boreholes Marl Hill 4 (MHD4; 367426 446752) and Cominco C9 (386010 463500) (Fig. 1b) were logged, sampled and assigned sedimentary facies (A-J) by Emmings et al. (2019). The stratigraphic framework was based on ammonoid biozones identified by Brandon et al. (1998). The sampling strategy was designed to minimise the potential for alteration due to modern weathering at outcrop, as implemented by Emmings et al. (2017) .

3.1. Palynology

34 palynology samples were processed using standard preparation methods (Wood et al., 1996), using hydrochloric (36% vol/vol) and hydrofluoric (HF) (40% vol/vol) acid to remove carbonate and silicate phases, respectively. Kerogen residues were sieved at 500 µm and 10 µm. Residues were spiked with *Lycopodium clavatum* spores (batch no. 3862, MPA66949-66953, 2 tablets in 5 g sample; MPA67171-68150, 3 tablets in 5 g sample) in order to calculate absolute abundances using the marker grain method (Maher, 1981; Stockmarr, 1971). Since AOM was the primary target in this study, and highly abundant compared to spores, this precluded calculation of absolute abundances using the marker grain method. A much larger spike (i.e., > 10 tablets) could potentially enable quantification of spore absolute

abundances (but not AOM) in this material. A subset of residues were oxidised for 7 minutes using fuming nitric acid.

Each sample residue was strew-mounted onto two slides and set in low fluorescing Elvacite™ resin. Microscopic observations were conducted using an Axio Imager M2m fitted with a motorized stage under transmitted light (brightfield and differential interference contrast) and incident green light. Green-light emission was attained using a 100 V tungsten filament (HVP) lamp at maximum brightness passed through the Zeiss 00 Propidium Iodide (PI) filter set (λ 530-585 nm excitation). A subset of slides were also analysed under a mercury HXP light source. Under green-light, the spectral irradiance for tungsten filament lamps and mercury lamps is similar (Lin and Davis, 1988). x10, x40 and x100 (oil immersion) EC Plan Neofluor objectives were utilised. Emitted light was red-light filtered (530-585 nm λ beam-splitter, filtering emission above λ 615 nm).

Green light fluorescence (coupled with red light filter) was used as a proxy for moderately quenched (i.e., polymerised) structures and highly ‘delocalised’ double bonds (Lin and Davis, 1988). Aromatic structures contain highly delocalised bonds, rather than acyclic compounds which may contain isolated double-bonds (e.g., alkenes, acyclic terpenoids). Thus green light fluorophors represent phenols and heteroatomic aromatic moieties contained within aliphatic polymers, and some aromatic (e.g., lignin-containing) substances. Highly polymerised substances that contain abundant delocalised bonds (e.g., humic compounds) promote quenching and are therefore typically non-fluorescent under all wavelengths (Lin and Davis, 1988).

Images were captured with an AxioCam MR R3 camera connected to a PC with Zen 2012 (Blue Edition) software. All images were captured in a dark room and under the same ambient light conditions. Particles were described and counted using an automatic stage, based on visual assessment and semi-automated analysis of extracted particle shape and fluorescence parameters using the Fiji ImageJ platform (Schindelin et al., 2012). Total AOM and AOMgr abundances are therefore relative and corrected for particle area. Palynofacies abundance data are provided in Appendix A.

3.2. Geochemistry

Samples selected for geochemical analysis were crushed and agate-milled to a fine powder. 193 samples were selected for pyrolysis, conducted on finely powdered samples in a Rock-Eval 6 pyrolyser (Vinci Technologies) in standard configuration and operated using the Bulk-Rock method (e.g., Słowakiewicz et al., 2015). The generated total organic carbon (TOC) and inorganic C (MINC) data were previously reported by Emmings et al. (2019).

Total carbon (C) and sulphur (TS) concentrations were measured on 110 samples using a LECO CS 230 elemental analyser. Major and trace element concentrations were measured on fused beads (109 samples) and powder briquettes (108 samples) with a PANalytical Axios Advanced X-Ray Fluorescence (XRF) spectrometer using default PANalytical SuperQ conditions. ‘Excess Si’ (*sensu*. Sholkovitz and Price, 1980) was calculated by Emmings et al. (2019) and interpreted primarily as a pelagic and biogenic (radiolarian) signal that did not migrate significantly during diagenesis.

Trace element enrichment factors (EFs) (e.g., Tribovillard et al. 2006) were utilised to normalise to abundances to the detrital fraction (Eq. 1), using Post-Archaean Average Shale (PAAS) (Taylor and McLennan, 1985). X is the element concentration (major elements; wt. % and trace elements; ppm).

$$\mathrm{EF_{element}} = \left[\frac{\mathrm{X}}{\mathrm{Al}}\right]_{\mathrm{sample}} / \left[\frac{\mathrm{X}}{\mathrm{Al}}\right]_{\mathrm{PAAS}} \qquad [\mathbf{Eq.\ 1}]$$

Fe species concentration data for 99 samples were measured via sequential extraction of 'highly reactive' Fe (Fe_{HR}; Poulton and Canfield, 2005; Eq. 2) phases, including carbonate-associated Fe (Fe_{carb}; e.g., siderite and ankerite), ferric (oxyhydr)oxides ($Fe_{ox;}$ e.g., goethite, hematite) and magnetite (Fe_{mag}). The extraction is a simplification of the method of Poulton and Canfield (2005). Fe_{carb}, Fe_{ox} and Fe_{mag} concentrations were measured using an Atomic Absorption Spectrometer (AAS).

The pyrite (Fe_{py}) fraction was estimated via extraction of sulphide S liberated by boiling chromous chloride solution, and titrated as Ag_2S (Canfield et al., 1986). This followed extraction of HCl-soluble (acid-volatile, Fe_{AVS}) sulphide S, in boiling HCl (Canfield et al., 1986), although in all samples Fe_{AVS} was only present as a trace component (below the limit of determination). Fe_{HR}/Fe_T (Fe_T; total Fe) and Fe_{py}/Fe_{HR} are compared with established thresholds for redox (Poulton and Canfield, 2011; Poulton and Raiswell, 2002; Raiswell and Canfield, 1998). Facies H-I Fe_{HR} is presented on a Fe_{mag}-free basis, due to the likely input of detrital Fe_{mag} (see Emmings, 2018).

$$\mathrm{Fe_{HR}} = \mathrm{Fe_{carb}} + \mathrm{Fe_{ox}} + \mathrm{Fe_{mag}} + \mathrm{Fe_{py}} \qquad [\mathbf{Eq.\ 2}]$$

37 sample powders (~1 g) were washed for 24 hours in 200 ml 10 wt/vol % NaCl in order to leach free sulphate (Kampschulte et al., 2001). Total S measured on NaCl-washed residues was compared with the total S of untreated powders, yielding an estimate for the sulphate S (S_{sul}) fraction, after correction for the mass loss assuming leaching of pure $CaSO_4$ (Appendix B). In most cases, estimated S_{sul} was within or close to ± 0.08 wt. % of the total (untreated) S (i.e., the long-term analytical precision). Therefore S_{sul} is negligible for most samples. S_{org} content was estimated by subtraction of S_{py} (Fe_{py}*1.15) and S_{sul} from TS (Eq. 3) (e.g., Tribovillard et al., 2001). Propagating the precision of TS, S_{py} and S_{sul} in quadrature yields a precision estimate of ± 0.12 wt. % S_{org}.

$$S_{org} = TS - S_{py} - S_{sul} \qquad [\mathbf{Eq.\ 3}]$$

S isotope ratios for chromium-reducible (S_{py}) extracts (as Ag_2S) were measured using a Thermo Finnigan Continuous Flow-Elemental Analysis-Isotope Ratio Mass Spectrometry (CF-EA-IRMS) system, comprising a Delta Plus XL isotope ratio mass spectrometer interfaced with a Flash 1112 elemental analyser. $^{36}S/^{34}S$ ratios of pyrite S are reported using $\delta^{34}S_{py}$ (‰) notation on the VCDT scale. S isotope ratios were drift-corrected using IAEA-S-3 (–32.3‰ VCDT) and calibrated using a linear two-point fit through IAEA-S-1 (–0.3‰ VCDT) and IAEA-S-3. $\delta^{34}S_{py}$ precision is estimated at ± 1.0‰, based on two standard deviations of repeat analyses, including IAEA-S-2 (+22.7‰ VCDT). Scanning electron microscopy (SEM) was conducted on uncoated ultrathin sections using an S-3600N Hitachi microscope with Oxford INCA 350 EDS. Electron microphotographs were acquired using backscattered electrons

(BSE) at 15 kV accelerating voltage, 50-66 µA filament current, in low-vacuum mode (25 Pa) and 15.0-16.3 mm (typically 16.1) working distance (WD).

4. Results and Discussion

4.1. Palynofacies and Palaeoredox

The palynofacies assemblage in sedimentary Facies A-G (see Fig. 2) is dominated by AOM, while spores and phytoclasts are a minor component (< 20 %), and marine palynomorphs are absent (Fig. 2; Table 1). In Facies H-I at Cominco S9, spores and phytoclasts are dominant (Fig. 3; Table 1). Nearly all AOM is 'heterogeneous' (e.g., Tyson, 1995) and subdivided into two main types; 'sharp-edged, pellet-like' AOM (AOMpel; Plate I) and 'granular' AOM (AOMgr; Plate II). AOMgr is rare in Facies A-F and is the dominant type of AOM in Facies G, whereas AOMpel is dominant Facies A-F and rare in Facies G.

Plotting heterogeneous AOM versus phytoclasts versus spores (Fig. 4) demonstrates most Facies A-G samples are sited in the 'distal suboxic-anoxic basin' and 'distal dysoxic-anoxic shelf' fields of Tyson (1995). Anoxic conditions in bottom waters during deposition of Facies A-F sediments are supported by enrichment in redox-sensitive trace elements Mo and U (e.g., Tribovillard et al., 2006) and $Fe_{HR}/Fe_T > 0.38$ (Figs. 2, 4-5; Table 1) (Poulton and Raiswell, 2002; Raiswell and Canfield, 1998). Facies H-I samples at Cominco S9 are sited in the 'heterolithic oxic (proximal) shelf' and 'mud-dominated oxic (distal) shelf' fields of Tyson (1995), respectively. Bottom water ventilation during deposition of Facies H-I is consistent with a lack of enrichment in Mo and U and $Fe_{HR}/Fe_T < 0.38$ (Figs. 2, 4-5; Table 1). Morridge Formation palynofacies data from the Edale Gulf and Widmerpool Gulf

297 (Hennissen et al., 2017) plot along a mixing line between the ‘distal suboxic-anoxic
298 basin’ and ‘marginal dysoxic-anoxic basin’ fields of Tyson (1995).
299
300 AOMpel is not comparable to AOM in contemporaneous mudstones from the nearby
301 Widmerpool Gulf paralic basin (Fig. 1a) (Hennissen et al., 2017; Könitzer et al.,
302 2016), but is similar to a variety of ‘well preserved’ AOM with Type I and II
303 composition. ‘Well preserved’ AOM is observed in the Kimmeridge Clay (Tyson,
304 1989; Tyson, 1995) and relatively aliphatic (H-rich) intervals from the Bowland Shale
305 in the Edale Gulf (Fig. 1a) (Hennissen et al., 2017), for example. AOMpel typically
306 exhibits pellet-like geometries (e.g., Plate I, 3, 5, 7). Thus AOMpel most likely
307 represent the faecal minipellets of zooplankton (e.g., Stoecker, 1984; Gowing and
308 Silver, 1985; Beaumont et al., 2002; Lampitt et al., 2009) and/or faecal pellets of
309 macro-zooplankton (e.g., Porter and Robbins, 1981; Bruland and Silver, 1981;
310 Cuomo and Chen, 1996; Henschke et al., 2016).
311
312 AOMgr (Plate II) exhibits a large particle diameter (500 μm, i.e., limit of the mesh
313 size), sheet-like, fragmented character (Plate II, 4) and contains candidate organic
314 sheaths (Plate II, 6, 7). AOMgr is comparable to ‘diffuse-edged AOM’ (Tyson, 1995)
315 and most AOM in contemporaneous mudstones from the paralic Widmerpool Gulf
316 (Fig. 1a), including AOMgr described by Hennissen et al. (2017), and AOMGr and
317 possibly AOMBr described by Könitzer et al. (2016). The relative abundance of
318 AOMgr increases significantly above the transition from anoxic (Facies F) to suboxic
319 or oxic (Facies G) bottom waters, indicated by a loss of enrichment of redox
320 sensitive trace elements, such as Mo and U (e.g., Tribovillard et al., 2006), Fe_{HR}/Fe_T
321 close to 0.38 (Poulton and Raiswell, 2002; Raiswell and Canfield, 1998), and

bioturbation in Facies G (Emmings et al., 2019). AOMgr dominates the palynofacies assemblage in Facies G (Fig. 2; Table 1) so that Facies G is sited in the 'distal suboxic-anoxic basin' and 'distal dysoxic-anoxic shelf' fields of Tyson (1995) (Figs. 4-5). This is slightly inconsistent with the palaeoredox proxy record which suggests deposition under dominantly oxic or suboxic conditions.

Presence of pyritised burrows, and early diagenetic nodular, aggregated and large framboidal pyrite forms in Facies G (Emmings et al., 2019) suggests highly sulphidic, and advective or stagnant conditions existed near seabed (Rickard, 2012). This is supported by high $\delta^{34}S_{py}$ values in Facies G (Fig. 2; Table 1; +6.4 and –8.9‰), which shows the bulk pyrite population formed under closed system conditions (e.g., Nissenbaum et al., 1972; Mossmann et al., 1991; Canfield et al., 1992). On this basis, AOMgr likely represents the remnants of extracellular polysaccharides (e.g., Pacton et al., 2007; 2011) produced by benthic microbial mats. This is supported by sedimentological interpretations (Emmings et al., 2019). Such mats potentially colonised a niche environment at the seabed as chemoautotrophic or chemoheterotrophic sulphide-oxidisers (e.g., Grunke et al., 2011).

4.2. Mechanisms for Sulphurization

Intervals 'A' (within Facies F) and 'B' (Facies G) exhibit $S_{org}/TOC > 0.04$, suggesting a bulk Type II-S kerogen composition (Orr, 1986). A microbial mat origin to AOMgr may explain the exceptionally high S_{org} content in Interval B (Facies G). Modern microbial mats oxidise H_2S using O_2 or NO_3^- as an electron acceptor across a strong redox gradient at the seabed (Bailey et al., 2009; Canfield and Teske, 1996; Grunke et al., 2011; Sievert et al., 2007; Wirsen et al., 2002), and are consortia of several

different types of bacteria. AOMgr is probably most comparable to the colourless sulphur bacterium *Arcobacter* (phylum Proteobacteria) that produces a 'cotton-ball'-like structure (Grunke et al., 2011; Wirsen et al., 2002) via fixation of S_{org} in filaments (Steudel, 1989). *Arcobacter* mats are present at cold seeps on the Nile Deep Sea Fan (Grunke et al., 2011), for example. AOMgr may also be comparable to *Thiopoloca*, a sulphide-oxidising denitrifier that is widespread beneath the upwelling Peru-Chile upwelling region (Fossing et al., 1995). Alternatively, the high S_{org} content in Interval A may be explained by direct reaction of H_2S with OM (e.g., Sinninghe Damsté and de Leeuw, 1990; Amrani, 2014). Regardless of S fixation mechanism, stagnation or advection of sulphidic porwaters near seabed implies relatively vigorous and sustained rates of SO_4-reduction (as the likely source of sulphide) and/or minimal buffering by reactive Fe in underlying sediments.

Ancient examples of benthic microbial mats are rare (Catuneanu, 2007; Schieber, 1986; Schieber et al., 2007a; Schieber et al., 2007b; Seckbach and Oren, 2010), especially regarding chemotrophs (Bailey et al., 2009). Early silica-cemented chemotrophic microbial mats are present in the Miocene Monterey Formation (Williams, 1984), which potentially contributed significantly to the petroleum system and Type II-S kerogen composition (Orr, 1986; Williams, 1984). S-rich filaments in modern chemosynthetic microbial mats can be sheathed by OM (Wirsen et al., 2002). Such sheaths are possibly observed within AOMgr (Plate II, 6, 7), although these are not a universal feature (Wirsen et al., 2002), and are not always preserved (Grant, 1991). Sulphide is toxic to infauna (Wang and Chapman, 1999). Thus predators to mats, such as gastropods (e.g., Tribovillard et al., 2000), were likely occluded from this environment due to the high redox gradient at seabed.

Interval A in Facies F overlying the E_{1a1} marine band exhibits relatively high S_{org} content yet contains minimal AOMgr (Fig. 2; Table 1). This package is distinctive because the palynological fraction is dominated by AOMpel that is coated by fine, microcrystalline pyrite ('AOMpyr'; Plate I, 6). AOMpel in Interval A also contains abundant orange, high-relief organic spheres within each particle (Plate III). Rarely, these spheres are also present within AOMgr in Facies G (Interval B; Fig. 2; Plate III, 6-9).

The spheres exhibit a finely reticulated texture in transmitted light that mimics pyrite framboids (Plate III, 3), and are best observed in oxidised slides following removal of the microcrystalline pyrite coatings on AOM. In some cases, each sphere contains a single pyrite framboid (Plate III, 1). The diameter of organic spheres in Interval A (Fig. 6) is similar to pyrite framboids in Facies F (Emmings et al., 2019). The orange colour of the organic spheres suggests sulphurized OM (e.g., Tribovillard et al., 2001), possibly comparable to orange gel-like AOM 'drops' (Aycard et al., 2003). AOM sulphurization is consistent with the relatively high S_{org} content in Interval A. The catalytic effect of S radicals associated with S_{org} during the thermal decomposition of kerogen (Lewan, 1998) may also explain the relatively low Rock-Eval T_{max} through Interval A. T_{max} through Interval A is approximately 15°C lower than the adjacent mudstone packages (Figs. 2, 7; Table 1). Such T_{max} inversions are not necessarily diagnostic of Type II-S OM, however, because a similar reduction in T_{max} is observed through the E_{1c1} marine band at Cominco S9 despite very low S_{org} content (Fig. 3). This suggests T_{max} is also influenced more broadly by OM composition (Type II versus III) and/or mineral matrix effects.

Sphere fluorescence under green light (Plate III, 5, 7, 9) suggests the presence of aromatic compounds within a moderately polymerised structure (Lin and Davis, 1988), potentially including S heteroatoms such as thiophenes (e.g., Eglinton et al., 1990). Since AOMgr in Interval B lacks fluorescence under green light and generally lacks $S_{org\text{-}PF}$, this suggests most S_{org} is present as (non-fluorescing) cross-linked (intermolecular) S polymers (e.g., Aizenshtat et al., 1995; Sinninghe Damsté et al., 1989).

The orange spherical texture in AOM is termed '$S_{org\text{-}PF}$', and is comparable to the texture originally described by Love (1957; 1962). Pyrite framboids are present in all sedimentary facies (Emmings et al., 2019), yet S_{org}-$_{PF}$ is only present in interval A, and rarely interval B. Clearly the microenvironment surrounding pyrite framboids within OM promoted sulphurization. Sulphurization of OM requires access to compounds prone to complexation with S (Adam et al., 2000) and available reactive S species in the local microenvironment. O contained within carbonyl groups, in particular, is prone to replacement by reduced S (e.g., Adam et al., 2000). Carbohydrates are also susceptible to sulphurization (Van Kaam-Peters et al., 1998). Reactive S species include H_2S, polysulphides, sulphites, or other S of intermediate oxidation states (Aizenshtat et al., 1995; Amrani, 2014; Amrani and Aizenshtat, 2004; Rickard, 2012; Sinninghe Damsté and Leeuw, 1990; Wasmund et al., 2017).

Under anoxic conditions, 'redox oscillation' between zones of SO_4 and Fe reduction (*sensu.* Aller, 1982; Aller, 1998) promotes sulphurization (Aplin and Macquaker, 1993; Filley et al., 2002) via S cycling and therefore generation of reactive S species

(e.g., Wasmund et al., 2017). Redox oscillation also enhances oxidation and/or dehydration of low-molecular weight compounds, such as alcohols, producing aldehydes or ketones (i.e., compounds with carbonyl functional groups; Burdige, 2006). These compounds are thought to be particularly susceptible to sulphurization, especially if they contain conjugate double bonds (Adam et al., 2000; Aizenshtat et al., 1995; Amrani, 2014; Grossi et al., 1998; Rontani et al., 1999).

Therefore redox oscillation *localised* to OM is the best explanation for $S_{org\text{-}PF}$ formation. This differs from the mechanism of sulphurization under persistently sulphidic (euxinic) conditions (e.g., Lewan, 1984; Orr, 1986; Hartgers et al., 1997), where H_2S potentially reacts directly with OM (Amrani, 2014; Sinninghe Damsté and De Leeuw, 1990). Under oscillatory redox conditions during early diagenesis, H_2S generation via SO_4-reduction likely proceeded only within the microenvironment local to particles of metabolisable OM (e.g., Burdige, 2006). This is consistent with the presence of pyrite that apparently nucleated on and/or within AOMpel within Interval A (Plate 1, 6).

Early diagenetic redox oscillation within Interval A is consistent with the Mo and U and $\delta^{34}S_{py}$ record (Table 1; Fig. 2). Firstly, high Mo relative to U in Interval A (Facies F mean Mo EF ~ 76 ± 86, U EF ~ 8 ± 3) suggests the presence of a relatively weak and unstable water column chemocline and development of 'particulate shuttle' conditions (Algeo and Tribovillard, 2009). This contrasts with moderate to high Mo *and* U contents in 'marine band' Facies A-C (mean Mo EF ~ 32 ± 39, U EF ~ 11 ± 11), which suggests relatively stable, moderately sulphidic conditions in bottom waters. Secondly, strongly negative (close

447 to – 40‰) $\delta^{34}S_{py}$ in Interval A suggests pyrite precipitation under long-lived open-
448 system conditions and/or large S fractionations via intermediate S cycling (e.g.,
449 Nissenbaum et al., 1972; Mossmann et al., 1991; Canfield et al., 1992; Canfield et
450 al., 2010).
451
452 H_2S that migrated into surrounding porewaters was likely oxidised to produce
453 sulphuric acid (e.g., Soetaert et al., 2007). This explains the lack of carbonate (Fig.
454 2), despite the presence of skeletal moulds (Emmings et al., 2019), in Intervals A
455 and B. Therefore the contacts between OM microenvironments and adjacent
456 porewaters exhibited an intermittently high redox-gradient (Fig. 8). This gradient was
457 likely strongest during periods of redoxcline deepening, where porewaters were
458 flooded by Fe-reducers. S cycling across these micro-redox fronts, local to each
459 framboid, provided the reactive S species required for sulphurization.
460
461 Pyrite nucleation within AOM likely formed initially as FeS, via reaction with dissolved
462 reduced Fe, sourced via dissimilatory Fe^{3+} reduction or direct reduction of particulate
463 FeOOH by H_2S (Fig. 8). FeS subsequently reacted with H_2S and/or polysulphides to
464 produce pyrite (e.g., Rickard, 2012). Microcrystalline pyrite coatings on OM (Plate I,
465 6) are therefore interpreted as a relict redox front, defined by reaction of H_2S
466 generated local to OM, and Fe^{3+} and/or FeOOH present in the surrounding
467 porewaters.
468
469 H_2 or short polysulphides are products of pyrite precipitation where FeS is the
470 reactant (Soetaert et al., 2007). H_2, as a key nutrient, potentially stimulated microbial
471 activity (Nissenbaum et al., 1972; Rickard, 2012), which in turn promoted

472 sulphurization local to the pyrite framboids. Thus $S_{org\text{-}PF}$ formed concomitantly with,
473 or following, pyrite (e.g., Filley et al., 2002), and are perhaps analogous to
474 'sulphurized biofilms' (MacLean et al., 2008). Microbial oxidisation of H_2 (as a
475 nutrient) coupled to dissimilatory elemental S reduction (Aizenshtat et al., 1995;
476 Sinninghe Damsté and De Leeuw, 1990) also generates reactive S species (e.g., via
477 elemental S or polysulphide-reducing bacteria; Ma et al., 1993; Ma et al., 2000;
478 Wasmund et al., 2017).
479
480 $S_{org\text{-}PF}$ is abundant in Interval A but rare in Interval B (compare Plate III, 2 and 8),
481 perhaps because pyrite framboids are also rare in Interval B (Emmings et al., 2019).
482 This suggests that H_2S and/or polysulphide in porewaters seldom attained the critical
483 supersaturation conditions required for framboid nucleation (Ohfuji and Rickard,
484 2005; Rickard, 2012). Together, this suggests that the steepest redox gradient
485 during deposition of Interval B was located near or at (and parallel to) the seabed,
486 likely utilised by microbial mats, and not local to OM. Thus pyrite nucleation and
487 growth in Interval B was uncoupled to sites of *in situ* H_2S production driven by OM
488 degradation, but instead driven by reaction of reduced Fe with upward-diffusing H_2S.
489 It is also possible AOMgr, as the dominant type of particulate OM in Interval B, was
490 relatively refractory and therefore relatively resistant to hydrolysis and degradation
491 by microbes. This limited the production of H_2S local to OM required for framboid
492 (and therefore $S_{org\text{-}PF}$) growth.
493
494 **4.3. Controls on Organic Matter Distribution**
495 The distribution of key palynofacies categories through the Upper Bowland Shale in
496 the Craven Basin is predictable and linked to changing bottom water redox

497 conditions and changing basin accommodation. Facies A-C muds deposited during
498 marine transgressions (Figs. 2-4, Table 1) lack $S_{org\text{-}PF}$ likely because the redoxcline
499 bounding zones of SO_4 and Fe reduction was fixed in the water column during
500 deposition (Fig. 9a). Marine maximum flooding is associated with a high
501 AOMpel/AOMgr and low abundance of spores and phytoclasts.
502
503 Intervals A and B overlie 'marine band' packages and were therefore likely deposited
504 during sea level fall (Emmings et al., 2019). An enhanced shelf-to-basin 'Fe shuttle'
505 during falling sea level (Lyons and Severmann, 2006) increased the Fe_{HR} supply to
506 the basin (Emmings, 2018). This process promoted buffering of H_2S by Fe_{HR} via
507 pyrite formation (including nucleation on AOM to generate AOMpyr), weakening and
508 destabilising the chemocline, stimulating early diagenetic redox oscillation and
509 triggering $S_{org\text{-}PF}$ formation (Interval A; Fig. 9b). Therefore $S_{org\text{-}PF}$ is a proxy for redox
510 oscillation between sulphidic and ferruginous anoxic micro-environments during early
511 diagenesis.
512
513 Pendle delta progradation during the E_{1b2} biozone triggered euphotic zone
514 desalination, which sufficiently reduced the export of autochthonous (marine) OM to
515 seabed and therefore promoted bottom water oxygenation (Emmings, 2018). Bottom
516 water ventilation promoted colonisation of the seabed by sulphide-oxidising microbial
517 mats (Fig. 9c). Therefore the transition from anoxic (Facies F) to oxic/suboxic
518 conditions (Facies G) exhibits a 'cross-over' between AOMpel and AOMgr (Fig. 2;
519 Table 1). The proportionality of AOMpel and AOMgr may therefore delineate ancient
520 redox fronts at or near seabed. Palynological assessment of AOM types should be

coupled with detailed sedimentological characterisation, however, in order to determine whether AOMgr particles are present *in situ* or as rip-up clasts.

Figure 10 integrates and summarises observations and interpretations spanning palynology and geochemistry (this study), sedimentology and pyrite microtextures described by Emmings (2018) and Emmings et al. (2019). A ternary plot of AOMpel + AOMpyr versus AOMgr versus spores + phytoclasts (Fig. 11) links palynofacies abundances to bottom and pore water redox conditions, water column productivity and proximity to fluvial (deltaic) supply of spores and phytoclasts. Field I delineates AOMgr-rich samples located in the paralic Widermerpool Gulf (Hennissen et al., 2017). Field I is a mixing line between AOMgr and spores and phytoclasts. Lack of AOMpel suggests relatively low productivity water column conditions. Dominance of AOMgr in Field I may indicate widespread occurrences of candidate microbial mats existed in these paralic basins, supported by a long-lived, restriction-driven redox gradient near or at seabed. Alternatively, it is possible AOMgr is generated via multiple pathways; perhaps AOMgr also includes a component of bacterially modified terrestrial OM (TOM). Field II is interpreted to indicate low to moderate water column productivity, dominantly oxic or suboxic bottom water conditions and sulphidic conditions near or at seabed (Figs. 11, 12a). The atomic S_{org}/TOC in Field II (Interval B) exceeds 0.04 (Table 1; Fig. 12b), the threshold for definition of Type II-S kerogen (Orr, 1986).

Field III represents moderate to high rates of water column productivity and autochthonous OM export to seabed, linked to anoxic and at least intermittently sulphidic bottom water conditions (Figs. 11; 12a). This field includes Type II-S

546 kerogen ($S_{org\text{-}PF}$) generated via early diagenetic redox oscillation (Fig. 9b). $S_{org\text{-}PF}$
547 exhibits a possible catalytic effect on T_{max} (Lewan, 1998). The majority of Bowland
548 Shale samples from the Craven Basin and contemporaneous mudstones from the
549 Edale Gulf (Hennissen et al., 2017) plot within this field. This suggests productivity
550 was relatively widespread, and perhaps stimulated by nutrient loading from the
551 nearby Pendle delta system (Figs. 1a, 9a-b) (Emmings, 2018). Field V represents
552 oxygenated conditions and/or close proximity to the supply of TOM (Figs. 9, 12a).
553 Facies H-I in Cominco S9, located proximal to the Pendle delta system and
554 deposited during reduced basin accommodation, are sited in this field. Thus Field IV
555 likely represents transitional settings defined by fluctuating oxic/suboxic and anoxic
556 conditions, or significant supply of spores and phytoclasts into anoxic bottom waters
557 (Fig. 11).
558
559 The mixing line between fields III and V (and therefore through Field IV; Fig. 11)
560 represents increasing proximity to fluvial sources and/or bottom and pore water
561 ventilation that was sufficiently gradual or diffuse. This inhibited development of a
562 high redox gradient at seabed. Candidate microbial mats (AOMgr) were unable to
563 colonise seabed in these settings. The mixing line between fields III and I represents
564 rapid bottom water ventilation and/or high frequency redox fluctuation, coupled to
565 persistently stagnant or advective, sulphidic porewaters near seabed. This
566 configuration supported colonisation by the candidate microbial mats.
567
568 Hydrogen index (HI), a key measure for hydrocarbon source rock potential, is
569 highest near Field I and III apices for all immature to early oil-mature data plotted
570 (Fig. 12c; including data from Hennissen et al., 2017). Absence of inorganic

571 geochemical data for Field I precludes assessment of the mechanism for high HI in
572 this field. However, assuming paralic basins were subject to long-lived and stable
573 redoxclines near seabed, it is plausible these conditions promoted condensation and
574 preservation of relatively labile (aliphatic) OM. High HI in Field III is best explained by
575 enhanced preservation of labile OM under sulphidic bottom water conditions beneath
576 a stable redoxcline.
577
578 Changing basin accommodation during deposition of the Bowland Shale is
579 considered at least partially equivalent to eustatic sea level systems tracts
580 (Posamentier et al., 1988). A sequence-stratigraphic control on OM type is important
581 for understanding the link between source rock heterogeneity and timing of
582 hydrocarbon generation and expulsion from this source rock. The effect of changing
583 sea level for biozones E_{1a1} to E_{1c1} is summarised using the ternary plot of
584 AOMpel + AOMpyr versus AOMgr versus spores + phytoclasts (Fig. 13). Key
585 intervals deposited during falling sea level contain bulk Type II-S OM, which likely
586 entered the oil window at a relatively low temperature (e.g., Dembicki, 2009).
587 Understanding the distribution and type of OM is important for exploring this
588 unconventional hydrocarbon resource in the UK (e.g., Andrews, 2013; Clarke et al.,
589 2018), especially if Type II-S intervals are laterally extensive. The possibility that
590 sulphide-oxidising microbial mats colonised seabed, and across several basins,
591 suggests nutrient and inorganic S and C cycling in epicontinental Mississippian
592 seaways likely operated in vastly different way compared to modern oceans.
593

5. Conclusions

Geochemical and palynological data were integrated through the Upper Bowland Shale unit in the Craven Basin (Lancashire, UK), a basin with ongoing hydrocarbon exploration. Fe-speciation, trace element geochemistry and $\delta^{34}S_{py}$ analyses were utilised in order to assess syngenetic and early diagenetic redox conditions. These data were integrated with sedimentological and palynological observations, in order to understand the controls on OM sulphurization and the distribution of AOM.

Particulate OM in the Upper Bowland Shale is dominated by two types of AOM; 'homogenous' AOM (AOMpel) and 'heterogeneous, granular' AOM (AOMgr). On the basis of textural observations, AOMpel most likely represent the faecal minipellets of zooplankton and/or pellets of macro-zooplankters. On the transition from anoxic to oxic bottom waters, AOMgr replaces AOMpel as the dominant type of AOM (Interval B). A large particle diameter (likely >500 μm), sheet-like, fragmented character, and presence of candidate organic sheaths suggests AOMgr at least partially represent fragments of benthic microbial mats, likely as sulphide-oxidisers.

Abundant orange, high-relief organic spheres are recognised within each AOM particle, particularly in one key interval (A) overlying the E_{1a1} marine band. These textures are associated with a high S_{org} content and are therefore interpreted as sulphurized OM local to pyrite framboids ($S_{org\text{-}PF}$). Sulphurization is linked to early diagenetic redox oscillation processes. Whilst the precise mechanism for sulphurization is unclear, we propose redox oscillation promoted sulphurization in two ways. Firstly, redox oscillation enhanced the degradation of OM. This produced organic compounds prone to sulphurization. Secondly, redox oscillation also

promoted S cycling across micro-redox fronts local to each framboid. Intermediate, and therefore reactive, S species were thus available for complexation with OM.

$S_{org\text{-}PF}$ formed primarily under anoxic conditions during periods of reduced sea level (Interval A), via an increased supply of Fe_{HR} from adjacent shelves. An increased supply of Fe_{HR} stimulated redox oscillation between ferruginous and euxinic conditions, which promoted acidification of porewaters near seabed. Redox oscillation was associated with S cycling required to generate reactive S species.

Both intervals A and B exhibit S_{org}/TOC > 0.04 and are therefore interpreted as Type II-S kerogen. A ternary plot of AOMpel + AOMpyr versus AOMgr versus spores + phytoclasts links the observed palynofacies and sulphurization (intervals A and B) to bottom and pore water redox conditions, water column productivity and proximity to fluvial (deltaic) supply of spores and phytoclasts. These variables were moderated by changing basin accommodation, driven primarily by eustatic sea level fluctuation. This is important for understanding the link between source rock heterogeneity and timing of hydrocarbon generation and expulsion from this source rock.

6. Acknowledgements

This study was funded by the Natural Environment Research Council (NERC), [grant no. NE/L002493/1], within the Central England Training Alliance (CENTA). The study also received CASE funding from the British Geological Survey. SWP acknowledges support from a Royal Society Wolfson Research Merit Award. Nick Riley (Carboniferous Ltd) is thanked for sharing biostratigraphic expertise and assistance.

644 Nick Marsh and Tom Knott are thanked for providing assistance during geochemical
645 analyses. Jane Flint is thanked for preparation of the palynological slides. BGS
646 authors publish with the approval of the Executive Director of the British Geological
647 Survey.

648

649 **7. References**

650 1 Adam, P., Schneckenburger, P., Schaeffer, P., Albrecht, P., 2000. Clues to
651 early diagenetic sulfurization processes from mild chemical cleavage of labile sulfur-
652 rich geomacromolecules. Geochimica et Cosmochimica Acta, 64(20): 3485-3503.

653 2 Aitkenhead, N., Bridge, D., Riley, N.J., Kimbell, S., 1992. Geology of the
654 country around Garstang: memoir for 1:50 000 sheet 67. HMSO, London.

655 3 Aizenshtat, Z., Krein, E.B., Vairavamurthy, M.A., Goldstein, T.P., 1995. Role
656 of Sulfur in the Transformations of Sedimentary Organic Matter: A Mechanistic
657 Overview, Geochemical Transformations of Sedimentary Sulfur. ACS Symposium
658 Series. American Chemical Society, pp. 16-37.

659 4 Algeo, T.J., Tribovillard, N., 2009. Environmental analysis of
660 paleoceanographic systems based on molybdenum–uranium covariation. Chemical
661 Geology, 268(3–4): 211-225.

662 5 Aller, R.C., 1982. Carbonate Dissolution in Nearshore Terrigenous Muds: The
663 Role of Physical and Biological Reworking. The Journal of Geology, 90(1): 79-95.

664 6 Aller, R.C., 1998. Mobile deltaic and continental shelf muds as suboxic,
665 fluidized bed reactors. Marine Chemistry, 61(3): 143-155.

666 7 Amrani, A., 2014. Organosulfur Compounds: Molecular and Isotopic Evolution
667 from Biota to Oil and Gas. Annual Review of Earth and Planetary Sciences, 42(1):
668 733-768.

669 8 Amrani, A., Aizenshtat, Z., 2004. Mechanisms of sulfur introduction chemically
670 controlled: δ34S imprint. Organic Geochemistry, 35(11): 1319-1336.

671 9 Andrews, I.J., 2013. The Carboniferous Bowland Shale gas study: geology
672 and resource estimation. British Geological Survey for Department of Energy and
673 Climate Change.

674 10 Aplin, A.C., Macquaker, J.H.S., 1993. Quantifying sedimentary geochemical
675 processes - C-S-Fe geochemistry of some modern and ancient anoxic marine muds
676 and mudstones. Philosophical Transactions of the Royal Society of London. Series
677 A: Physical and Engineering Sciences, 344(1670): 89-100.

678 11 Arthurton, R.S., 1984. The Ribblesdale fold belt, NW England—a Dinantian-
679 early Namurian dextral shear zone. Geological Society, London, Special
680 Publications, 14(1): 131-138.

681 12 Aycard, M. et al., 2003. Formation pathways of proto-kerogens in Holocene
682 sediments of the upwelling influenced Cariaco Trench, Venezuela. Organic
683 Geochemistry, 34(6): 701-718.

684 13 Bailey, J.V., Orphan, V.J., Joye, S.B., Corsetti, F.A., 2009. Chemotrophic
685 microbial mats and their potential for preservation in the rock record. Astrobiology,
686 9(9): 843-59.

687 14 Beaumont, K., L, Nash, G., V, Davidson, A., T, 2002. Ultrastructure,
688 morphology and flux of microzooplankton faecal pellets in an east Antarctic fjord.
689 Marine Ecology Progress Series, 245: 133-148.

690 15 Bisat, W.S., 1923. The Carboniferous Goniatites Of The North Of England
691 And Their Zones. Proceedings of the Yorkshire Geological Society, 20(1): 40-124.

692 16 Brandon, A. et al., 1998. Geology of the country around Lancaster: memoir for
693 1:50 000 sheet 59. The Stationary Office, London.

694 17 Bruland, K.W., Silver, M.W., 1981. Sinking rates of fecal pellets from
695 gelatinous zooplankton (Salps, Pteropods, Doliolids). Marine Biology, 63(3): 295-
696 300.

697 18 Burdige, D.J., 2006. Geochemistry of Marine Sediments. Princeton University
698 Press, USA.

699 19 Canfield, D.E., Farquhar, J., Zerkle, A.L., 2010. High isotope fractionations
700 during sulfate reduction in a low-sulfate euxinic ocean analog. Geology, 38(5): 415-
701 418.

702 20 Canfield, D.E., Raiswell, R., Bottrell, S.H., 1992. The reactivity of sedimentary
703 iron minerals toward sulfide. American Journal of Science, 292(9): 659-683.

704 21 Canfield, D.E., Raiswell, R., Westrich, J.T., Reaves, C.M., Berner, R.A., 1986.
705 The use of chromium reduction in the analysis of reduced inorganic sulfur in
706 sediments and shales. Chemical Geology, 54(1): 149-155.

707 22 Canfield, D.E., Teske, A., 1996. Late Proterozoic rise in atmospheric oxygen
708 concentration inferred from phylogenetic and sulphur-isotope studies. Nature, 382:
709 127.

710 23 Catuneanu, O., 2007. Sequence stratigraphic context of microbial mat
711 features. In: Schieber, J. et al. (Eds.), Atlas of microbial mat features preserved
712 within the clastic rock record. Elsevier, pp. 276-283.

713 24 Clarke, H., Turner, P., Bustin, R.M., Riley, N., Besly, B., 2018. Shale gas
714 resources of the Bowland Basin, NW England: a holistic study. Petroleum
715 Geoscience.

716 25 Cuomo, M.C., Chen, Y.Y., 1996. Pellets and Epifluorescence. In: Jansonius,
717 J., McGregor, D. (Eds.), Palynology: Principles and Applications (1): American
718 Association of Stratigraphic Palynologists Foundation,, pp. 1092-1097.

719 26 Davies, R.J., Austin, R., Moore, D., 1993. Environmental controls of
720 Brigantian conodont-distribution: evidence from the Gayle limestone of the Yoredale
721 Group in Northern England. Annales de la Société géologique de Belgique,
722 116(Fascicule 2 - Carboniferous biostratigraphy): 221-241.

723 27 Davies, S., Hampson, G., Flint, S., Elliott, T., 1999. Continental-scale
724 sequence stratigraphy of the Namurian, Upper Carboniferous and its applications to
725 reservoir prediction. Geological Society, London, Petroleum Geology Conference
726 Series, 5: 757-770.

727 28 Davies, S.J., 2008. The record of Carboniferous sea-level change in low-
728 latitude sedimentary successions from Britain and Ireland during the onset of the late
729 Paleozoic ice age. Geological Society of America Special Papers, 441: 187-204.

730 29 Davydov, V.I., Korn, D., Schmitz, M., 2012. The Carboniferous Period.
731 Geologic Time Scale 2012 2-Volume Set. Elsevier.

732 30 Dembicki, H., 2009. Three common source rock evaluation errors made by
733 geologists during prospect or play appraisals. AAPG Bulletin, 93(3): 341-356.

734 31 Earp, J.R., 1961. Geology of the country around Clitheroe and Nelson (one-
735 inch geological sheet 68, new series). H.M.S.O.

736 32 Eglinton, T.I., Sinninghe Damsté, J.S., Kohnen, M.E.L., de Leeuw, J.W., 1990.
737 Rapid estimation of the organic sulphur content of kerogens, coals and asphaltenes
738 by pyrolysis-gas chromatography. Fuel, 69(11): 1394-1404.

739 33 Emmings, J., 2018. Controls on UK Lower Namurian Shale Gas Prospectivity:
740 Understanding the Spatial and Temporal Distribution of Organic Matter in Siliciclastic
741 Mudstones. PhD Thesis, University of Leicester.

742 34 Emmings, J. et al., 2019. From Marine Bands to Hybrid Flows: Sedimentology
743 of a Mississippian Black Shale. Sedimentology, ACCEPTED MANUSCRIPT.

744 35 Emmings, J. et al., 2017. Stream and Slope Weathering Effects on Organic-
745 rich Mudstone Geochemistry and Implications for Hydrocarbon Source Rock
746 Assessment: A Bowland Shale Case Study. Chemical Geology, 471: 74-91.

747 36 Espitalie, J., Madec, M., Tissot, B., Mennig, J.J., Leplat, P., 1977. Source
748 Rock Characterization Method for Petroleum Exploration. Offshore Technology
749 Conference.

750 37 Filley, T.R., Freeman, K.H., Wilkin, R.T., Hatcher, P.G., 2002. Biogeochemical
751 controls on reaction of sedimentary organic matter and aqueous sulfides in holocene
752 sediments of Mud Lake, Florida. Geochimica et Cosmochimica Acta, 66(6): 937-954.

753 38 Fossing, H. et al., 1995. Concentration and transport of nitrate by the mat-
754 forming sulphur bacterium Thioploca. Nature, 374: 713.

755 39 Fraser, A.J., Gawthorpe, R.L., 1990. Tectono-stratigraphic development and
756 hydrocarbon habitat of the Carboniferous in northern England. Geological Society of
757 London Special Publication, 55(1): 49-86.

758 40 Gastaldo, R.A., Purkyňová, E., Šimůnek, Z., Schmitz, M.D., 2009. Ecological
759 Persistence In The Late Mississippian (Serpukhovian, Namurian A) Megafloral
760 Record Of The Upper Silesian Basin, Czech Republic. Palaios, 24(6): 336-350.

761 41 Gawthorpe, R., 1987. Tectono-sedimentary evolution of the Bowland Basin, N
762 England, during the Dinantian. Journal of the Geological Society, 144: 59 - 71.

763 42 Gowing, M.M., Silver, M.W., 1985. Minipellets: A new and abundant size class
764 of marine fecal pellets. Journal of Marine Research, 43(2): 395-418.

765 43 Grant, C.W., 1991. Lateral and vertical distributions and textural features of
766 filamentous bacterial (Beggiatoa sp.) mats in Santa Barbara basin, California, AAPG
767 Bulletin Annual meeting of the American Association of Petroleum Geologists
768 (AAPG), Dallas, TX (United States), 7-10 Apr 1991. ; None, pp. Medium: X; Size:
769 Pages: 585.

770 44 Grossi, V. et al., 1998. Biotransformation pathways of phytol in recent anoxic
771 sediments. Organic Geochemistry, 29(4): 845-861.

772 45 Grunke, S. et al., 2011. Niche differentiation among mat-forming, sulfide-
773 oxidizing bacteria at cold seeps of the Nile Deep Sea Fan (Eastern Mediterranean
774 Sea). Geobiology, 9(4): 330-48.

775 46 Hartgers, W.A. et al., 1997. Sulfur-binding in recent environments: II.
776 Speciation of sulfur and iron and implications for the occurrence of organo-sulfur
777 compounds. Geochimica et Cosmochimica Acta, 61(22): 4769-4788.

778 47 Hennissen, J.A.I. et al., 2017. The prospectivity of a potential shale gas play:
779 An example from the southern Pennine Basin (central England, UK). Marine and
780 Petroleum Geology.

781 48 Henschke, N., Everett, J.D., Richardson, A.J., Suthers, I.M., 2016. Rethinking
782 the Role of Salps in the Ocean. Trends in Ecology & Evolution, 31(9): 720-733.

783 49 Holdsworth, B., Collinson, J.D., 1988. Millstone Grit cyclicity revisited. In:
784 Besly, B.M., Kelling, G. (Eds.), Sedimentation in a Synorogenic Basin Complex: The
785 Upper Carboniferous of Northwest Europe. Blackie, Glasgow, pp. 132 - 152.

786 50 Jarvie, D.M., 2012. Shale resource systems for oil and gas: Part 1 - Shale-gas
787 resource systems. Shale reservoirs - Giant resources for the 21st century: AAPG
788 Memoir 97.

789 51 Kampschulte, A., Bruckschen, P., Strauss, H., 2001. The sulphur isotopic
790 composition of trace sulphates in Carboniferous brachiopods: implications for coeval
791 seawater, correlation with other geochemical cycles and isotope stratigraphy.
792 Chemical Geology, 175(1): 149-173.

793 52 Kane, I.A., 2010. Development and flow structures of sand injectities: The
794 Hind Sandstone Member injectite complex, Carboniferous, UK. Marine and
795 Petroleum Geology, 27: 1200 - 1215.

796 53 Kerschke, D., Schulz, H.-M., 2013. The shale gas potential of Tournaisian,
797 Visean, and Namurian black shales in North Germany: baseline parameters in a
798 geological context. Environmental Earth Sciences, 70(8): 3817-3837.

799 54 Kirby, G.A. et al., 2000. Structure and evolution of the Craven Basin and
800 adjacent areas. Subsurface Memoir of the British Geological Survey.

801 55 Könitzer, S.F., Stephenson, M.H., Davies, S.J., Vane, C.H., Leng, M.J., 2016.
802 Significance of sedimentary organic matter input for shale gas generation potential of
803 Mississippian Mudstones, Widmerpool Gulf, UK. Review of Palaeobotany and
804 Palynology, 224, Part 2: 146-168.

805 56 Lampitt, R.S., Salter, I., Johns, D., 2009. Radiolaria: Major exporters of
806 organic carbon to the deep ocean. Global Biogeochemical Cycles, 23(1): n/a-n/a.

807 57 Leeder, M.R., 1982. Upper Palaeozoic basins of the British Isles—Caledonide
808 inheritance versus Hercynian plate margin processes. Journal of the Geological
809 Society, 139(4): 479-491.

810 58 Lewan, M.D., 1984. Factors controlling the proportionality of vanadium to
811 nickel in crude oils. Geochimica et Cosmochimica Acta, 48(11): 2231-2238.

812 59 Lewan, M.D., 1998. Sulphur-radical control on petroleum formation rates.
813 Nature, 391(6663): 164-166.

814 60 Lin, R., Davis, A., 1988. The Chemistry of Coal Maceral Fluorescence with
815 Special Reference to the Huminite/Vitrinite Group, Energy and Fuels Research
816 Center, College of Earth and Mineral Sciences, The Pennsylvania State University.

817 61 Love, L.G., 1957. Micro-organisms and the presence of syngenetic pyrite.
818 Quarterly Journal of the Geological Society, 113(1-4): 429-436,NP,437-440.

819 62 Love, L.G., 1962. Further studies on micro-organisms and the presence of
820 syngenetic pyrite. Palaeontology, 5.

821 63 Lyons, T.W., Severmann, S., 2006. A critical look at iron paleoredox proxies:
822 New insights from modern euxinic marine basins. Geochimica et Cosmochimica
823 Acta, 70(23): 5698-5722.

824 64 Ma, K., Schicho, R.N., Kelly, R.M., Adams, M.W., 1993. Hydrogenase of the
825 hyperthermophile Pyrococcus furiosus is an elemental sulfur reductase or
826 sulfhydrogenase: evidence for a sulfur-reducing hydrogenase ancestor. Proceedings
827 of the National Academy of Sciences, 90(11): 5341-5344.

828 65 MacLean, L.C. et al., 2008. A high-resolution chemical and structural study of
829 framboidal pyrite formed within a low-temperature bacterial biofilm. Geobiology, 6(5):
830 471-80.

66 Maher, L.J., 1981. Statistics for microfossil concentration measurements employing samples spiked with marker grains. Review of Palaeobotany and Palynology, 32(2): 153-191.

67 Martinsen, O.J., Collinson, J.D., Holdsworth, B.K., 1995. Millstone Grit Cyclicity Revisited, II: Sequence Stratigraphy and Sedimentary Responses to Changes of Relative Sea-Level, Sedimentary Facies Analysis. Blackwell Publishing Ltd., pp. 305-327.

68 Menning, M. et al., 2006. Global time scale and regional stratigraphic reference scales of Central and West Europe, East Europe, Tethys, South China, and North America as used in the Devonian–Carboniferous–Permian Correlation Chart 2003 (DCP 2003). Palaeogeography, Palaeoclimatology, Palaeoecology, 240(1–2): 318-372.

69 Moseley, F., 1952. The Namurian of the Lancaster Fells. Quarterly Journal of the Geological Society, 109(1-4): 423-450,NP,451-454.

70 Moseley, F., 1962. The Structure Of The South-Western Part Of The Sykes Anticline, Bowland, West Yorkshire. Proceedings of the Yorkshire Geological and Polytechnic Society, 33(3): 287-314.

71 Mossmann, J.-R., Aplin, A.C., Curtis, C.D., Coleman, M.L., 1991. Geochemistry of inorganic and organic sulphur in organic-rich sediments from the Peru Margin. Geochimica et Cosmochimica Acta, 55(12): 3581-3595.

72 Nissenbaum, A., Presley, B.J., Kaplan, I.R., 1972. Early diagenesis in a reducing fjord, Saanich Inlet, British Columbia—I. chemical and isotopic changes in major components of interstitial water. Geochimica et Cosmochimica Acta, 36(9): 1007-1027.

73 Nyhuis, C.J., Riley, D., Kalasinska, A., 2015. Thin section petrography and chemostratigraphy: Integrated evaluation of an upper Mississippian mudstone dominated succession from the southern Netherlands. Netherlands Journal of Geosciences - Geologie en Mijnbouw, 95(1): 3-22.

74 Ohfuji, H., Rickard, D., 2005. Experimental syntheses of framboids—a review. Earth-Science Reviews, 71(3–4): 147-170.

75 Orr, W., 1986. Kerogen/asphaltene/sulfur relationships in sulfur-rich Monterey oils. Advances in Organic Geochemistry, 10: 499-516.

76 Pacton, M., Fiet, N., Gorin, G.E., 2007. Bacterial Activity and Preservation of Sedimentary Organic Matter: The Role of Exopolymeric Substances. Geomicrobiology Journal, 24(7-8): 571-581.

77 Pacton, M., Gorin, G.E., Vasconcelos, C., 2011. Amorphous organic matter — Experimental data on formation and the role of microbes. Review of Palaeobotany and Palynology, 166(3–4): 253-267.

78 Pitrat, C.W., 1970. Phytoplankton and the Late Paleozoic wave of extinction. Palaeogeography, Palaeoclimatology, Palaeoecology, 8(1): 49-54.

79 Porter, K.G., Robbins, E.I., 1981. Zooplankton Fecal Pellets Link Fossil Fuel and Phosphate Deposits. Science, 212(4497): 931-933.

80 Posamentier, H.W., Jervey, M.T., Vail, P.R., 1988. Eustatic Controls on Clastic Deposition I - Conceptual Framework. Society of Economic Paleontologists and Mineralogists Special Publication(42).

81 Poulton, S.W., Canfield, D.E., 2005. Development of a sequential extraction procedure for iron: implications for iron partitioning in continentally derived particulates. Chemical Geology, 214(3): 209-221.

82 Poulton, S.W., Canfield, D.E., 2011. Ferruginous Conditions: A Dominant Feature of the Ocean through Earth's History. Elements, 7(2): 107-112.

83 Poulton, S.W., Raiswell, R., 2002. The low-temperature geochemical cycle of iron: From continental fluxes to marine sediment deposition. American Journal of Science, 302(9): 774-805.

84 Raiswell, R., Canfield, D., 1998. Sources of iron for pyrite formation in marine sediments. American Journal of Science, 298(3): 219-245.

85 Ramsbottom, W.H.C., 1977. Major cycles of transgression and regression (mesothems) in the Namurian. Proceedings of the Yorkshire Geological and Polytechnic Society, 41(3): 261-291.

86 Ramsbottom, W.H.C., Saunders, W.B., 1985. Evolution and Evolutionary Biostratigraphy of Carboniferous Ammonoids. Journal of Paleontology, 59(1): 123-139.

87 Rickard, D., 2012. Chapter 6 - Sedimentary Pyrite. In: David, R. (Ed.), Developments in Sedimentology. Elsevier, pp. 233-285.

88 Riegel, W., 1996. The geologic significance of the Late Paleozoic phytoplankton blackout, IX IPC Meeting, Houston, Texas, USA abstracts, pp. 133-134.

89 Riegel, W., 2008. The Late Palaeozoic phytoplankton blackout — Artefact or evidence of global change? Review of Palaeobotany and Palynology, 148(2): 73-90.

90 Riley, N. et al., 1993. Geochronometry and geochemistry of the European mid-Carboniferous boundary global stratotype proposal, Stonehead Beck, North Yorkshire, UK. Annales de la Societe geologique de Belgique, T. 116 (fascicule 2): 275-289.

91 Rontani, J.-F., Bonin, P.C., Volkman, J.K., 1999. Biodegradation of Free Phytol by Bacterial Communities Isolated from Marine Sediments under Aerobic and Denitrifying Conditions. Applied and Environmental Microbiology, 65(12): 5484-5492.

92 Schieber, J., 1986. The possible role of benthic microbial mats during the formation of carbonaceous shales in shallow Mid-Proterozoic basins. Sedimentology, 33(4): 521-536.

93 Schieber, J., Sur, S., Banerjee, S., 2007a. Benthic microbial mats in black shale units from the Vindhyan Supergroup, Middle Proterozoic of India: the challenges of recognizing the genuine article. In: Schieber, J. et al. (Eds.), Atlas of microbial mat features preserved within the clastic rock record. Elsevier, pp. 189-197.

94 Schieber, J., Sur, S., Banerjee, S., 2007b. Microbial Mats on Muddy Substrates - Examples of Possible Sedimentary Features and Underlying Processes. In: Schieber, J. et al. (Eds.), Atlas of microbial mat features preserved within the clastic rock record. Elsevier, pp. 189-197.

95 Schindelin, J. et al., 2012. Fiji: an open-source platform for biological-image analysis. Nature Methods, 9: 676.

96 Seckbach, J., Oren, A., 2010. Microbial Mats: Modern and Ancient Microorganisms in Stratified Systems. Cellular Origin, Life in Extreme Habitats and Astrobiology, 14.

97 Servais, T., Martin, R.E., Nützel, A., 2016. The impact of the 'terrestrialisation process' in the late Palaeozoic: pCO2, pO2, and the 'phytoplankton blackout'. Review of Palaeobotany and Palynology, 224, Part 1: 26-37.

98 Sholkovitz, E.R., Price, N.B., 1980. The major-element chemistry of suspended matter in the Amazon Estuary. Geochimica et Cosmochimica Acta, 44(2): 163-171.

99 Sievert, S.M., Wieringa, E.B., Wirsen, C.O., Taylor, C.D., 2007. Growth and mechanism of filamentous-sulfur formation by Candidatus Arcobacter sulfidicus in opposing oxygen-sulfide gradients. Environ Microbiol, 9(1): 271-6.

100 Sinninghe Damsté, J.S., De Leeuw, J.W., 1990. Analysis, structure and geochemical significance of organically-bound sulphur in the geosphere: State of the art and future research. Advances in Organic Geochemistry, 16(4-6): 1077-1101.

101 Sinninghe Damsté, J.S., Leeuw, J.W.d., 1990. Organic sulfur compounds and other biomarkers as indicators of palaeosalinity. In: Orr, W., White, W. (Eds.), Geochemistry of Sulfur in Fossil Fuels. American Chemical Society.

102 Słowakiewicz, M. et al., 2015. Shale-Gas Potential Of The Mid-Carboniferous Bowland-Hodder Unit In The Cleveland Basin (Yorkshire), Central Britain. Journal of Petroleum Geology, 38(1): 59-75.

103 Soetaert, K., Hofmann, A.F., Middelburg, J.J., Meysman, F.J.R., Greenwood, J., 2007. The effect of biogeochemical processes on pH. Marine Chemistry, 105(1): 30-51.

104 Steudel, R., 1989. On the Nature of the "Elemental Sulfur" (S^0) Produced by Sulfur-oxidising Bacteria - a Model for S^0 Globules. In: Schlegel, H., Bowien, B. (Eds.), Biological of Autotrophic Bacteria. Science Technology Publishing, Madison, USA.

948 105 Stockmarr, J., 1971. Tablets with spores used in absolute pollen analysis.
949 Pollen et spores, XIII(4).

950 106 Stoecker, D.K., 1984. Particle production by planktonic ciliates. Limnology and
951 Oceanography, 29(5): 930-940.

952 107 Tappan, H., 1970. Phytoplankton abundance and Late Paleozoic extinctions:
953 A reply. Palaeogeography, Palaeoclimatology, Palaeoecology, 8(1): 56-66.

954 108 Taylor, S., McLennan, S., 1985. The Continental Crust: Its Composition and
955 Evolution. Blackwell Scientific, London, 312 pp.

956 109 Tribovillard, N., Algeo, T., Lyons, T., Riboulleau, A., 2006. Trace metals as
957 paleoredox and paleoproductivity proxies: An update. Chemical Geology, 232: 12 -
958 32.

959 110 Tribovillard, N., Bialkowski, A., Tyson, R.V., Lallier-Vergès, E., Deconinck,
960 J.F., 2001. Organic facies variation in the late Kimmeridgian of the Boulonnais area
961 (northernmost France). Marine and Petroleum Geology, 18(3): 371-389.

962 111 Tribovillard, N., Trentesaux, A., Trichet, J., Défarge, C., 2000. A Jurassic
963 counterpart for modern kopara of the Pacific atolls:: lagoonal, organic matter-rich,
964 laminated carbonate of Orbagnoux (Jura Mountains, France). Palaeogeography,
965 Palaeoclimatology, Palaeoecology, 156(3): 277-288.

966 112 Tyson, R., 1989. Late Jurassic palynofacies trends, Piper and Kimmeridge
967 Clay Formations, UK onshore and offshire. In: Batter, D., Keen, M. (Eds.), Northwest
968 European Micropalaeontology and Palynology. British Micropalaeontological Society
969 Series. Ellis Horwood, Chichester, pp. 135-172.

970 113 Tyson, R., 1995. Sedimentary Organic Matter: Organic Facies and
971 Palynofacies, London.

972 114 Van Kaam-Peters, H.M.E., Schouten, S., Köster, J., Sinninghe Damstè, J.S.,
973 1998. Controls on the molecular and carbon isotopic composition of organic matter
974 deposited in a Kimmeridgian euxinic shelf sea: evidence for preservation of
975 carbohydrates through sulfurisation. Geochimica et Cosmochimica Acta, 62(19):
976 3259-3283.

977 115 Veevers, J.J., Powell, C.M., 1987. Late Paleozoic glacial episodes in
978 Gondwanaland reflected in transgressive-regressive depositional sequences in
979 Euramerica. Geological Society of America Bulletin, 98(4): 475-487.

980 116 Wang, F., Chapman, P.M., 1999. Biological implications of sulfide in
981 sediment—a review focusing on sediment toxicity. Environmental Toxicology and
982 Chemistry, 18(11): 2526-2532.

983 117 Warr, L.N., 2000. The Variscan Orogeny: the welding of Pangaea. In:
984 Woodcock, N.H., Strachan, R. (Ed.), Geological History of Britain and Ireland. Wiley-
985 Blackwell, Hoboken, USA, pp. 271 - 294.

118 Wasmund, K., Mußmann, M., Loy, A., 2017. The life sulfuric: microbial ecology of sulfur cycling in marine sediments. Environmental Microbiology Reports, 9(4): 323-344.

119 Waters, C.N., Browne, M.A.E., Dean, M.T., Powell, J.H., 2007. Lithostratigraphical framework for Carboniferous successions of Great Britain (Onshore). British Geological Survey Research Report, RR/07/01.

120 Waters, C.N., Condon, D.J., 2012. Nature and timing of Late Mississippian to Mid-Pennsylvanian glacio-eustatic sea-level changes of the Pennine Basin, UK. Journal of the Geological Society, 169(1): 37-51.

121 Waters, C.N., Davies, S.J., 2006. Carboniferous: extensional basins, advancing deltas and coal swamps. In: Brenchley, P.J. (Ed.), The geology of England and Wales. Geological Society of London, London, England, pp. 173 - 223.

122 Waters, C.N., Waters, R.A., Barclay, W.J., Davies, J.R., 2009. A lithostratigraphical framework for the Carboniferous successions of southern Great Britain (onshore). British Geological Survey Research Report, RR/09/01.

123 Wignall, P.B., Newton, R., 1998. Pyrite framboid diameter as a measure of oxygen deficiency in ancient mudrocks. American Journal of Science, 298(7): 537-552.

124 Williams, L.A., 1984. Subtidal stromatolites in Monterey Formation and other organic-rich rocks as suggested source contributors to petroleum formation. AAPG Bulletin, 68(12): 1879-1893.

125 Wirsen, C.O. et al., 2002. Characterization of an autotrophic sulfide-oxidizing marine Arcobacter sp. that produces filamentous sulfur. Appl Environ Microbiol, 68(1): 316-25.

126 Wood, G.D., Gabriel, A.M., Lawson, J.C., 1996. Palynological techniques - processing and microscopy. In: Jansonius, J., McGregor, D. (Eds.), Palynology: Principles and Applications (1): American Association of Stratigraphic Palynologists Foundation,, pp. 29 - 50.

Figure Captions

Fig. 1. a) Regional basin structure modified from Waters et al. (2007), including the Craven Basin, study positions Hind Clough (A), MHD4 (B) and Cominco S9 (C), and UK coastline. Palynological studies by Hennissen et al., (2017) and Könitzer et al., (2014; 2016) through the broadly time equivalent (Pendleian to Arnsbergian) Morridge Formation from the Widmerpool Gulf (D) and Edale Gulf (E) are also plotted for reference. LDH = Lake District High; AIB = Alston Block; ST = Stainmore

Trough; AB = Askrigg Block; BH = Bowland High; CLH = Central Lancashire High; GT = Gainsborough Trough; EG = Edale Gulf; WG = Widermerpool Gulf; HH = Holme High; b) The Bowland Shale Formation is exposed as part of the Ribblesdale Fold Belt, including Westphalian structural elements (Fraser and Gawthorpe, 1990) and study sites Hind Clough (outcrop) and borehole Marl Hill 4 (MHD4). Outcrop extent data are based on DigMapGB-625, published with permission of the British Geological Survey. c) Generalised Lower Namurian stratigraphy and Craven Basin composite after Brandon et al. (1998). Marine band areal extent data from Waters and Condon (2012), including diagnostic ammonoid fauna from Riley et al. (1993). Mesothems from Ramsbottom (1973). HS = Hind Sandstone Member. PG = Pendle Grit Member.

Fig. 2. Sedimentary logs through Hind Clough (a) and borehole MHD4 (b), from Emmings et al. (2019), plotted with selected geochemical data including RockEval pyrolysis total organic carbon (TOC), inorganic C content and T_{max}, organic S (S_{org}), bulk pyrite $\delta^{34}S_{py}$, enrichment factors (EFs) for redox-sensitive trace elements (Mo, U) and Fe speciation redox proxies. See Materials and Methods for derivation of 'excess Si' and calculation of trace element enrichment factors (EFs). Intervals A and B exhibit relatively high S_{org} content. Interval A contains abundant sulphurized AOM spheres surrounding pyrite framboids ($S_{org\text{-}PF}$).

Fig. 3. Sedimentary log through borehole Cominco S9, from Emmings et al. (2019), plotted with selected geochemical data including RockEval pyrolysis total organic carbon (TOC), inorganic C content and T_{max}, organic S (S_{org}), bulk pyrite $\delta^{34}S_{py}$, enrichment factors (EFs) for redox-sensitive trace elements (Mo, U) and Fe

speciation redox proxies. See Materials and Methods for derivation of 'excess Si' and calculation of trace element enrichment factors (EFs). See Fig. 2 for key to sedimentary facies. **Facies H-I Fe_{HR} is presented on a Fe_{mag}-free basis, due to the likely input of detrital Fe_{mag} (see Emmings, 2018 for discussion).

Fig. 4. 'APP' ternary plot of heregeneous AOM (defined as AOMpyr + AOMpel + AOMgr) versus phytoclasts + homogenous AOM (the latter is typically negligible in samples in this study) versus spores (terrestrial palynomorphs). Fields and interpreted processes are from Tyson (1995). See Fig. 2 and Emmings et al., (2019) for sedimentary facies description. Palynofacies abundance data for the Morridge Formation in the Edale Gulf (borehole Karenight 1) and Widmerpool Gulf (borehole Carsington DRC3), from Hennissen et al., (2017), are also plotted for comparison.

Fig. 5. 'APP' ternary plot (see Fig. 4 for details) with palaeoredox proxies (a) Fe_{HR}/Fe_T and (b) Mo enrichment factors (EFs) mapped to each sample. See text for discussion.

Fig. 6. $S_{org\text{-}PF}$ diameter versus frequency in Interval A (Facies F). N = number of spheres counted, MFD = maximum framboid diameter (Wignall and Newton, 1998).

Fig. 7. Rock-Eval pyrolysis T_{max} versus organic S/C, with point size and colour mapped to the relative abundance of AOMgr, and with Type II-S field (S/C > 0.04) from Orr (1986). Several turbidites, debrites and hybrid flow deposits exhibit moderate S/C and contain AOMgr interpreted as rip-up clasts (Emmings et al.,

2019). Interval A is possibly positioned at the end of a mixing line defined by the catalytical effect of S radicals during hydrocarbon maturation (Lewan, 1998).

Fig. 8. Proposed mechanism for formation of $S_{org\text{-}PF}$ local to pyrite framboids in Interval A (and rarely B), via capture of reactive S species across a local redoxcline between zones of Fe- and SO_4-reduction, and/or via microbial reduction of intermediate S species perhaps via H_2 nutrient loading local to framboids. These conditions are likely favoured during early diagenetic redox oscillation under relatively high Fe_{HR} loadings. Fe mono-sulphide and pyrite nucleation equations (labelled A and B, respectively) from Soetaert et al. (2007).

Fig. 9. Basin accommodation control on the distribution of $S_{org\text{-}PF}$, after the model for anoxia in the Craven Basin described by Emmings (2018). a) Deposition of 'marine band' facies during periods of high sea level and euxinic bottom waters driven by relatively high rates of primary productivity (enhanced AOMpel export). Fixation of the redoxcline within the water column, bounding zones of Fe and SO_4-reduction, limited $S_{org\text{-}PF}$ formation in sediments. b) Falling sea level promoted Fe_{HR} shuttling into deep waters (via mobilisation of the shelfal Fe_{HR} sink) and triggered early diagenetic redox oscillation in porewaters (likely between zones of Fe- and SO_4-reduction). These conditions promoted pyrite precipitation on AOM (AOMpyr) and $S_{org\text{-}PF}$ formation in Interval A. c) Bottom waters became progressively oxygenated during the late stages of deposition of the Bowland Shale. AOMpel is replaced by AOMgr as the dominant type of AOM, which may represent sulphide-oxidising microbial mats that utilised the high redox gradient near seabed. These conditions

1095 are linked to limited $S_{org\text{-}PF}$ formation but possibly promoted intermolecular fixation of
1096 S_{org} (Interval B).
1097
1098 Fig. 10. Summary of key observations and interpretations spanning palynology and
1099 organic geochemistry (this study) and sedimentology (Emmings et al., 2019).
1100 Backscattered electron microphotographs are also reported by Emmings (2018). All
1101 scale bars = 50 μm. Generalized geochemistry includes mean Mo and U EFs with
1102 uncertainty quantified as two standard deviations.
1103
1104 Fig. 11. Ternary plot of AOMpel + AOMpyr versus AOMgr versus
1105 spores + phytoclasts. See Fig. 2 and Emmings et al., (2019) for sedimentary facies
1106 description. Palynofacies abundance data for the Morridge Formation in the Edale
1107 Gulf (borehole Karenight 1) and Widmerpool Gulf (borehole Carsington DRC3), from
1108 Hennissen et al., (2017), are also plotted for comparison.
1109
1110 Fig. 12. Ternary plot of AOMpel + AOMpyr versus AOMgr versus
1111 spores + phytoclasts (see Fig. 11 for details), with (a) Fe_{HR}/Fe_T; (b) organic S/C, and;
1112 (c) hydrogen index (HI) mapped to each data point. Palynofacies abundance data for
1113 the Morridge Formation in the Edale Gulf (borehole Karenight 1) and Widmerpool
1114 Gulf (borehole Carsington DRC3), from Hennissen et al., (2017), are also plotted
1115 with HI. See text for discussion.
1116
1117 Fig. 13. Ternary plot of AOMpel + AOMpyr versus AOMgr versus
1118 spores + phytoclasts (see Fig. 11 for details), with organic S/C mapped to each data
1119 point and interpreted basin accommodation pathways from Emmings et al., (2019).

Basin accommodation pathways are at least partially equivalent to the eustatic sea level systems tracts of Posamentier et al., (1988). TST = transgressive systems tract; HST = highstand systems tract; FSST = falling stage systems tract; LST = lowstand systems tract.

Plate I. ‘Sharp-edged’ heterogeneous amorphous organic matter (AOMpel) example transmitted light microphotographs. Scale bars = 50 μm unless otherwise stated. 1-4. MPA68143. 5. MPA68144. 6. MPA66949. 7-9. MPA68145.

Plate II. ‘Diffuse-edged, granular’ heterogeneous amorphous organic matter (AOMgr) example transmitted light microphotographs. Scale bars = 50 μm unless otherwise stated. 1-4. MPA68138. 5-7. MPA68139 (6-7; arrows indicate candidate sheaths). 8. MPA68140. 9. MPA68128.

Plate III. Sulphurized AOM local to pyrite framboids ($S_{org\text{-}PF}$; arrows indicate examples). Scale bars = 50 μm. 1-5. Interval A. 1-4. MPA66949 (oxidised slide 4, transmitted light). 5. MPA66949 (oxidised slide 4, incident green light, red light filtered). 6-9. Interval B. 6, 8. MPA68139 (oxidised slide 4, transmitted light). 7, 9. (Incident green light, red light filtered).

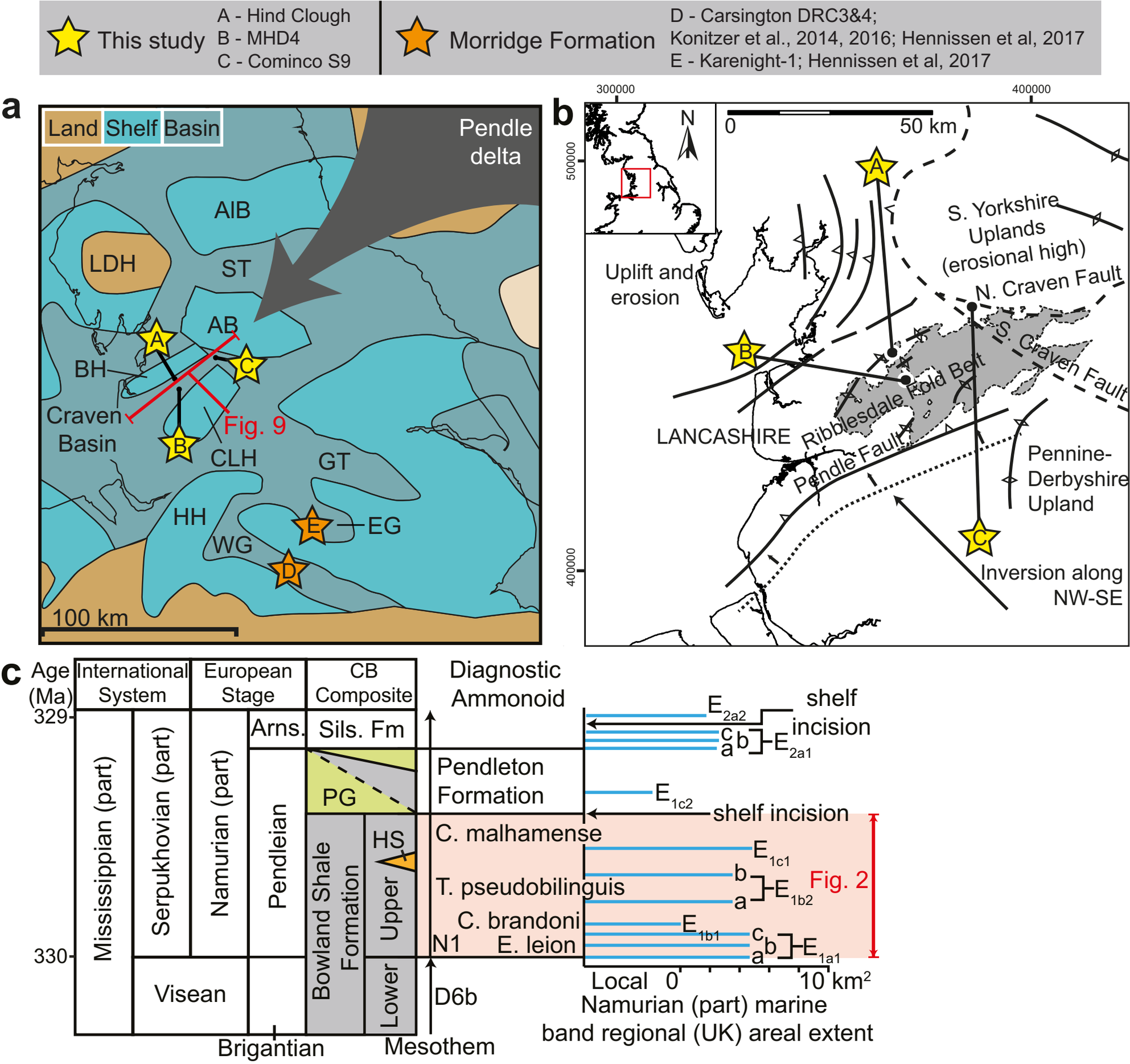
This study
A - Hind Clough
B - MHD4
C - Cominco S9
Morridge Formation
D - Carsington DRC3&4;
Konitzer et al., 2014, 2016; Hennissen et al, 2017
E - Karenight-1; Hennissen et al, 2017
a
Land
Shelf
Basin
Pendle delta
AlB
LDH
ST
AB
BH
Craven Basin
Fig. 9
CLH
GT
HH
WG
EG
100 km
b
300000
400000
500000
400000
N
0
50 km
Uplift and erosion
S. Yorkshire Uplands (erosional high)
N. Craven Fault
S. Craven Fault
Ribblesdale Fold Belt
LANCASHIRE
Pendle Fault
Pennine-Derbyshire Upland
Inversion along NW-SE
c
Age (Ma)
International System
European Stage
CB Composite
Diagnostic Ammonoid
329
330
Mississippian (part)
Serpukhovian (part)
Namurian (part)
Pendleian
Arns.
Sils. Fm
PG
Pendleton Formation
Bowland Shale Formation
HS
Upper
Lower
Visean
Brigantian
Mesothem
D6b
N1
E. leion
C. brandoni
T. pseudobilinguis
C. malhamense
E2a2
E2a1
E1c2
E1c1
E1b2
E1b1
E1a1
shelf incision
shelf incision
Fig. 2
Local 0
10 km²
Namurian (part) marine band regional (UK) areal extent

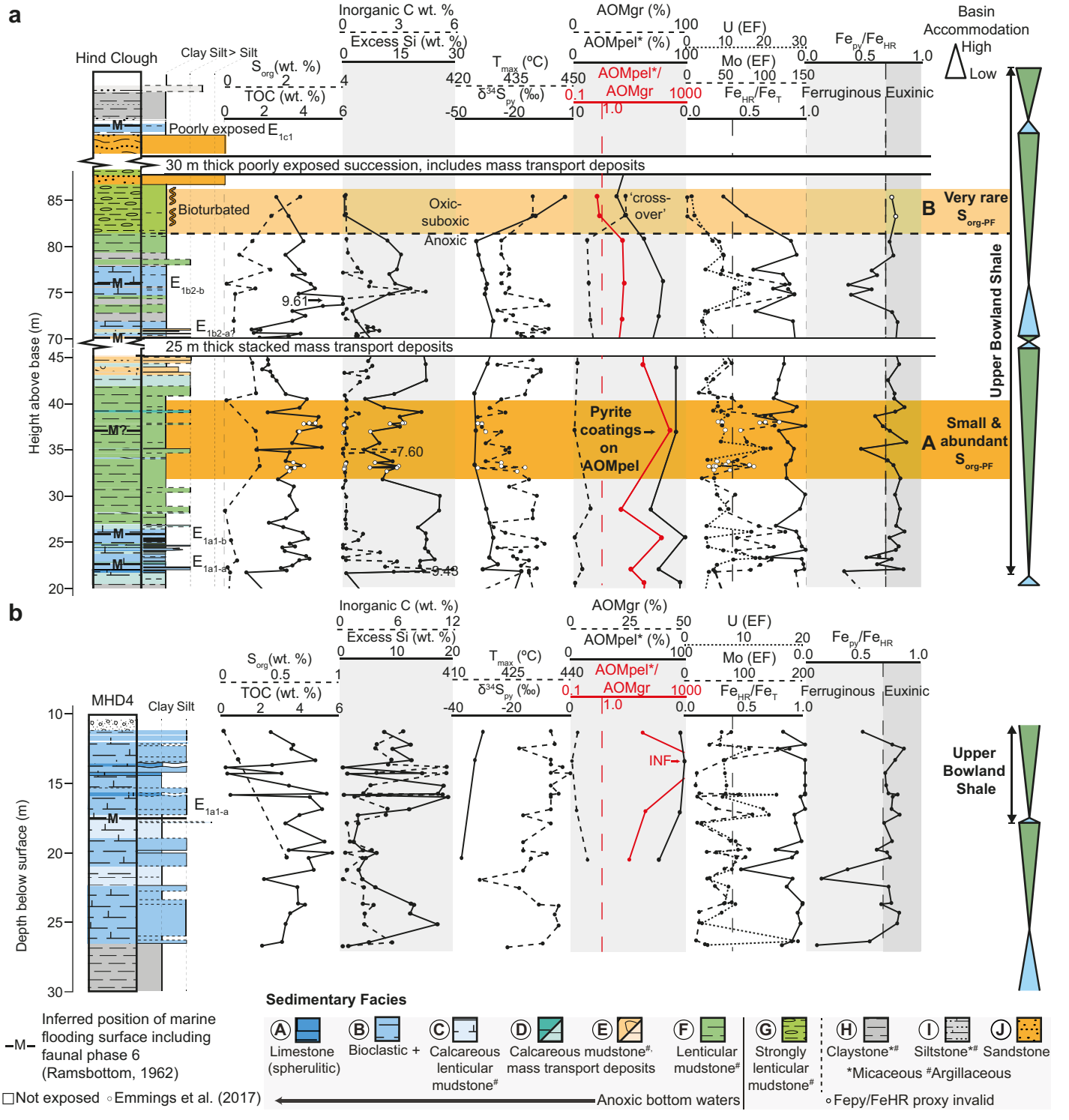
a
Hind Clough
Clay Silt > Silt
Inorganic C wt. %
Excess Si (wt. %)
AOMgr (%)
AOMpel* (%)
U (EF)
Mo (EF)
Basin Accommodation
High
Low
Poorly exposed E1c1
30 m thick poorly exposed succession, includes mass transport deposits
Bioturbated
Oxic-suboxic
Anoxic
'cross-over'
B
Very rare Sorg-PF
E1b2-b
E1b2-a
9.61
25 m thick stacked mass transport deposits
Pyrite coatings on AOMpel
7.60
9.48
A
Small & abundant Sorg-PF
Upper Bowland Shale
Height above base (m)
b
MHD4
Clay Silt
E1a1-a
INF
Upper Bowland Shale
Depth below surface (m)
Sedimentary Facies
A Limestone (spherulitic)
B Bioclastic +
C Calcareous lenticular mudstone#
D Calcareous mass transport deposits
E mudstone#.
F Lenticular mudstone#
G Strongly lenticular mudstone#
H Claystone*#
I Siltstone*#
J Sandstone
*Micaceous #Argillaceous
Inferred position of marine flooding surface including faunal phase 6 (Ramsbottom, 1962)
Not exposed
Emmings et al. (2017)
Anoxic bottom waters
Fepy/FeHR proxy invalid

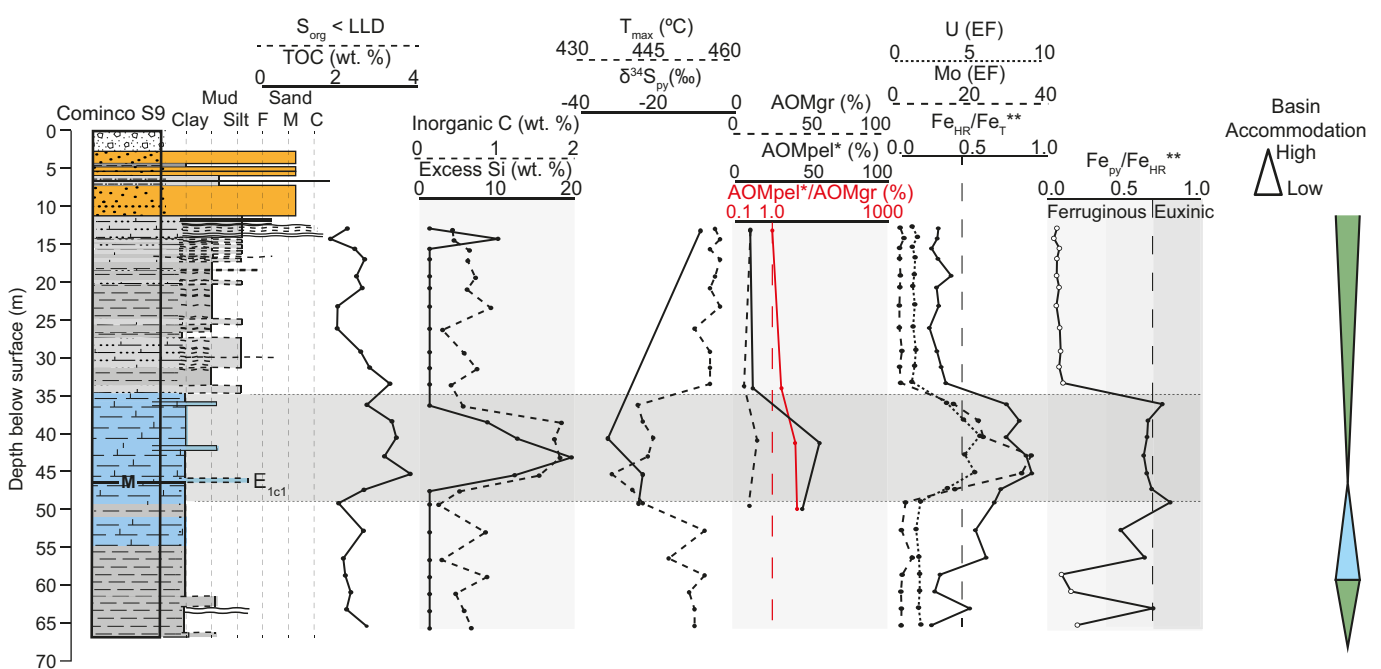
Cominco S9
Depth below surface (m)
Mud
Clay
Silt
Sand
F
M
C
S_{org} < LLD
TOC (wt. %)
0
2
4
T_{max} (ºC)
430
445
460
$\delta^{34}S_{py}$(‰)
-40
-20
0
U (EF)
0
5
10
Mo (EF)
0
20
40
AOMgr (%)
0
50
100
Fe_{HR}/Fe_T**
0.0
0.5
1.0
Inorganic C (wt. %)
0
1
2
Excess Si (wt. %)
0
10
20
AOMpel* (%)
0
50
100
AOMpel*/AOMgr (%)
0.1
1.0
1000
Fe_{py}/Fe_{HR}**
0.0
0.5
1.0
Ferruginous
Euxinic
M
E_{1c1}
Basin Accommodation
High
Low

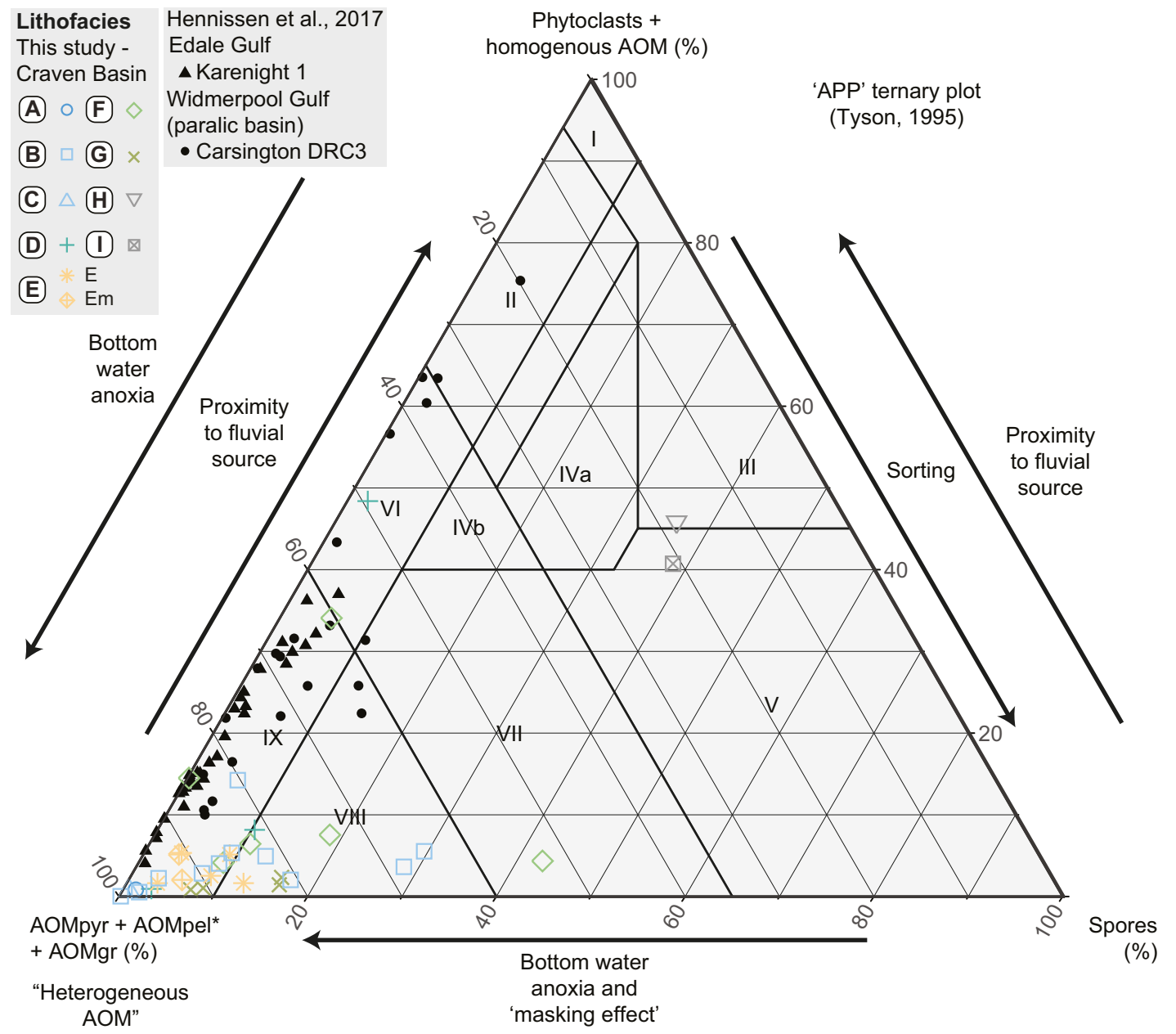

I - Highly proximal shelf or basin
II - Marginal dysoxic-anoxic basin
III - Heterolithic oxic (proximal) shelf
IVa - Dysoxic-suboxic slope
IVb - Suboxic-anoxic slope
V - Mud-dominated oxic (distal) shelf
VI - Proximal suboxic-anoxic shelf
VII - Distal dysoxic-oxic shelf
VIII - Distal dysoxic-anoxic shelf
IX - Distal suboxic-anoxic basin

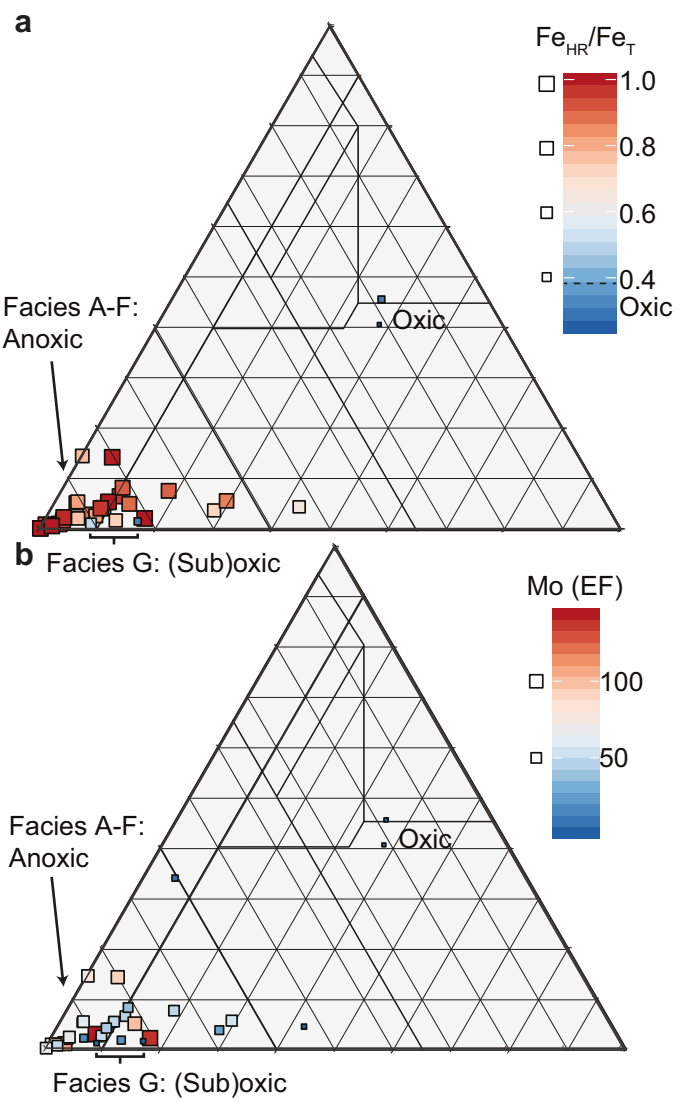
a
Fe_{HR}/Fe_T
1.0
0.8
0.6
0.4
Oxic
Facies A-F:
Anoxic
Oxic
b
Facies G: (Sub)oxic
Mo (EF)
100
50
Facies A-F:
Anoxic
Oxic
Facies G: (Sub)oxic

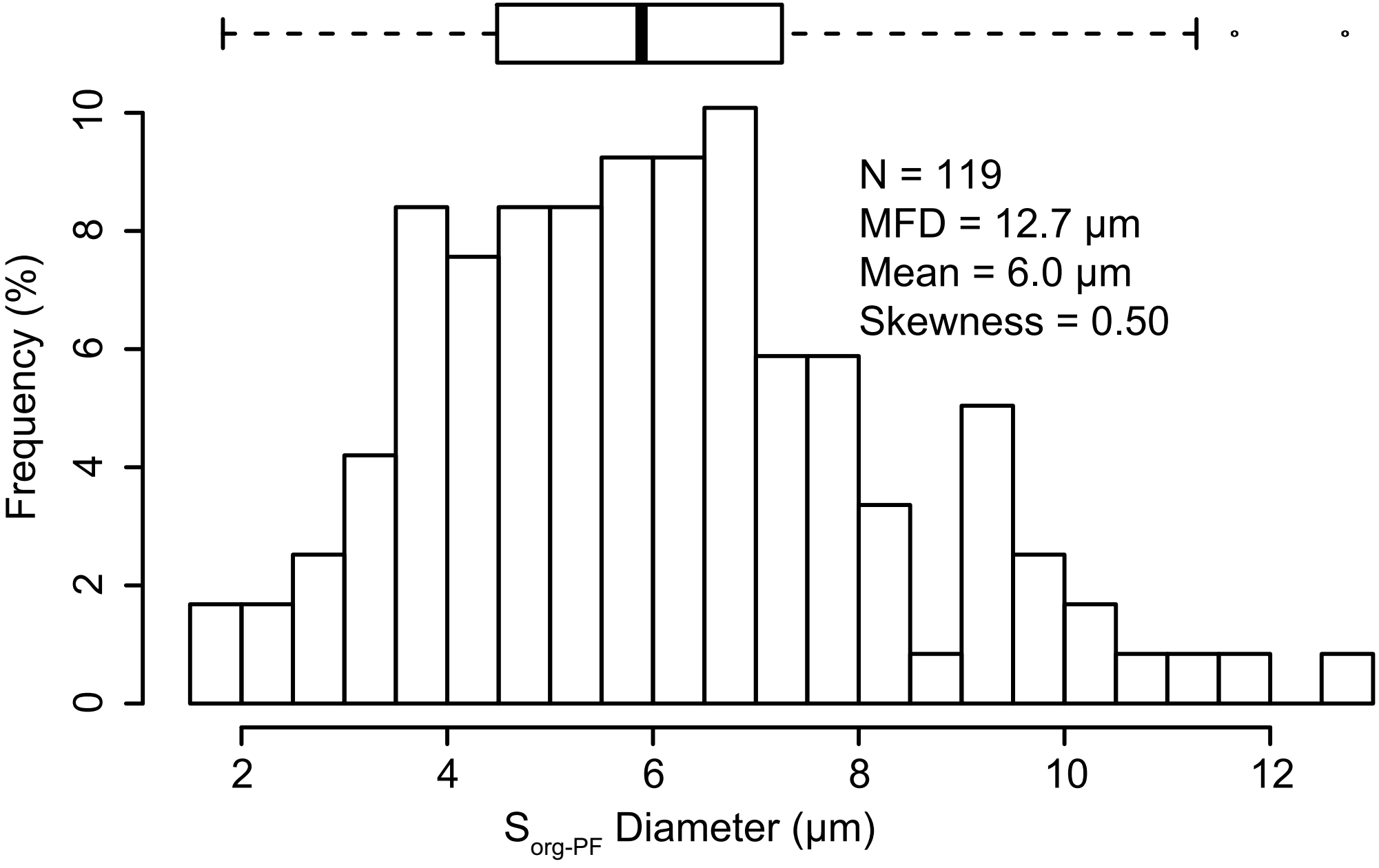
N = 119
MFD = 12.7 µm
Mean = 6.0 µm
Skewness = 0.50
Frequency (%)
0
2
4
6
8
10
2
4
6
8
10
12
S org-PF Diameter (µm)

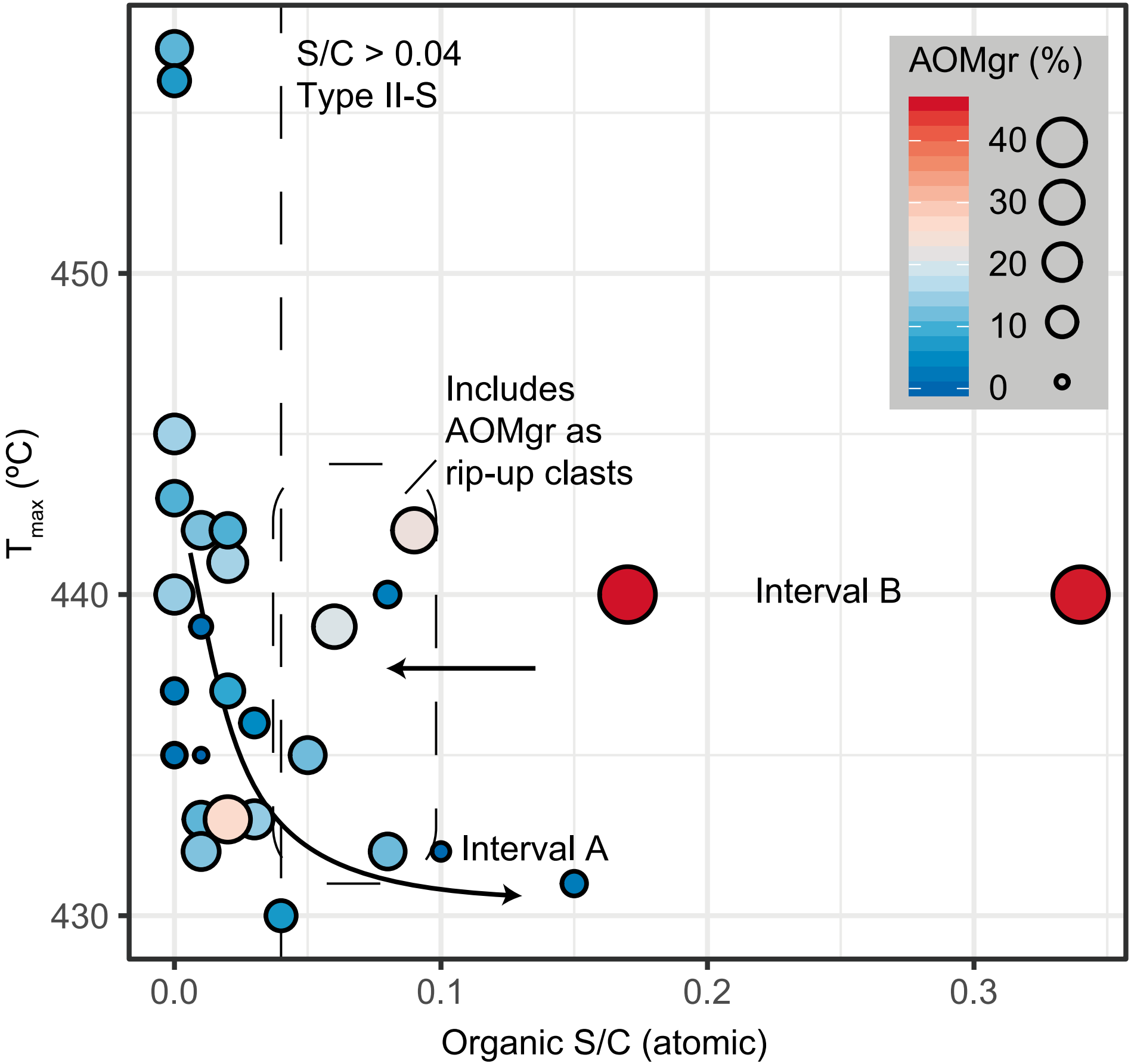
S/C > 0.04
Type II-S
AOMgr (%)
40
30
20
10
0
Includes
AOMgr as
rip-up clasts
Interval B
Interval A
450
440
430
0.0
0.1
0.2
0.3
T max (°C)
Organic S/C (atomic)

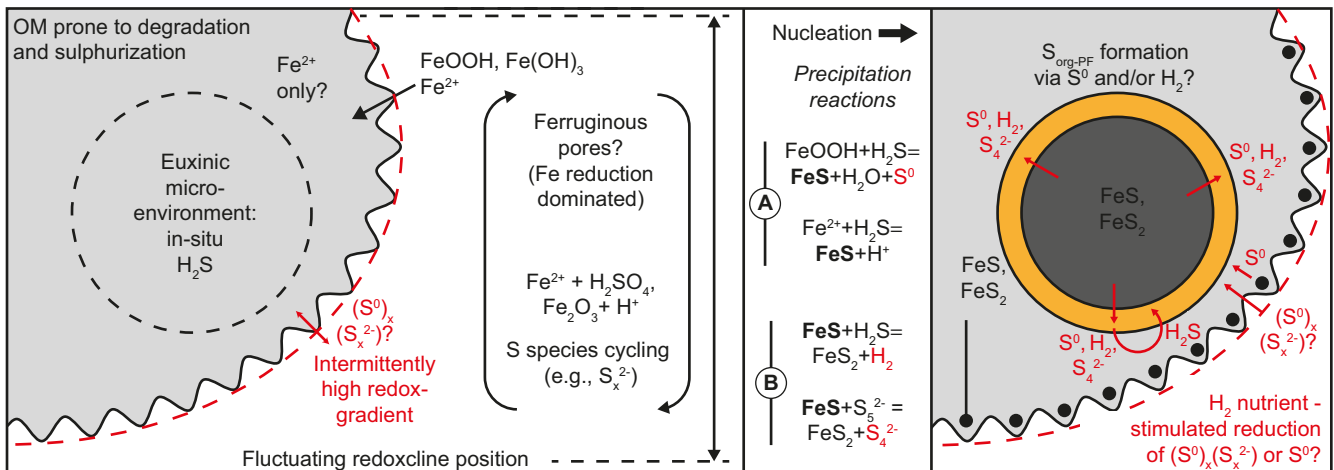
OM prone to degradation and sulphurization
Fe2+ only?
FeOOH, Fe(OH)3
Fe2+
Euxinic micro-environment: in-situ H2S
Ferruginous pores? (Fe reduction dominated)
Fe2+ + H2SO4, Fe2O3 + H+
S species cycling (e.g., Sx2-)
(S0)x (Sx2-)?
Intermittently high redox-gradient
Fluctuating redoxcline position
Nucleation
Precipitation reactions
A
FeOOH+H2S= FeS+H2O+S0
Fe2+ +H2S= FeS+H+
B
FeS+H2S= FeS2+H2
FeS+S52- = FeS2+S42-
Sorg-PF formation via S0 and/or H2?
S0, H2, S42-
FeS, FeS2
S0
H2S
(S0)x (Sx2-)?
H2 nutrient - stimulated reduction of (S0)x(Sx2-) or S0?

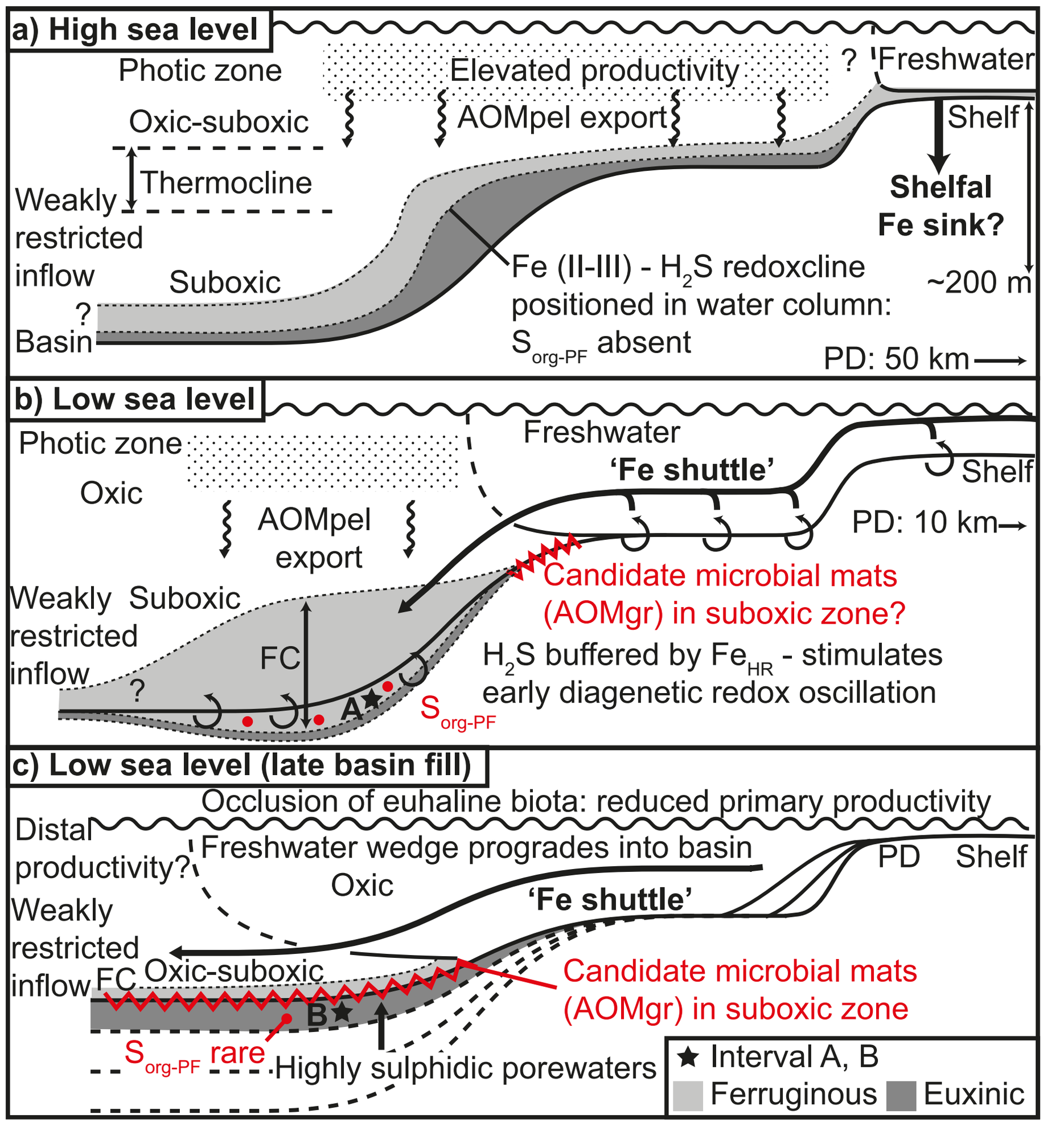
a) High sea level
Photic zone
Elevated productivity
? Freshwater
Oxic-suboxic
AOMpel export
Shelf
Thermocline
Weakly restricted inflow
Shelfal Fe sink?
Suboxic
Fe (II-III) - H2S redoxcline positioned in water column:
~200 m
?
Basin
Sorg-PF absent
PD: 50 km
b) Low sea level
Photic zone
Freshwater
'Fe shuttle'
Shelf
Oxic
AOMpel export
PD: 10 km
Candidate microbial mats (AOMgr) in suboxic zone?
Weakly restricted inflow
Suboxic
FC
H2S buffered by FeHR - stimulates early diagenetic redox oscillation
?
A
Sorg-PF
c) Low sea level (late basin fill)
Occlusion of euhaline biota: reduced primary productivity
Distal productivity?
Freshwater wedge progrades into basin
PD
Shelf
Oxic
'Fe shuttle'
Weakly restricted inflow
FC
Oxic-suboxic
Candidate microbial mats (AOMgr) in suboxic zone
B
Sorg-PF rare
Highly sulphidic porewaters
Interval A, B
Ferruginous
Euxinic

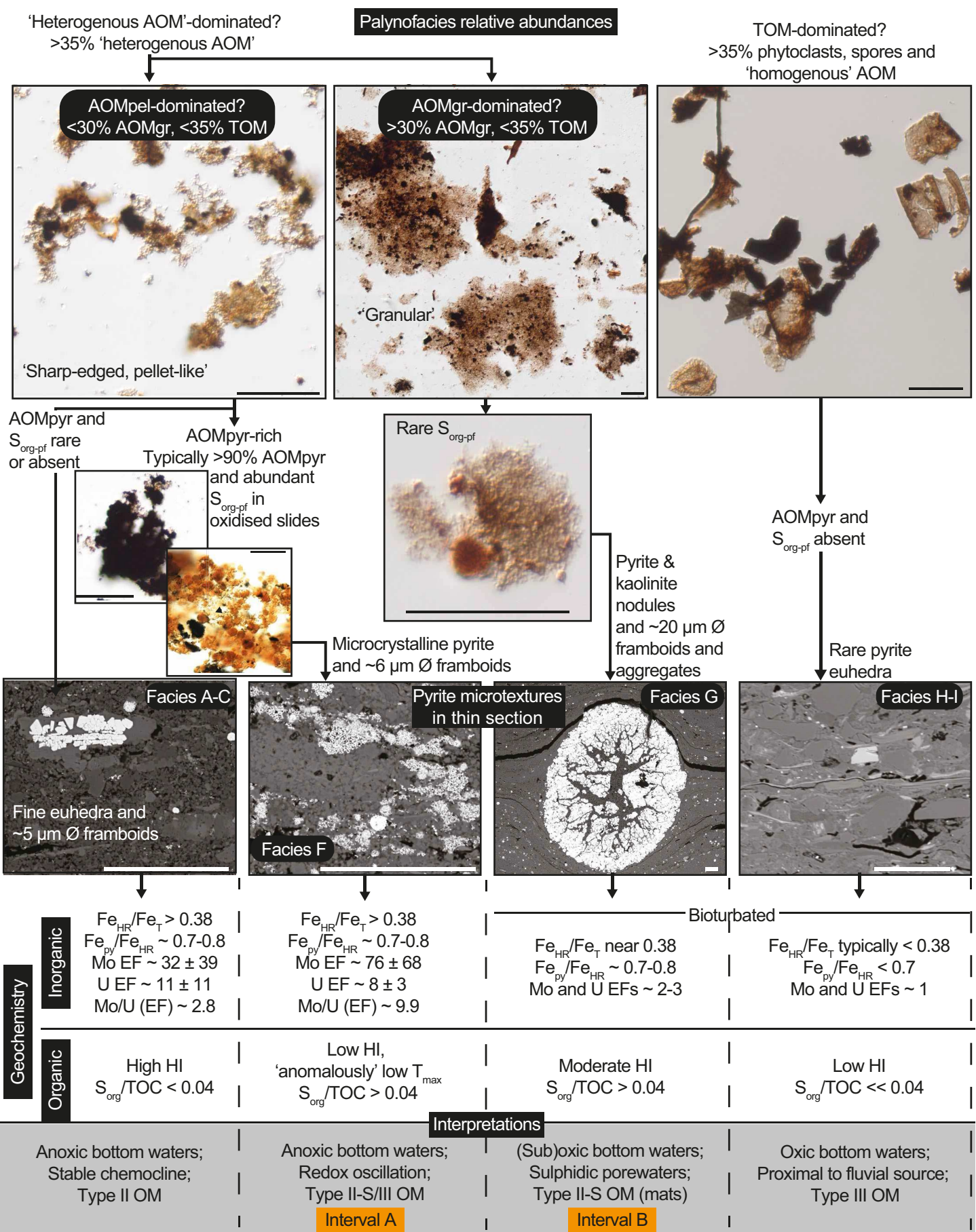
'Heterogenous AOM'-dominated?
>35% 'heterogenous AOM'
Palynofacies relative abundances
TOM-dominated?
>35% phytoclasts, spores and
'homogenous' AOM
AOMpel-dominated?
<30% AOMgr, <35% TOM
'Sharp-edged, pellet-like'
AOMgr-dominated?
>30% AOMgr, <35% TOM
'Granular'
AOMpyr and
S org-pf rare
or absent
AOMpyr-rich
Typically >90% AOMpyr
and abundant
S org-pf in
oxidised slides
Rare S org-pf
AOMpyr and
S org-pf absent
Microcrystalline pyrite
and ~6 µm Ø framboids
Pyrite &
kaolinite
nodules
and ~20 µm Ø
framboids and
aggregates
Rare pyrite
euhedra
Facies A-C
Fine euhedra and
~5 µm Ø framboids
Pyrite microtextures
in thin section
Facies F
Facies G
Facies H-I
Bioturbated
Geochemistry
Inorganic
Fe HR/Fe T > 0.38
Fe py/Fe HR ~ 0.7-0.8
Mo EF ~ 32 ± 39
U EF ~ 11 ± 11
Mo/U (EF) ~ 2.8
Fe HR/Fe T > 0.38
Fe py/Fe HR ~ 0.7-0.8
Mo EF ~ 76 ± 68
U EF ~ 8 ± 3
Mo/U (EF) ~ 9.9
Fe HR/Fe T near 0.38
Fe py/Fe HR ~ 0.7-0.8
Mo and U EFs ~ 2-3
Fe HR/Fe T typically < 0.38
Fe py/Fe HR < 0.7
Mo and U EFs ~ 1
Organic
High HI
S org/TOC < 0.04
Low HI,
'anomalously' low T max
S org/TOC > 0.04
Moderate HI
S org/TOC > 0.04
Low HI
S org/TOC << 0.04
Interpretations
Anoxic bottom waters;
Stable chemocline;
Type II OM
Anoxic bottom waters;
Redox oscillation;
Type II-S/III OM
Interval A
(Sub)oxic bottom waters;
Sulphidic porewaters;
Type II-S OM (mats)
Interval B
Oxic bottom waters;
Proximal to fluvial source;
Type III OM

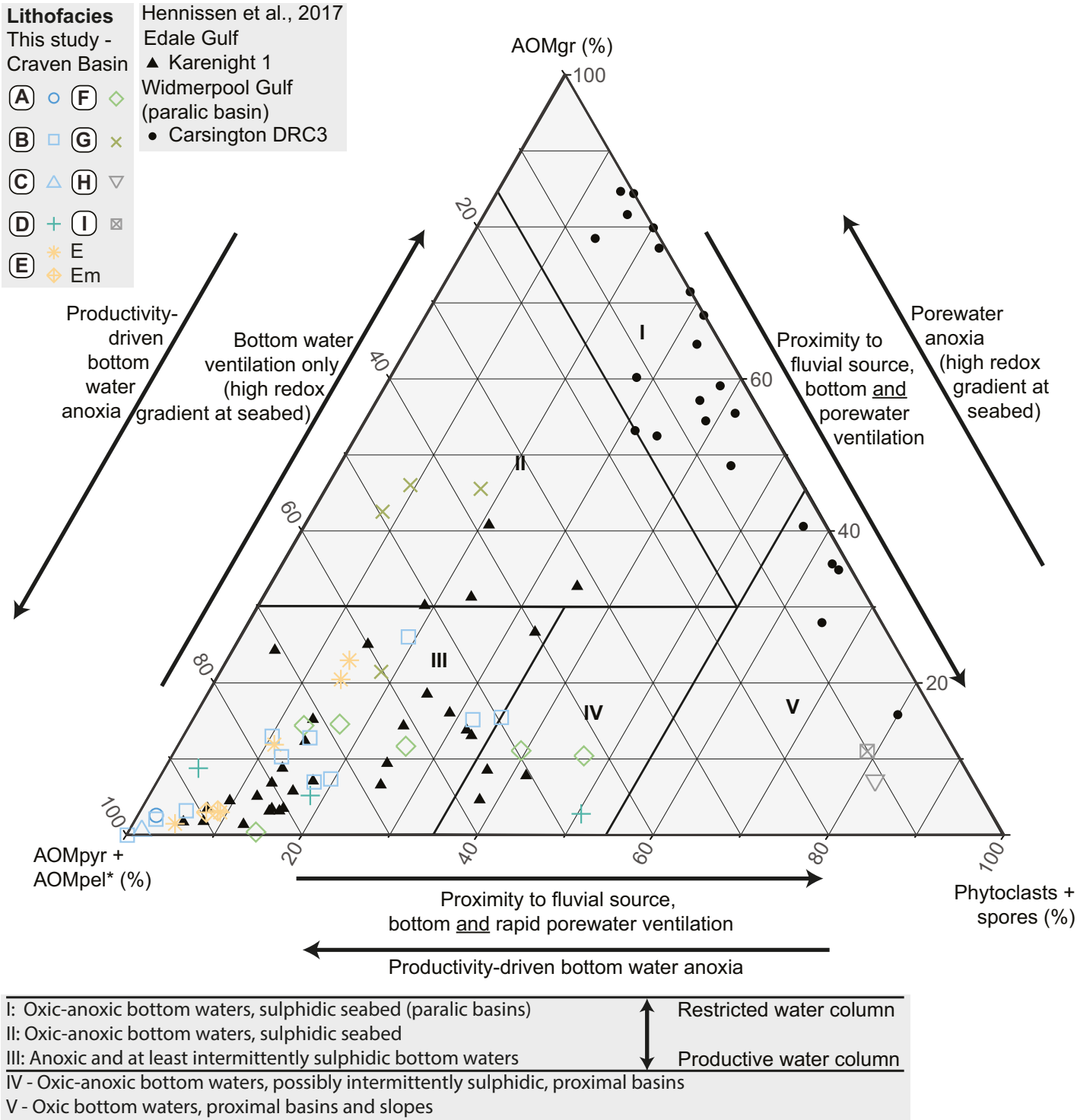
Lithofacies
This study - Craven Basin
A
B
C
D
E
F
G
H
I
E
Em
Hennissen et al., 2017
Edale Gulf
▲ Karenight 1
Widmerpool Gulf (paralic basin)
● Carsington DRC3
AOMgr (%)
100
20
40
60
80
Productivity-driven bottom water anoxia
Bottom water ventilation only (high redox gradient at seabed)
Proximity to fluvial source, bottom and porewater ventilation
Porewater anoxia (high redox gradient at seabed)
I
II
III
IV
V
AOMpyr + AOMpel* (%)
Phytoclasts + spores (%)
Proximity to fluvial source, bottom and rapid porewater ventilation
Productivity-driven bottom water anoxia
I: Oxic-anoxic bottom waters, sulphidic seabed (paralic basins)
II: Oxic-anoxic bottom waters, sulphidic seabed
III: Anoxic and at least intermittently sulphidic bottom waters
Restricted water column
Productive water column
IV - Oxic-anoxic bottom waters, possibly intermittently sulphidic, proximal basins
V - Oxic bottom waters, proximal basins and slopes

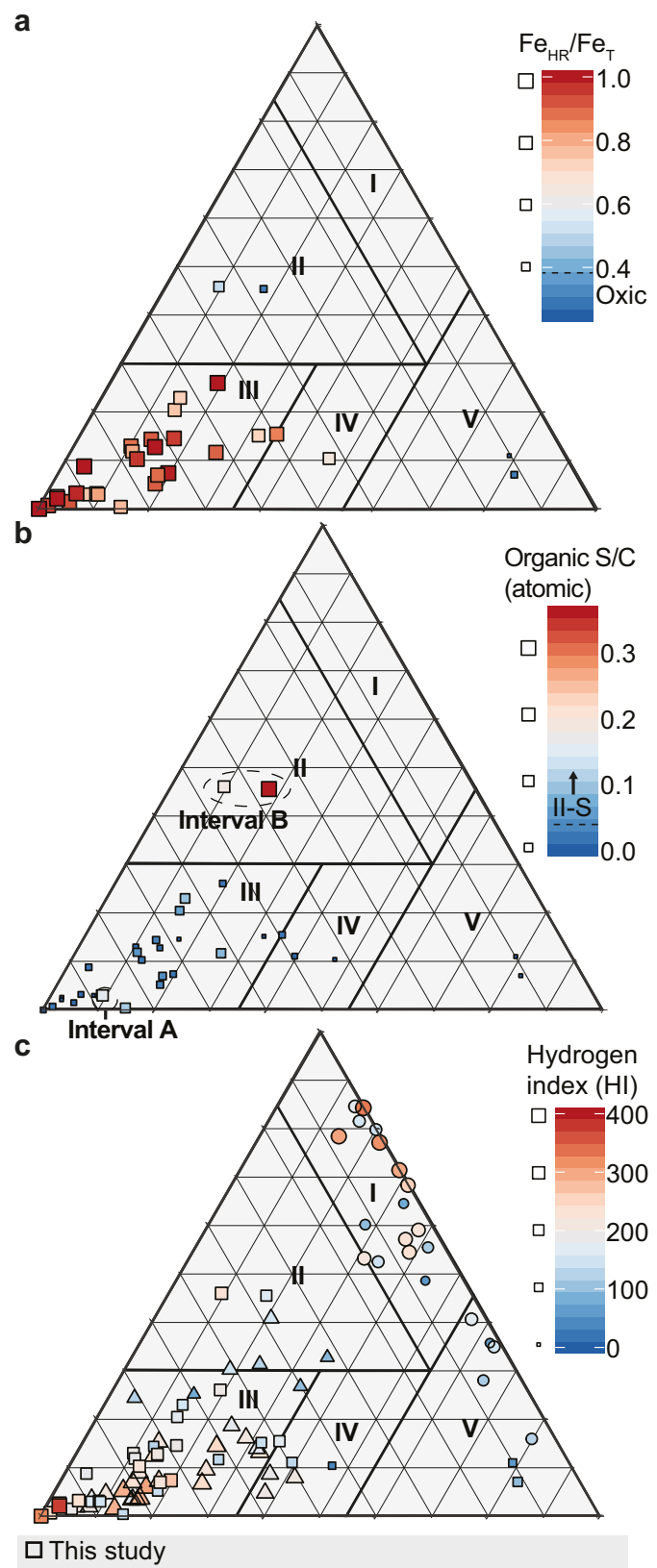

□ This study

Hennissen et al., 2017:

Edale Gulf	Widmerpool Gulf (paralic basin)
△ Karenight 1	○ Carsington DRC3

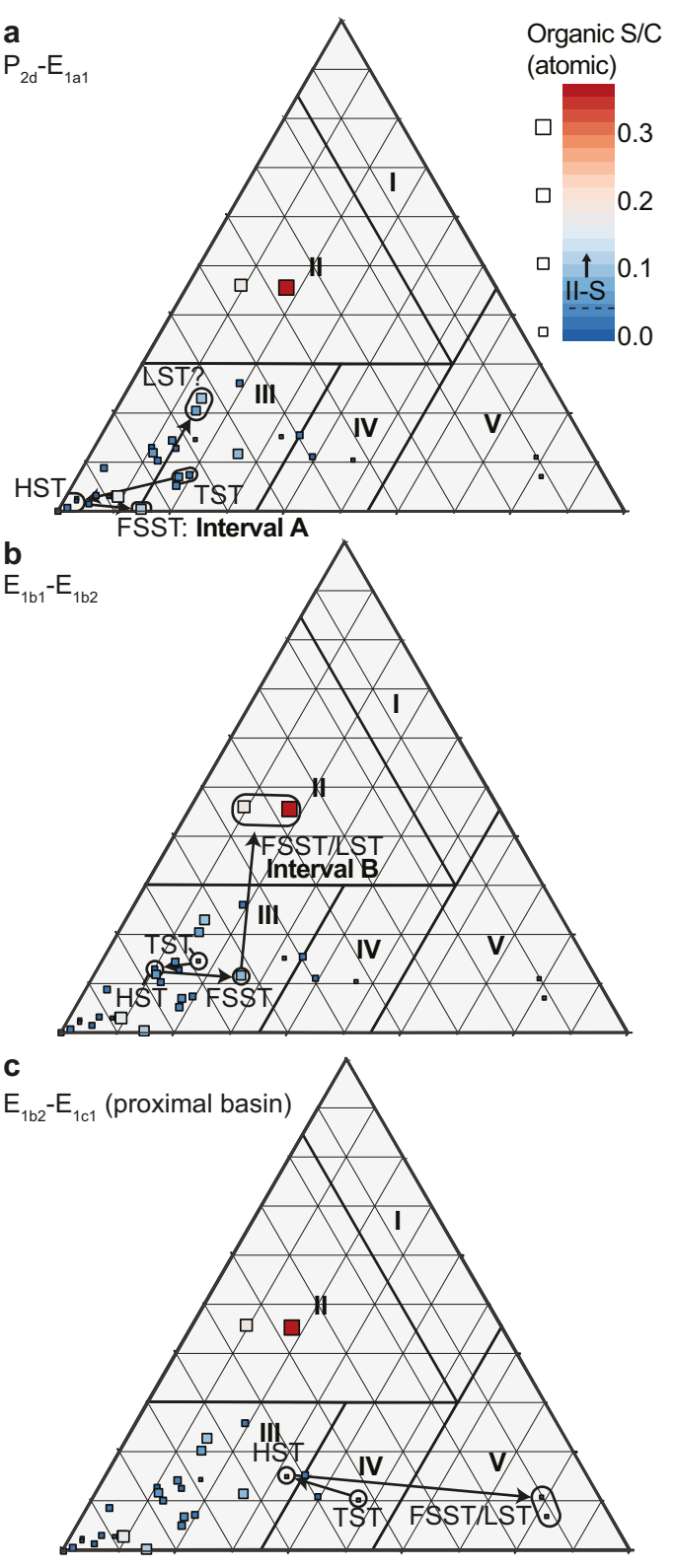
a
P2d-E1a1
Organic S/C
(atomic)
0.3
0.2
0.1
0.0
II-S
I
II
III
IV
V
LST?
HST
TST
FSST: Interval A
b
E1b1-E1b2
I
II
FSST/LST
Interval B
III
IV
V
TST
HST
FSST
c
E1b2-E1c1 (proximal basin)
I
II
III
HST
IV
V
TST
FSST/LST

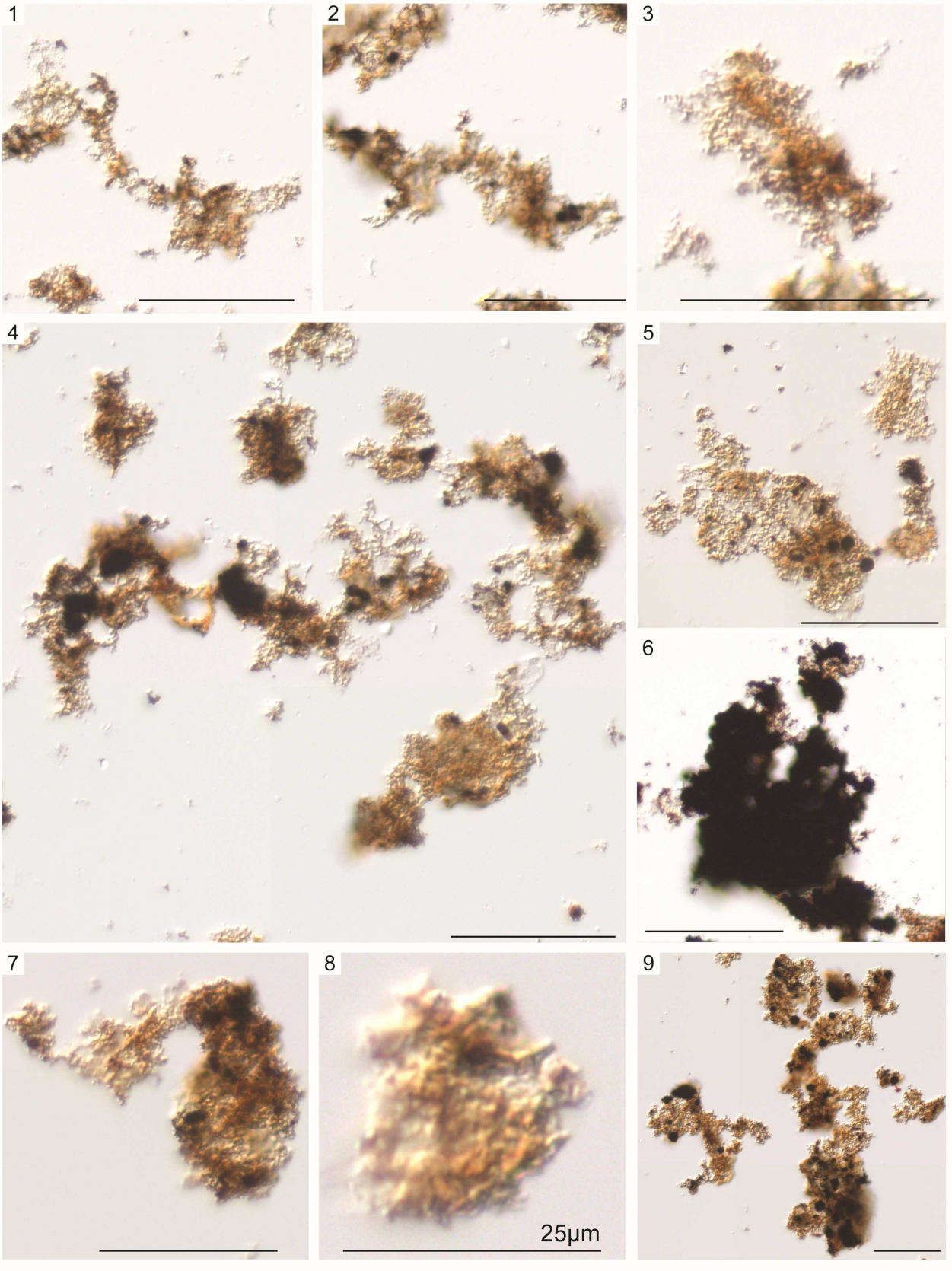
1
2
3
4
5
6
7
8
9
25µm

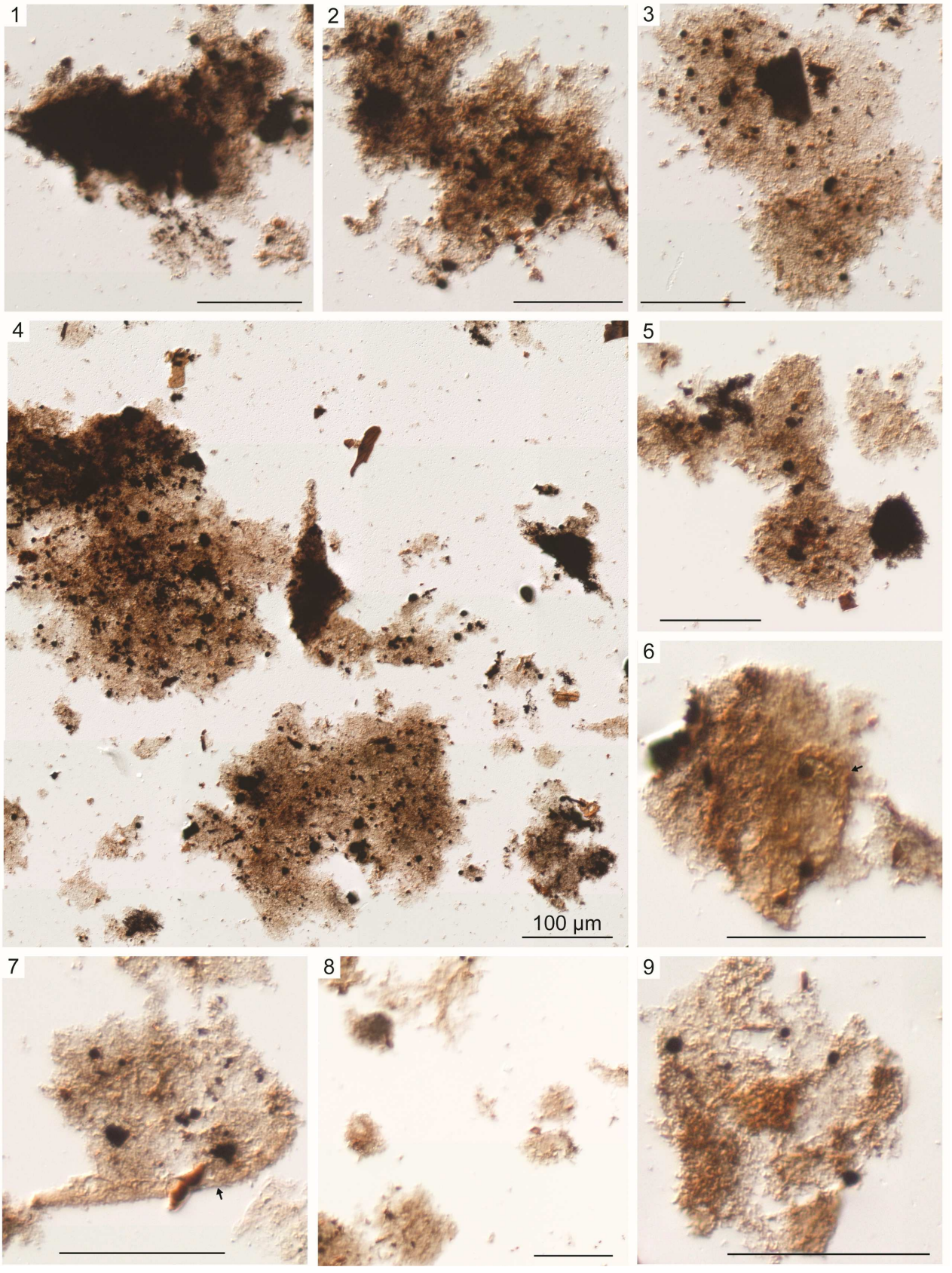
1
2
3
4
5
6
100 µm
7
8
9

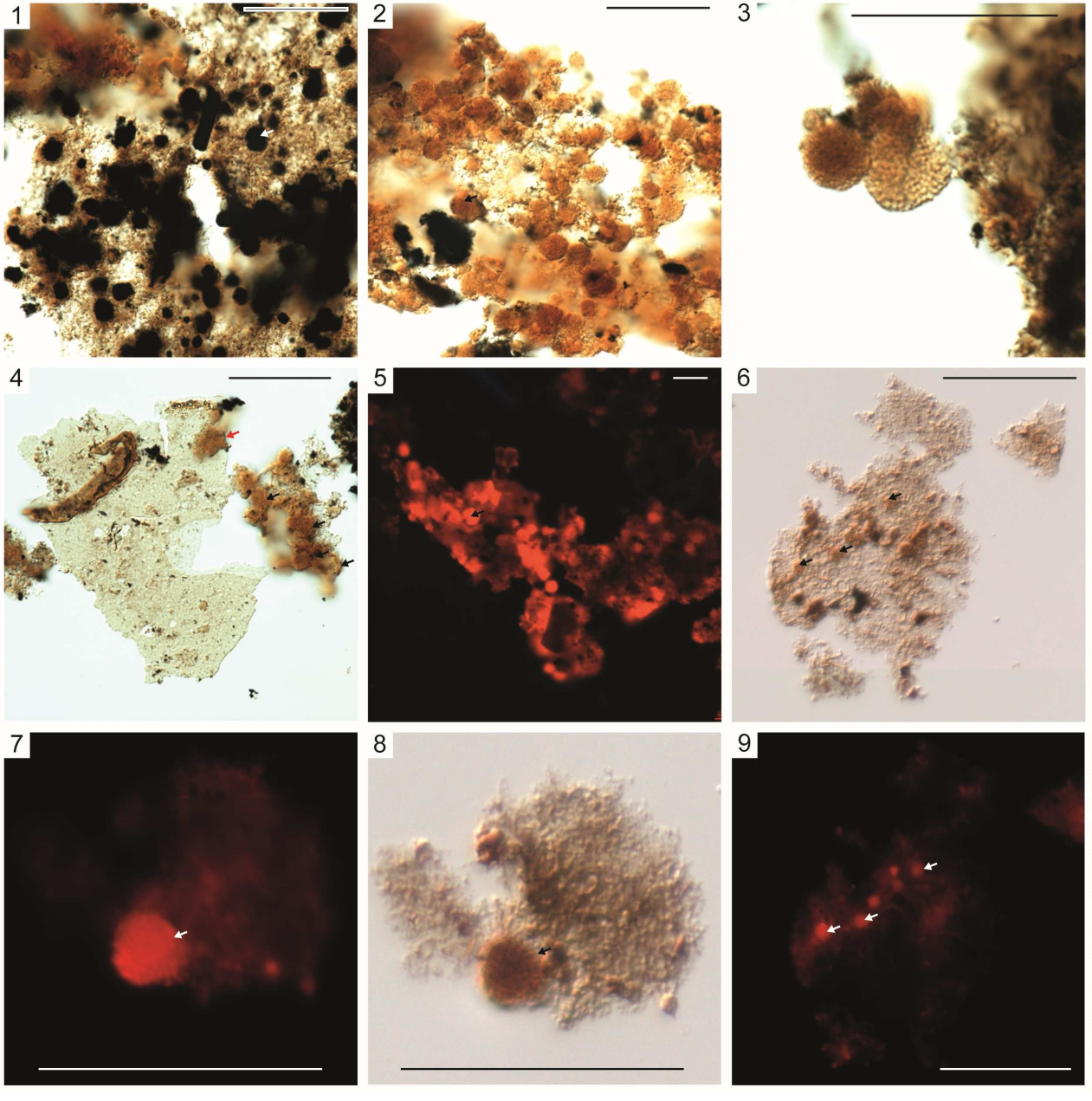
1
2
3
4
5
6
7
8
9

Table 1. Selected palynofacies abundances and geochemical data.

Sample	Depth /	Location	Facies	AOMpel* (%)	AOMgr (%)	TOM (%)	Total AOM (%)	AOMpel/ AOMgr	TOM/ AOMpel	T_{max} (°C)	TOC (%)	MINC (%)	S (%)	S_{py} (%)	S_{sul} (%)	S_{org} (%)	Atomic S/C	$\delta^{34}S_{py}$ (‰)	Fe_{HR}/Fe_T	Fe_{py}/Fe_{HR}	Mo (EF)	U (EF)
SSK61352	11.9	C-S9	I	10.1	11.0	78.8	21.1	0.9	7.8	457	2.17	0.30	0.047	0.04	0.01	<LLD	-	–8.6	0.25	0.04	1.00	0.80
SSK61392	33.28	C-S9	H	11.4	7.2	83.3	18.6	1.6	7.3	456	3.26	0.28	0.14	0.09	-	<LLD	-	–	0.3	0.08	1.10	0.8
SSK61404	40.72	C-S9	B	53.0	15.2	31.9	68.2	3.5	0.6	445	3.42	1.63	1.61	1.47	0.10	0.04	0.00	–32.1	0.72	0.67	26.60	5.80
SSK61420	49.74	C-S9	F	42.6	10.4	46.8	53.0	4.1	1.1	443	1.95	0.12	3.07	2.95	0.28	<LLD	-	–24.4	0.64	0.83	2.70	1.4
HC02_198	114	HC	F	49.5	11.1	39.4	60.6	4.5	0.8	433	3.1	0.2	0.22	0.09	0.05	0.08	0.01	–35.5	-	-	6.7	3.1
HC02_191	85.7	HC	G	36.9	45.6	17.6	82.5	0.8	0.5	440	2.7	0.2	4.05	1.23	0.26	2.56	0.34	6.4	0.31	0.74	2.9	2.0
HC02_188	83.6	HC	G	44.5	45.9	9.3	90.4	1.0	0.2	440	3.3	0.2	3.61	1.93	0.12	1.56	0.17	–8.9	0.51	0.78	3.3	2.7
HC02_184	80.83	HC	F	62.4	11.7	26.0	74.1	5.3	0.4	432	4.1	0.2	4.81	3.66	0.24	0.91	0.08	–39.5	0.90	0.73	48.9	7.0
HC02_174	76.1	HC	B	76.9	13.0	10.1	89.9	5.9	0.1	432	4.5	1.5	3.51	2.04	1.37	0.10	0.01	–34.0	0.88	0.37	143.9	15.9
HC02_166	72.02	HC	F	72.5	14.4	13.0	86.9	5.0	0.2	433	3.5	0.2	3.63	3.27	0.08	0.27	0.03	–30.8	0.91	0.79	25.1	4.5
HC02_127	62.78	HC	B	54.9	26.1	19.1	81.0	2.1	0.3	433	4.92	0.21	2.90	2.56	<LLD	0.34	0.02	–37.2	1.00	0.73	137.8	7.9
HC02_125	62.44	HC	D	87.4	8.8	3.8	96.2	9.9	0.0	437	1.59	3.19	1.43	1.19	0.13	0.11	0.02	–27.9	1.00	0.55	108.6	15.7
HC02_120	61.6	HC	Em	89.5	3.0	7.6	92.5	29.8	0.1	437	1.61	0.08	0.45	0.51	<LLD	<LLD	-	–27.0	0.75	0.75	18.1	5.3
HC02_106	56.35	HC	E	65.4	20.5	14.2	85.9	3.2	0.2	439	3.45	1.71	2.81	2.07	0.12	0.63	0.06	–29.7	0.75	0.60	26.4	6.2
HC02_101	54.7	HC	E	93.9	1.5	4.8	95.4	62.6	0.1	439	2.43	0.38	1.61	1.48	0.05	0.08	0.01	–24.8	0.92	0.70	21.5	4.8
HC02_87	51.86	HC	E	77.2	11.9	10.9	89.1	6.5	0.1	435	3.77	1.21	3.72	2.71	0.52	0.50	0.05	–34.3	0.80	0.73	50.8	8.6
HC02_75	48.82	HC	E	63.1	23.0	13.9	86.1	2.7	0.2	442	1.71	1.13	1.75	1.23	0.09	0.44	0.09	–23.0	0.73	0.63	19.8	4.2
HC02_73	48.14	HC	Em	87.9	3.2	8.8	91.1	27.5	0.1	440	2.19	1.14	2.40	1.75	0.16	0.49	0.08	–28.5	0.82	0.65	34.4	5.5
HC02_67	44.77	HC	E	87.9	3.0	9.2	90.9	29.3	0.1	431	2.27	1.57	3.94	2.88	0.12	0.93	0.15	–34.1	0.81	0.73	64.6	9.7
HC01_04B[#]	37.37	HC	F	84.8	0.4	14.5	85.2	212.0	0.2	432	3.87	0.09	4.88	2.94	0.89	1.05	0.10	–40.1	0.77	0.65	77.5	9.7
HC02_37	28.7	HC	F	68.4	14.6	17.0	83.0	4.7	0.2	440	3.75	0.17	1.16	0.97	0.20	<LLD	-	–34.6	0.95	0.74	47.6	10.4
HC02_31	25.52	HC	C	97.8	0.7	1.4	98.5	139.7	0.0	441	4.33	0.82	1.25	0.97	0.09	0.19	0.02	–31.0	0.94	0.65	72.5	5.1
HC02_21	22.02	HC	B	73.1	7.4	19.6	80.5	9.9	0.3	441	2.92	0	2.28	2.12	<LLD	0.16	0.02	–36.5	0.99	0.77	91.7	6.8
HC02_16	16.4	HC	B	91.4	3.2	5.2	94.6	28.6	0.1	442	3.55	3.65	1.29	1.16	0.07	0.06	0.01	–25.3	0.98	0.65	66.9	3.5
HC02_14	12.9	HC	B	49.6	15.5	35.0	65.1	3.2	0.7	441	2.95	3.66	1.75	1.56	0.06	0.13	0.02	–33.0	0.86	0.61	55.4	3.5
HC02_13	11.6	HC	B	72.7	12.8	14.5	85.5	5.7	0.2	442	3.31	2.03	1.73	1.48	0.16	0.13	0.01	–30.1	1.00	0.76	49.6	4.8
HC02_11	5.9	HC	D	76.3	5.2	18.3	81.5	14.7	0.2	436	2.18	4.04	3.01	2.61	0.21	0.19	0.03	–29.6	0.91	0.73	36.9	10.8
HC02_2	0.68	HC	B	77.1	10.3	12.5	87.4	7.5	0.2	442	3.43	3.09	2.09	1.75	0.13	0.21	0.02	–30.8	0.96	0.77	43.0	4.4
SSK60768	10.8	MHD4	A	95.3	2.6	2.1	97.9	36.7	0.0	435	2.66	6.78	1.04	0.91	0.12	0.01	0.00	–29.3	0.82	0.51	74.8	5.8
SSK60774	12.9	MHD4	B	99.8	0	0.1	99.8	INF	0.0	435	4.87	5.51	2.15	1.87	0.14	0.14	0.01	–32.1	1.00	0.80	64.2	6.2
SSK60787	16.55	MHD4	B	95.4	2.1	2.3	97.5	45.4	0.0	435	5.2	5.09	1.81	1.55	0.51	<LLD	-	–34.6	1.00	0.77	49.6	12.9
SSK60798	20.18	MHD4	B	75.2	7.0	17.9	82.2	10.7	0.2	430	4.54	2.41	4.92	3.72	0.65	0.55	0.04	–36.7	0.89	0.75	98.6	8.4

Notes: *This fraction is dominated by AOMpel (including AOMpyr) but also includes other possible sub-types of heterogeneous, sharp-edged AOM. See Emmings et al., (2019) for sedimentary facies description and interpretations. See Emmings (2018) for Fe-speciation and Mo and U data and interpretations. Facies E and Em likely represent mass transport deposits (Emmings et al., 2019), and therefore contain S_{org}-rich AOMgr as rip-up clasts. Highlighted rows indicate Interval A (bottom) and B (top) as detailed in Fig. 2. TOM = terrestrial palynomorphs (spores) and phytoclasts. MINC = inorganic C. C-S9 = Cominco S9. HC = Hind Clough. MHD4 = Marl Hill 4. Facies H-I Fe_{HR} is presented on a Fe_{mag}-free basis, due to the likely input of detrital Fe_{mag} (see Emmings, 2018 for discussion).[#]RockEval pyrolysis and major and trace element data reported by Emmings et al. (2017).

Table A-1. Palynofacies abundance data (untreated kerogen) [%].

Sample	Depth / Height (m)	Location	Facies	MPA	AOMpyr	AOMpel*	AOMgr	Spores	Phytoclasts
SSK61352	11.9	C-S9	I	68147	-	10.1	11.0	38.2	40.6
SSK61392	33.28	C-S9	H	68148	-	11.4	7.2	36.8	46.5
SSK61404	40.72	C-S9	B	68149	7.2	53.0	15.2	28.3	3.6
SSK61420	49.74	C-S9	F	68150	6.9	42.6	10.4	42.5	4.3
HC02_198	114	HC	F	68142	5.2	49.5	11.1	5.4	34.0
HC02_196	100	HC	G	68141	0.2	60.3	21.5	16.0	2.3
HC02_194	91.15	HC	G	68140	0.1	49.5	42.5	7.1	0.8
HC02_191	85.7	HC	G	68139	0.8	36.9	45.6	16.2	1.4
HC02_188	83.6	HC	G	68138	0.2	44.5	45.9	8.3	1.0
HC02_184	80.83	HC	F	68137	4.3	62.4	11.7	18.5	7.5
HC02_174	76.1	HC	B	68136	0.1	76.9	13.0	7.3	2.8
HC02_166	72.02	HC	F	68135	0.4	72.5	14.4	8.9	4.1
HC02_127	62.78	HC	B	68134	0.8	54.9	26.1	17.1	2.0
HC02_125	62.44	HC	D	68133	0	87.4	8.8	2.9	0.9
HC02_120	61.6	HC	Em	68132	0.2	89.5	3.0	5.6	2.0
HC02_106	56.35	HC	E	68131	0.7	65.4	20.5	9.1	5.1
HC02_101	54.7	HC	E	68130	0.1	93.9	1.5	3.2	1.6
HC02_87	51.86	HC	E	68129	0.3	77.2	11.9	8.4	2.5
HC02_75	48.82	HC	E	68128	0.4	63.1	23.0	12.3	1.6
HC02_73	48.14	HC	Em	67181	0.9	87.9	3.2	3.7	5.1
HC02_67	44.77	HC	E	67180	1.3	87.9	3.0	3.9	5.3
HC01_04B	37.37	HC	F	66949	81.7	84.8	0.4	0.1	14.4
HC02_37	28.7	HC	F	67179	10.5	68.4	14.6	10.6	6.4
HC02_31	25.52	HC	C	67178	0	97.8	0.7	0.6	0.8
HC02_21	22.02	HC	B	67177	44.3	73.1	7.4	5.4	14.2
HC02_19	20.5	HC	D	67176	9.4	46.8	2.8	2.1	48.3
HC02_16	16.4	HC	B	67175	0.1	91.4	3.2	3.0	2.2
HC02_14	12.9	HC	B	67174	3.2	49.6	15.5	29.5	5.5
HC02_13	11.6	HC	B	67173	2.1	72.7	12.8	9.2	5.3
HC02_11	5.9	HC	D	67172	2.4	76.3	5.2	10.2	8.1
HC02_2	0.68	HC	B	67171	1.5	77.1	10.3	8.5	4.0
SSK60768	10.8	MHD4	A	68143	0	95.3	2.6	1.3	0.8
SSK60774	12.9	MHD4	B	68144	0	99.8	0	0.1	0
SSK60787	16.55	MHD4	B	68145	0	95.4	2.1	1.8	0.5
SSK60798	20.18	MHD4	B	68146	0.1	75.2	7.0	13	4.9

Notes
*Includes AOMpel sub-classes

The following data and methods are also reported in Emmings (2018).

Table B-1. Selected Major Element (XRF) Data (wt. %) and LECO S and C (wt. %).

Sample	Location	Depth / Height [m]	Facies	Bead	Al	Fe	S	C
SSK60768	MHD4	10.80	A	LF41303R	3.02	1.87	1.04	9.51
SSK60776	MHD4	13.44	A	LF41307	0.33	0.26	0.26	12.10
SSK60778	MHD4	13.90	A	LF41309	0.32	0.22	0.31	11.90
SSK60783	MHD4	15.48	A	LF41312	0.35	0.62	0.55	12.00
HC02_20	HC	21.80	A	LF41374R	2.44	3.85	1.08	10.60
HC02_2	HC	0.68	B	LF41373	4.27	2.04	2.09	6.48
HC02_13	HC	11.60	B	LF41359	4.17	1.66	1.73	5.36
SSK60774	HC	12.90	B	LF41306	3.99	2.00	2.15	8.68
HC02_14	MHD4	12.90	B	LF41360	2.58	2.58	1.75	8.50
SSK60777	MHD4	13.87	B	LF41308	3.19	1.69	1.65	7.18
SSK60782	MHD4	15.40	B	LF41311	3.46	2.05	2.05	7.97
SSK60785	MHD4	15.64	B	LF41313	3.97	2.13	2.17	6.17
HC02_16	HC	16.40	B	LF41361	4.72	1.59	1.29	7.19
SSK60787	MHD4	16.55	B	LF41314R	2.20	1.71	1.81	10.40
SSK60788	MHD4	16.99	B	LF41315	4.73	3.98	3.92	8.93
SSK60791	MHD4	17.60	B	LF41316	9.17	3.12	3.25	3.97
SSK60794	MHD4	18.97	B	LF41317	8.16	5.04	5.27	6.51
SSK60795	MHD4	19.60	B	LF41318	4.53	8.38	8.21	7.11
SSK60797	MHD4	19.80	B	LF41319	8.54	2.37	2.17	6.12
SSK60798	MHD4	20.18	B	LF41320	6.51	4.81	4.92	7.11
SSK60800	MHD4	21.06	B	LF41321	7.48	5.96	6.10	5.79
SSK60801	MHD4	21.75	B	LF41322	6.46	7.89	7.67	2.56
HC02_21	HC	22.02	B	LF41375	3.54	2.42	2.28	5.46
SSK60804	MHD4	22.35	B	LF41323	5.88	5.40	5.52	6.44
HC02_23	HC	22.58	B	LF41376	4.05	1.44	1.06	5.81
HC02_24	HC	23.15	B	LF41377	3.21	1.61	1.38	6.82
HC02_25	HC	23.32	B	LF41378	4.96	1.22	1.16	4.31
SSK60806	MHD4	23.57	B	LF41324	4.78	4.41	4.59	6.52
SSK60807	MHD4	23.66	B	LF41325	4.38	1.35	1.17	8.05
HC02_27	HC	24.16	B	LF41379	3.52	2.12	1.92	5.16
SSK60808	MHD4	24.30	B	LF41326	4.26	2.70	2.81	6.39
SSK60809	MHD4	25.10	B	LF41327	4.24	2.03	2.09	5.93
SSK60812	MHD4	26.44	B	LF41328	3.43	1.77	1.22	8.88
SSK61400	C-S9	38.47	B	LF41342	7.41	3.24	2.22	5.03
SSK61404	C-S9	40.72	B	LF41343	6.61	2.65	1.61	5.06
SSK61408	C-S9	43.28	B	LF41344	4.92	2.07	1.40	4.85
SSK61412	C-S9	45.72	B	LF41345	6.80	3.26	2.14	5.11
SSK61416	C-S9	47.91	B	LF41346	10.59	4.43	2.67	3.01
SSK61424	C-S9	53.55	B	LF41348	12.87	6.24	1.94	3.55
HC02_127	HC	62.78	B	LF41358	5.05	2.92	2.90	5.08

Sample	Location	Depth / Height [m]	Facies	Bead	Al	Fe	S	C
HC02_172	HC	75.00	B	LF41364	3.29	5.68	2.98	8.51
HC02_173	HC	75.60	B	LF41365	4.48	4.31	3.64	5.96
HC02_174	HC	76.10	B	LF41403	5.34	5.47	3.51	5.27
HC02_177	HC	77.15	B	LF41366	6.21	4.43	4.00	4.62
HC02_178	HC	77.67	B	LF41367	6.30	3.92	3.43	4.52
SSK60770	MHD4	11.75	C	LF41304R	3.64	2.21	2.28	7.86
SSK60772	MHD4	12.06	C	LF41305R	3.13	8.47	9.22	7.55
SSK60781	MHD4	14.80	C	LF41310	2.96	1.44	1.61	6.30
HC02_31	HC	25.52	C	LF41381	4.84	1.37	1.25	4.99
HC02_32	HC	26.20	C	LF41382	3.97	3.55	3.49	5.16
HC02_11	HC	5.90	D	LF41402	4.00	3.41	3.01	6.20
HC02_49A	HC	35.37	D	LF41388R	2.45	5.46	2.54	9.35
HC02_58	HC	39.50	D	LF41392	4.76	3.57	2.99	3.01
HC02_63	HC	43.00	D	LF41396	4.73	2.26	1.84	3.61
HC02_125	HC	62.44	D	LF41357	1.70	1.83	1.43	5.20
HC02_67	HC	44.77	E	LF41397	3.68	4.20	3.94	3.74
HC02_75	HC	48.82	E	LF41399	4.59	2.31	1.75	2.74
HC02_87	HC	51.86	E	LF41400	6.12	4.02	3.72	4.73
HC02_101	HC	54.70	E	LF41354	5.26	2.00	1.61	2.71
HC02_106	HC	56.35	E	LF41355	6.10	3.97	2.81	5.16
HC02_73	HC	48.14	Em	LF41398	5.01	2.86	2.40	3.24
HC02_120	HC	61.60	Em	LF41356	5.32	0.79	0.45	1.67
HC02_28	HC	24.55	F	LF41380	3.92	7.66	8.20	2.92
HC02_33	HC	26.83	F	LF41383	4.87	5.77	5.92	2.98
HC02_37	HC	28.70	F	LF41384	4.76	1.19	1.16	3.82
HC02_40	HC	30.30	F	LF41385	4.82	1.20	1.09	3.35
HC02_43	HC	32.10	F	LF41386	8.63	2.23	2.11	2.76
HC01_14B	HC	33.00	F	LF40522	7.01	6.73	6.92	3.52
HC01_13B	HC	33.38	F	LF40521	5.68	8.84	7.38	3.53
HC01_11B	HC	33.42	F	LF40519	8.68	5.25	5.52	3.22
HC01_10B	HC	33.58	F	LF40518	6.34	5.47	5.50	3.86
HC01_09B	HC	33.95	F	LF40517	7.91	5.04	5.09	4.18
HC02_47	HC	34.10	F	LF41387	5.95	8.00	8.53	3.04
HC02_51	HC	36.10	F	LF41389	7.08	7.30	7.56	3.33
HC01_04B	HC	37.37	F	LF40511	8.50	5.09	4.88	4.03
HC02_54	HC	37.90	F	LF41390	5.23	7.73	7.73	4.78
HC01_01B	HC	38.22	F	LF40509	6.60	6.97	7.35	4.31
HC01_05AB	HC	38.30	F	LF40512	5.56	6.65	6.49	4.57
HC01_05BB	HC	38.30	F	LF40513	6.08	5.35	5.58	4.91
HC02_57	HC	39.00	F	LF41391	5.53	6.83	6.74	4.56
HC02_59	HC	40.00	F	LF41393	6.86	6.52	6.64	3.71
HC02_61	HC	40.95	F	LF41394	8.35	5.95	5.88	4.03

Sample	Location	Depth / Height [m]	Facies	Bead	Al	Fe	S	C
HC02_62	HC	41.50	F	LF41395	7.49	2.99	2.81	3.06
SSK61420	C-S9	49.74	F	LF41347	13.99	4.82	3.07	2.01
HC02_166	HC	72.02	F	LF41362	9.86	3.92	3.63	3.41
HC02_168	HC	73.10	F	LF41363	8.71	8.67	8.76	3.34
HC02_181	HC	79.31	F	LF41368	6.63	4.06	4.09	3.11
HC02_184	HC	80.83	F	LF41369	7.17	4.89	4.81	4.04
HC02_198	HC	114.00	(F)	LF41372	8.74	1.01	0.22	3.17
HC02_188	HC	83.60	G	LF41370	14.16	4.23	3.61	3.30
HC02_191	HC	85.70	G	LF41371	14.23	4.66	4.05	2.60
SSK61376	C-S9	22.62	H	LF41336	12.25	4.31	0.06	2.78
SSK61380	C-S9	25.66	H	LF41337	13.25	4.15	0.05	2.08
SSK60813	MHD4	26.72	(H)	LF41329	8.20	6.15	5.47	2.39
SSK61392	C-S9	33.28	H	LF41340	11.54	3.25	0.14	3.44
SSK61396	C-S9	36.18	H	LF41341	10.55	4.41	3.20	3.12
SSK61428	C-S9	57.36	H	LF41349	13.71	4.14	2.44	2.17
SSK61432	C-S9	59.71	H	LF41350	11.86	4.93	0.12	2.90
SSK61440	C-S9	64.37	H	LF41352	13.01	5.41	2.36	2.63
SSK61352	C-S9	11.90	I	LF41330	12.35	3.60	0.05	2.36
SSK61356	C-S9	13.32	I	LF41331	8.84	3.69	0.03	2.04
SSK61360	C-S9	14.69	I	LF41332	11.95	4.74	0.07	2.81
SSK61364	C-S9	16.13	I	LF41333	12.14	4.60	0.06	3.04
SSK61368	C-S9	18.47	I	LF41334	11.73	5.11	0.16	2.90
SSK61372	C-S9	20.09	I	LF41335	12.17	4.45	0.08	2.93
SSK61384	C-S9	28.86	I	LF41338	11.40	3.69	0.07	2.89
SSK61388	C-S9	31.06	I	LF41339	12.04	4.60	0.09	3.34
SSK61436	C-S9	62.03	I	LF41351	13.19	2.96	0.09	2.58
SSK61444	C-S9	66.69	I	LF41353	13.53	3.91	0.16	3.18

Table B-2. Selected Trace Element (XRF) Data

Sample	Location	Depth / Height [m]	Facies	Pellet	Mo	U
SSK60768	MHD4	10.80	A	L54886	23.6	5.7
SSK60783	MHD4	15.48	A	L54896	3.3	1.7
HC02_20	HC	21.80	A	L54960	10.4	4.6
HC02_2	HC	0.68	B	L54959	19.1	6.0
HC02_13	HC	11.60	B	L54944	21.5	6.5
SSK60774	HC	12.90	B	L54889	26.7	8.0
HC02_14	MHD4	12.90	B	L54945	14.9	2.9
SSK60777	MHD4	13.87	B	L54892	5.7	6.6
SSK60782	MHD4	15.40	B	L54895	7.8	7.3
SSK60785	MHD4	15.64	B	L54897	7.4	7.7

HC02_16	HC	16.40	B	L54946	33.0	5.4
SSK60787	MHD4	16.55	B	L54898	11.4	9.1
SSK60788	MHD4	16.99	B	L54899	54.4	21.1
SSK60791	MHD4	17.60	B	L54900	17.1	7.3
SSK60794	MHD4	18.97	B	L54901	62.8	21.7
SSK60795	MHD4	19.60	B	L54902	50.0	12.6
SSK60797	MHD4	19.80	B	L54903	30.5	13.5
SSK60798	MHD4	20.18	B	L54904	67.0	17.6
SSK60800	MHD4	21.06	B	L54905	49.7	18.3
SSK60801	MHD4	21.75	B	L54906	26.1	7.1
HC02_21	HC	22.02	B	L54961	33.8	7.8
SSK60804	MHD4	22.35	B	L54907	29.3	13.3
HC02_23	HC	22.58	B	L54962	44.7	10.1
HC02_24	HC	23.15	B	L54963	41.0	12.1
HC02_25	HC	23.32	B	L54964	51.1	28.9
SSK60806	MHD4	23.57	B	L54908	37.8	9.9
SSK60807	MHD4	23.66	B	L54909	28.7	11.6
HC02_27	HC	24.16	B	L54965	26.2	10.5
SSK60808	MHD4	24.30	B	L54910	9.5	8.0
SSK60809	MHD4	25.10	B	L54911	9.3	3.5
SSK60812	MHD4	26.44	B	L54912	5.8	20.9
SSK61400	C-S9	38.47	B	L54926	19.3	11.0
SSK61404	C-S9	40.72	B	L54927	18.4	12.5
SSK61408	C-S9	43.28	B	L54928	21.5	7.6
SSK61412	C-S9	45.72	B	L54929	27.1	11.9
SSK61416	C-S9	47.91	B	L54930	19.3	11.5
SSK61424	C-S9	53.55	B	L54932	1.9	4.6
HC02_127	HC	62.78	B	L54943	72.7	13.0
HC02_172	HC	75.00	B	L54949	53.9	16.6
HC02_173	HC	75.60	B	L54950	69.3	17.8
HC02_174	HC	76.10	B	L54951	80.2	27.5
HC02_177	HC	77.15	B	L54952	49.1	18.0
HC02_178	HC	77.67	B	L54953	35.2	10.9
SSK60770	MHD4	11.75	C	L54887	14.6	6.5
SSK60772	MHD4	12.06	C	L54888	56.5	10.7
SSK60781	MHD4	14.80	C	L54894	4.7	6.4
HC02_31	HC	25.52	C	L54967	36.6	8.0
HC02_32	HC	26.20	C	L54968	58.7	20.5
HC02_11	HC	5.90	D	L54940	15.4	14.0
HC02_49A	HC	35.37	D	L54974	28.3	16.3
HC02_58	HC	39.50	D	L54978	24.6	10.5
HC02_63	HC	43.00	D	L54982	18.9	7.9
HC02_125	HC	62.44	D	L54942	19.3	8.7
HC02_67	HC	44.77	E	L54983	24.8	11.5

HC02_75	HC	48.82	E	L54985	9.5	6.3
HC02_87	HC	51.86	E	L54986	32.4	16.9
HC02_101	HC	54.70	E	L54938	11.8	8.2
HC02_106	HC	56.35	E	L54939	16.8	12.2
HC02_73	HC	48.14	Em	L54984	18.0	8.9
HC02_120	HC	61.60	Em	L54941	10.0	9.2
HC02_28	HC	24.55	F	L54966	51.2	7.0
HC02_33	HC	26.83	F	L54969	52.7	8.2
HC02_37	HC	28.70	F	L54970	23.6	16.1
HC02_40	HC	30.30	F	L54971	35.1	12.0
HC02_43	HC	32.10	F	L54972	19.6	19.6
HC01_14B	HC	33.00	F	L54255	45.6	15.7
HC01_13B	HC	33.38	F	L54254	57.3	10.5
HC01_11B	HC	33.42	F	L54252	38.2	19.6
HC01_10B	HC	33.58	F	L54251	59.6	20.1
HC01_09B	HC	33.95	F	L54250	49.5	19.6
HC02_47	HC	34.10	F	L54973	45.4	10.5
HC02_51	HC	36.10	F	L54975	63.9	19.8
HC01_04B	HC	37.37	F	L54244	68.8	26.7
HC02_54	HC	37.90	F	L54976	68.9	15.1
HC01_01B	HC	38.22	F	L54242	72.4	19.2
HC01_05AB	HC	38.30	F	L54245	77.3	14.3
HC01_05BB	HC	38.30	F	L54246	71.8	17.5
HC02_57	HC	39.00	F	L54977	69.7	18.4
HC02_59	HC	40.00	F	L54979	55.9	17.5
HC02_61	HC	40.95	F	L54980	56.2	21.3
HC02_62	HC	41.50	F	L54981	13.8	14.2
SSK61420	C-S9	49.74	F	L54931	4.0	6.5
HC02_166	HC	72.02	F	L54947	25.8	14.5
HC02_168	HC	73.10	F	L54948	29.6	14.7
HC02_181	HC	79.31	F	L54954	38.3	20.5
HC02_184	HC	80.83	F	L54955	36.6	16.2
HC02_198	HC	114.00	(F)	L54958	6.1	8.7
HC02_188	HC	83.60	G	L54956	4.9	12.2
HC02_191	HC	85.70	G	L54957	4.4	9.0
SSK61376	C-S9	22.62	H	L54920	1.0	3.9
SSK61380	C-S9	25.66	H	L54921	1.0	3.8
SSK60813	MHD4	26.72	(H)	L54913	26.3	9.2
SSK61392	C-S9	33.28	H	L54924	1.4	3.0
SSK61396	C-S9	36.18	H	L54925	18.8	11.2
SSK61428	C-S9	57.36	H	L54933	6.9	5.9
SSK61432	C-S9	59.71	H	L54934	2.1	5.3
SSK61440	C-S9	64.37	H	L54936	1.9	5.4
SSK61352	C-S9	11.90	I	L54914	1.3	3.2

SSK61356	C-S9	13.32	I	L54915	2.1	3.4
SSK61360	C-S9	14.69	I	L54916	1.0	3.1
SSK61364	C-S9	16.13	I	L54917	1.1	4.0
SSK61368	C-S9	18.47	I	L54918	1.3	3.7
SSK61372	C-S9	20.09	I	L54919	1.2	3.3
SSK61384	C-S9	28.86	I	L54922	1.9	4.1
SSK61388	C-S9	31.06	I	L54923	1.1	3.9
SSK61436	C-S9	62.03	I	L54935	1.8	5.9
SSK61444	C-S9	66.69	I	L54937	1.9	6.5

*Table B-3. Fe Speciation Data (Fe_{mag}, Fe_{carb} and Fe_{ox} via sequential extraction and Fe_{py} via chromous chloride distillation, wt. %). #Excluding Fe_{mag} from Fe_{HR} *Excluding Fe_{carb} from Fe_{HR}; only applied to Cominco S9 Facies H and I samples.*

Sample	Location	Depth / Height [m]	Facies	Fe_{AVS}	Fe_{mag}	Fe_{carb}	Fe_{ox}	Fe_{py}	Fe_{un}	Fe_{HR}	Fe_{HR}*	Fe_{HR} / Fe_T	Fe_{HR} / Fe_T#	Fe_{HR} / Fe_T*	Fe_{py} / Fe_{HR}	Fe_{py} / Fe_{HR}#	Fe_{py} / Fe_{HR}*
SSK60768	MHD4	10.80	A	-	0.010	0.635	0.100	0.79	0.34	1.53	0.90	0.82	0.82	0.48	0.51	0.51	0.88
SSK60783	MHD4	15.48	A	-	0.004	0.094	0.018	0.54	0.00	0.65	0.56	1.00	1.05	0.90	0.82	0.82	0.96
HC02_20	HC	21.80	A	-	0.000	2.519	0.097	0.91	0.32	3.53	1.01	0.92	0.92	0.26	0.26	0.26	0.90
HC02_2	HC	0.68	B	-	0.000	0.390	0.054	1.52	0.08	1.97	1.58	0.96	0.96	0.77	0.77	0.77	0.97
HC02_13	HC	11.60	B	-	0.000	0.362	0.051	1.29	0.00	1.70	1.34	1.00	1.03	0.81	0.76	0.76	0.96
HC02_14	HC	12.90	B	-	0.000	0.736	0.132	1.36	0.36	2.22	1.49	0.86	0.86	0.58	0.61	0.61	0.91
SSK60774	MHD4	12.90	B	-	0.013	0.326	0.066	1.62	0.00	2.03	1.70	1.00	1.02	0.85	0.80	0.80	0.95
SSK60777	MHD4	13.87	B	-	0.015	0.403	0.076	1.23	0.00	1.72	1.32	1.00	1.02	0.78	0.71	0.71	0.93
SSK60782	MHD4	15.40	B	T	0.021	0.390	0.138	1.57	0.00	2.12	1.73	1.00	1.03	0.84	0.74	0.74	0.91
SSK60785	MHD4	15.64	B	-	0.022	0.334	0.096	1.59	0.08	2.05	1.71	0.96	0.96	0.80	0.78	0.78	0.93
HC02_16	HC	16.40	B	-	0.000	0.498	0.053	1.00	0.03	1.56	1.06	0.98	0.98	0.67	0.65	0.65	0.95
SSK60787	MHD4	16.55	B	-	0.008	0.350	0.048	1.35	0.00	1.75	1.40	1.00	1.03	0.82	0.77	0.77	0.96
SSK60788	MHD4	16.99	B	-	0.024	0.395	0.156	3.05	0.35	3.62	3.23	0.91	0.91	0.81	0.84	0.84	0.94
SSK60791	MHD4	17.60	B	-	0.032	0.666	0.155	2.02	0.24	2.87	2.21	0.92	0.92	0.71	0.70	0.70	0.92
SSK60794	MHD4	18.97	B	-	0.034	0.800	0.275	3.77	0.15	4.88	4.08	0.97	0.97	0.81	0.77	0.77	0.92
SSK60795	MHD4	19.60	B	-	0.066	1.185	1.051	4.05	2.03	6.35	5.17	0.76	0.76	0.62	0.64	0.64	0.78
SSK60797	MHD4	19.80	B	-	0.019	0.458	0.118	1.61	0.16	2.20	1.75	0.93	0.93	0.74	0.73	0.73	0.92
SSK60798	MHD4	20.18	B	-	0.034	0.698	0.320	3.23	0.52	4.29	3.59	0.89	0.89	0.75	0.75	0.75	0.90
SSK60800	MHD4	21.06	B	-	0.046	0.739	0.956	1.08	3.15	2.82	2.08	0.47	0.47	0.35	0.38	0.38	0.52
SSK60801	MHD4	21.75	B	-	0.049	4.358	1.593	1.07	0.82	7.07	2.71	0.90	0.90	0.34	0.15	0.15	0.39
HC02_21	HC	22.02	B	-	0.000	0.451	0.096	1.84	0.02	2.39	1.94	0.99	0.99	0.80	0.77	0.77	0.95
SSK60804	MHD4	22.35	B	-	0.043	0.869	0.266	3.40	0.82	4.58	3.71	0.85	0.85	0.69	0.74	0.74	0.92
HC02_23	HC	22.58	B	-	0.000	0.565	0.080	0.76	0.03	1.41	0.84	0.98	0.98	0.59	0.54	0.54	0.91
HC02_24	HC	23.15	B	-	0.000	0.432	0.085	1.04	0.05	1.56	1.13	0.97	0.97	0.70	0.67	0.67	0.92
HC02_25	HC	23.32	B	-	0.000	0.159	0.290	0.37	0.41	0.82	0.66	0.67	0.67	0.54	0.45	0.45	0.56
SSK60806	MHD4	23.57	B	-	0.030	0.822	0.153	3.31	0.09	4.32	3.50	0.98	0.98	0.79	0.77	0.77	0.95
SSK60807	MHD4	23.66	B	-	0.012	0.362	0.050	0.89	0.03	1.32	0.95	0.98	0.98	0.71	0.68	0.68	0.93
HC02_27	HC	24.16	B	-	0.000	0.538	0.092	1.50	0.00	2.13	1.59	1.00	1.01	0.75	0.70	0.70	0.94
SSK60808	MHD4	24.30	B	-	0.016	0.331	0.068	2.12	0.17	2.53	2.20	0.94	0.94	0.81	0.84	0.84	0.96
SSK60809	MHD4	25.10	B	-	0.016	0.285	0.053	1.60	0.08	1.95	1.67	0.96	0.96	0.82	0.82	0.82	0.96

Sample	Location	Depth / Height [m]	Facies	Fe_{AVS}	Fe_{mag}	Fe_{carb}	Fe_{ox}	Fe_{py}	Fe_{un}	Fe_{HR}	Fe_{HR}*	Fe_{HR} / Fe_T	Fe_{HR} / Fe_T#	Fe_{HR} / Fe_T*	Fe_{py} / Fe_{HR}	Fe_{py} / Fe_{HR}#	Fe_{py} / Fe_{HR}*
SSK60812	MHD4	26.44	B	-	0.012	0.586	0.068	0.91	0.20	1.57	0.99	0.89	0.89	0.56	0.58	0.58	0.92
SSK61400	C-S9	38.47	B	-	0.041	0.735	0.073	1.79	0.60	2.63	1.90	0.81	0.81	0.59	0.68	0.68	0.94
SSK61404	C-S9	40.72	B	-	0.046	0.522	0.062	1.28	0.74	1.91	1.39	0.72	0.72	0.52	0.67	0.67	0.92
SSK61408	C-S9	43.28	B	-	0.036	0.528	0.060	1.16	0.29	1.78	1.25	0.86	0.86	0.61	0.65	0.65	0.92
SSK61412	C-S9	45.72	B	-	0.054	0.834	0.081	1.96	0.33	2.93	2.10	0.90	0.90	0.64	0.67	0.67	0.94
SSK61416	C-S9	47.91	B	-	0.101	0.680	0.115	2.13	1.40	3.02	2.34	0.68	0.68	0.53	0.70	0.70	0.91
SSK61424	C-S9	53.55	B	-	1.067	1.302	0.317	1.55	2.01	4.23	2.93	0.68	0.51	0.47	0.37	0.49	0.53
HC02_127	HC	62.78	B	-	0.024	0.491	0.309	2.22	0.00	3.05	2.56	1.00	1.05	0.88	0.73	0.73	0.87
HC02_172	HC	75.00	B	-	0.018	2.993	0.204	2.05	0.41	5.27	2.28	0.93	0.93	0.40	0.39	0.39	0.90
HC02_173	HC	75.60	B	-	0.017	0.962	0.396	1.82	1.12	3.20	2.23	0.74	0.74	0.52	0.57	0.57	0.82
HC02_174	HC	76.10	B	-	0.490	1.816	0.759	1.77	0.63	4.84	3.02	0.88	0.88	0.55	0.37	0.37	0.59
HC02_177	HC	77.15	B	-	0.067	0.849	0.490	2.26	0.76	3.67	2.82	0.83	0.83	0.64	0.62	0.62	0.80
HC02_178	HC	77.67	B	-	0.018	0.692	0.253	1.27	1.68	2.24	1.54	0.57	0.57	0.39	0.57	0.57	0.82
SSK60770	MHD4	11.75	C	-	0.015	0.400	0.090	1.74	0.00	2.25	1.85	1.00	1.02	0.84	0.78	0.78	0.94
SSK60772	MHD4	12.06	C	-	0.048	0.615	0.131	5.77	1.91	6.56	5.95	0.77	0.77	0.70	0.88	0.88	0.97
SSK60781	MHD4	14.80	C	-	0.015	0.309	0.086	1.06	0.00	1.47	1.16	1.00	1.02	0.81	0.72	0.72	0.91
HC02_31	HC	25.52	C	-	0.012	0.382	0.061	0.84	0.08	1.30	0.92	0.94	0.94	0.67	0.65	0.65	0.92
HC02_32	HC	26.20	C	-	0.014	0.555	0.150	2.55	0.28	3.26	2.71	0.92	0.92	0.76	0.78	0.78	0.94
HC02_11	HC	5.90	D	-	0.002	0.734	0.116	2.27	0.29	3.12	2.39	0.91	0.91	0.70	0.73	0.73	0.95
HC02_49A	HC	35.37	D	T	0.002	2.754	0.179	1.98	0.54	4.92	2.16	0.90	0.90	0.40	0.40	0.40	0.92
HC02_58	HC	39.50	D	-	0.016	0.806	0.130	2.22	0.40	3.17	2.37	0.89	0.89	0.66	0.70	0.70	0.94
HC02_63	HC	43.00	D	-	0.001	0.563	0.064	1.10	0.52	1.73	1.17	0.77	0.77	0.52	0.64	0.64	0.94
HC02_125	HC	62.44	D	-	0.008	0.702	0.122	1.03	0.00	1.87	1.16	1.00	1.02	0.64	0.55	0.55	0.89
HC02_67	HC	44.77	E	-	0.015	0.785	0.113	2.51	0.78	3.42	2.64	0.81	0.81	0.63	0.73	0.73	0.95
HC02_75	HC	48.82	E	-	0.000	0.570	0.056	1.07	0.62	1.69	1.12	0.73	0.73	0.49	0.63	0.63	0.95
HC02_87	HC	51.86	E	-	0.014	0.694	0.141	2.35	0.82	3.20	2.51	0.80	0.80	0.62	0.73	0.73	0.94
HC02_101	HC	54.70	E	-	0.011	0.490	0.055	1.28	0.16	1.84	1.35	0.92	0.92	0.67	0.70	0.70	0.95
HC02_106	HC	56.35	E	-	0.009	1.056	0.112	1.80	1.00	2.97	1.92	0.75	0.75	0.48	0.60	0.60	0.94
HC02_73	HC	48.14	Em	-	0.003	0.728	0.077	1.53	0.52	2.33	1.61	0.82	0.82	0.56	0.65	0.65	0.95
HC02_120	HC	61.60	Em	-	0.000	0.092	0.058	0.45	0.20	0.60	0.50	0.75	0.75	0.63	0.75	0.75	0.89
HC02_28	HC	24.55	F	-	0.017	1.694	0.292	5.41	0.25	7.41	5.72	0.97	0.97	0.75	0.73	0.73	0.95
HC02_33	HC	26.83	F	-	0.043	0.800	0.411	3.03	1.48	4.29	3.49	0.74	0.74	0.60	0.71	0.71	0.87
HC02_37	HC	28.70	F	-	0.000	0.220	0.074	0.84	0.05	1.13	0.91	0.95	0.95	0.77	0.74	0.74	0.92
HC02_40	HC	30.30	F	-	0.000	0.273	0.088	0.84	0.00	1.20	0.93	1.00	1.00	0.77	0.70	0.70	0.90
HC02_43	HC	32.10	F	-	0.000	0.403	0.073	1.39	0.37	1.86	1.46	0.84	0.84	0.66	0.74	0.74	0.95
HC01_10B	HC	33.58	F	-	0.038	0.974	0.425	3.12	0.92	4.55	3.58	0.83	0.83	0.65	0.68	0.68	0.87
HC02_47	HC	34.10	F	-	0.028	2.325	0.208	4.43	1.01	6.99	4.67	0.87	0.87	0.58	0.63	0.63	0.95
HC02_51	HC	36.10	F	-	0.036	0.860	0.363	4.91	1.13	6.17	5.31	0.85	0.85	0.73	0.80	0.80	0.92
HC01_04B	HC	37.37	F	-	0.031	0.925	0.403	2.55	1.17	3.91	2.99	0.77	0.77	0.59	0.65	0.65	0.85
HC02_54	HC	37.90	F	-	0.034	3.012	0.336	4.90	0.00	8.28	5.27	1.00	1.07	0.68	0.59	0.59	0.93
HC02_57	HC	39.00	F	-	0.060	1.127	0.634	2.02	2.99	3.84	2.71	0.56	0.56	0.40	0.53	0.53	0.74
HC02_59	HC	40.00	F	-	0.046	0.812	0.466	4.71	0.49	6.03	5.22	0.93	0.93	0.80	0.78	0.78	0.90

Sample	Location	Depth / Height [m]	Facies	Fe_{AVS}	Fe_{mag}	Fe_{carb}	Fe_{ox}	Fe_{py}	Fe_{un}	Fe_{HR}	Fe_{HR}*	Fe_{HR} / Fe_T	Fe_{HR} / Fe_T#	Fe_{HR} / Fe_T*	Fe_{py} / Fe_{HR}	Fe_{py} / Fe_{HR}#	Fe_{py} / Fe_{HR}*
HC02_61	HC	40.95	F	-	0.039	0.884	0.413	2.97	1.64	4.31	3.43	0.72	0.72	0.58	0.69	0.69	0.87
HC02_62	HC	41.50	F	-	0.003	0.473	0.209	1.55	0.76	2.24	1.76	0.75	0.75	0.59	0.69	0.69	0.88
SSK61420	C-S9	49.74	F	-	0.117	0.398	0.113	2.57	1.63	3.20	2.80	0.66	0.64	0.58	0.80	0.83	0.92
HC02_166	HC	72.02	F	-	0.024	0.525	0.185	2.85	0.33	3.58	3.06	0.91	0.91	0.78	0.79	0.79	0.93
HC02_168	HC	73.10	F	-	0.084	0.894	0.312	3.80	3.58	5.09	4.20	0.59	0.59	0.48	0.75	0.75	0.91
HC02_181	HC	79.31	F	-	0.019	0.590	0.317	2.92	0.22	3.84	3.25	0.95	0.95	0.80	0.76	0.76	0.90
HC02_184	HC	80.83	F	-	0.026	0.763	0.416	3.19	0.50	4.39	3.63	0.90	0.90	0.74	0.73	0.73	0.88
HC02_188	HC	83.60	G	-	0.000	0.253	0.222	1.67	2.08	2.15	1.90	0.51	0.51	0.45	0.78	0.78	0.88
HC02_191	HC	85.70	G	-	0.000	0.255	0.117	1.07	3.22	1.44	1.18	0.31	0.31	0.25	0.74	0.74	0.90
SSK61376	C-S9	22.62	H	-	0.983	0.891	0.149	0.04	2.25	2.06	1.17	0.48	0.25	0.27	0.02	0.04	0.03
SSK61380	C-S9	25.66	H	-	0.480	0.597	0.130	0.05	2.89	1.25	0.66	0.30	0.19	0.16	0.04	0.06	0.07
SSK60813	MHD4	26.72	H	-	0.030	3.063	1.325	0.55	1.18	4.97	1.91	0.81	0.81	0.31	0.11	0.11	0.29
SSK61392	C-S9	33.28	H	-	0.266	0.779	0.110	0.08	2.01	1.24	0.46	0.38	0.30	0.14	0.07	0.08	0.18
SSK61396	C-S9	36.18	H	-	0.054	0.621	0.086	2.48	1.17	3.24	2.62	0.73	0.72	0.59	0.77	0.78	0.95
SSK61428	C-S9	57.36	H	-	0.076	0.388	0.444	1.57	1.66	2.48	2.09	0.60	0.58	0.51	0.63	0.65	0.75
SSK61432	C-S9	59.71	H	-	1.241	1.026	0.158	0.10	2.41	2.52	1.49	0.51	0.26	0.30	0.04	0.07	0.06
SSK61440	C-S9	64.37	H	-	0.823	0.578	0.142	1.81	2.06	3.35	2.77	0.62	0.47	0.51	0.54	0.72	0.65
SSK61352	C-S9	11.90	I	-	0.401	0.642	0.217	0.04	2.30	1.30	0.65	0.36	0.25	0.18	0.03	0.04	0.06
SSK61356	C-S9	13.32	I	-	0.607	0.690	0.180	0.02	2.19	1.50	0.81	0.41	0.24	0.22	0.01	0.02	0.02
SSK61360	C-S9	14.69	I	-	1.054	0.714	0.178	0.06	2.74	2.00	1.29	0.42	0.20	0.27	0.03	0.06	0.04
SSK61364	C-S9	16.13	I	-	0.955	0.898	0.179	0.05	2.52	2.08	1.18	0.45	0.24	0.26	0.02	0.04	0.04
SSK61368	C-S9	18.47	I	-	0.910	1.406	0.243	0.07	2.48	2.63	1.22	0.51	0.34	0.24	0.03	0.04	0.06
SSK61372	C-S9	20.09	I	-	0.965	0.810	0.180	0.06	2.44	2.02	1.20	0.45	0.24	0.27	0.03	0.06	0.05
SSK61384	C-S9	28.86	I	-	0.676	0.699	0.117	0.06	2.14	1.55	0.85	0.42	0.24	0.23	0.04	0.07	0.07
SSK61388	C-S9	31.06	I	-	1.035	0.990	0.176	0.07	2.33	2.27	1.28	0.49	0.27	0.28	0.03	0.06	0.05
SSK61436	C-S9	62.03	I	-	0.488	0.472	0.095	0.09	1.81	1.15	0.67	0.39	0.22	0.23	0.08	0.14	0.14
SSK61444	C-S9	66.69	I	-	0.990	0.528	0.111	0.15	2.13	1.77	1.25	0.45	0.20	0.32	0.08	0.19	0.12

Table B-4. S Species and S Isotope Data

Sample	Location	Depth / Height [m]	Facies	TS [%]	S_{py} [%]	S_{sul} [%]	S_{org} [%]	Atomic S/C	$\delta^{34}S_{py}$ [‰]	$\delta^{34}S_{bulk}$ [‰]	$\delta^{34}S_{org}$ [‰]
SSK60768	MHD4	10.80	A	1.04	0.91	0.12	0.01	0.00	-29.32	-	-
HC02_20	HC	21.80	A	1.08	1.05	0.06	<LLD	-	-16.51	-	-
HC02_2	HC	0.68	B	2.09	1.75	0.13	0.21	0.02	-30.82	-29.06	-14.77
HC02_13	HC	11.60	B	1.73	1.48	0.16	0.13	0.01	-30.05	-	-
SSK60774	MHD4	12.90	B	2.15	1.87	0.14	0.14	0.01	-32.10	-29.09	11.78
HC02_14	HC	12.90	B	1.75	1.56	0.06	0.13	0.02	-33.00	-31.65	-15.06
HC02_16	HC	16.40	B	1.29	1.16	0.07	0.06	0.01	-25.32	-	-
SSK60787	MHD4	16.55	B	1.81	1.55	0.51	<LLD	-	-34.57	-	-
SSK60794	MHD4	18.97	B	5.27	-	-	-	-	-	-	-
SSK60798	MHD4	20.18	B	4.92	3.72	0.65	0.55	0.04	-36.71	-35.66	-28.62
SSK60801	MHD4	21.75	B	7.67	-	-	-	-	-	-	-

Sample	Location	Depth / Height [m]	Facies	TS [%]	S_{py} [%]	S_{sul} [%]	S_{org} [%]	Atomic S/C	$\delta^{34}S_{py}$ [‰]	$\delta^{34}S_{bulk}$ [‰]	$\delta^{34}S_{org}$ [‰]
HC02_21	HC	22.02	B	2.28	2.12	<LLD	0.16	0.02	-36.50	-35.72	-25.36
HC02_23	HC	22.58	B	1.06	0.88	0.10	0.08	0.01	-28.79	-26.98	-6.49
HC02_25	HC	23.32	B	1.16	0.42	0.33	0.41	0.03	-33.06	-27.85	-22.43
SSK61404	C-S9	40.72	B	1.61	1.47	0.10	0.04	0.00	-32.13	-	-
SSK61412	C-S9	45.72	B	2.14	2.25	0.17	<LLD	-	-23.27	-	-
HC02_127	HC	62.78	B	2.9	2.56	<LLD	0.34	0.02	-37.23	-36.53	-31.28
HC02_172	HC	75.00	B	2.98	2.36	0.30	0.32	0.03	-35.11	-33.98	-25.66
HC02_173	HC	75.60	B	3.64	2.10	0.53	1.02	0.08	-34.59	-32.62	-28.58
HC02_174	HC	76.10	B	3.51	2.04	1.37	<LLD	0.00	-34.03	-38.11	-
HC02_178	HC	77.67	B	3.43	1.46	0.44	1.53	0.14	-36.37	-37.07	-37.75
HC02_31	HC	25.52	C	1.25	0.97	0.09	0.19	0.02	-31.02	-30.90	-30.27
HC02_11	HC	5.90	D	3.01	2.61	0.21	0.19	0.03	-29.59	-28.42	-12.53
HC02_58	HC	39.50	D	2.99	-	-	-	-	-	-	-
HC02_125	HC	62.44	D	1.43	1.19	0.13	0.11	0.02	-27.94	-27.25	-19.55
HC02_67	HC	44.77	E	3.94	2.88	0.12	0.93	0.15	-34.05	-33.31	-31.02
HC02_75	HC	48.82	E	1.75	1.23	0.09	0.44	0.09	-23.01	-22.22	-20.02
HC02_87	HC	51.86	E	3.72	2.71	0.52	0.50	0.05	-34.31	-34.83	-37.64
HC02_101	HC	54.70	E	1.61	1.48	0.05	0.08	0.01	-24.78	-	-
HC02_106	HC	56.35	E	2.81	2.07	0.12	0.63	0.06	-29.72	-27.07	-18.34
HC02_73	HC	48.14	Em	2.4	1.75	0.16	0.49	0.08	-28.52	-28.08	-26.49
HC02_120	HC	61.60	Em	0.445	0.51	<LLD	<LLD	-	-26.98	-	-
HC02_28	HC	24.55	F	8.2	-	-	-	-	-	-	-
HC02_33	HC	26.83	F	5.92	-	-	-	-	-	-	-
HC02_37	HC	28.70	F	1.16	0.97	0.20	<LLD	-	-34.64	-34.20	-
HC02_40	HC	30.30	F	1.09	-	-	-	-	-	-	-
HC02_43	HC	32.10	F	2.11	-	-	-	-	-	-	-
HC01_10B	HC	33.58	F	5.5	3.58	0.74	1.18	0.10	-40.68	-40.28	-39.06
HC02_47	HC	34.10	F	8.53	-	-	-	-	-	-	-
HC02_51	HC	36.10	F	7.56	-	-	-	-	-	-	-
HC01_04B	HC	37.37	F	4.88	2.94	0.89	1.05	0.10	-40.10	-38.94	-35.67
HC02_54	HC	37.90	F	7.73	-	-	-	-	-	-	-
HC02_57	HC	39.00	F	6.74	-	-	-	-	-	-	-
HC02_59	HC	40.00	F	6.64	-	-	-	-	-	-	-
HC02_61	HC	40.95	F	5.88	-	-	-	-	-	-	-
HC02_62	HC	41.50	F	2.81	5.41	0.17	1.06	0.10	-40.81	-39.61	-33.50
SSK61420	C-S9	49.74	F	3.07	2.95	0.28	<LLD	-	-24.37	-	-
HC02_166	HC	72.02	F	3.63	3.27	0.08	0.27	0.03	-30.83	-29.35	-11.64
HC02_168	HC	73.10	F	8.76	-	-	-	-	-	-	-
HC02_181	HC	79.31	F	4.09	3.35	0.28	0.46	0.05	-38.39	-36.30	-21.11
HC02_184	HC	80.83	F	4.81	3.66	0.24	0.91	0.08	-39.51	-32.27	-3.15
HC02_198	HC	114.00	(F)	0.217	0.09	0.05	0.08	0.01	-35.48	-	-
HC02_188	HC	83.60	G	3.61	1.93	0.12	1.56	0.17	-8.93	-6.01	-2.41

Sample	Location	Depth / Height [m]	Facies	TS [%]	S_{py} [%]	S_{sul} [%]	S_{org} [%]	Atomic S/C	$\delta^{34}S_{py}$ [‰]	$\delta^{34}S_{bulk}$ [‰]	$\delta^{34}S_{org}$ [‰]
HC02_191	HC	85.70	G	4.05	1.23	0.26	2.56	0.34	6.41	8.69	9.79
SSK60813	MHD4	26.72	(H)	5.47	-	-	-	-	-	-	-
SSK61428	C-S9	57.36	H	2.44	-	-	-	-	-	-	-
SSK61352	C-S9	11.90	I	0.047	0.04	0.01	<LLD	-	-8.57	-	-

Sample powders (~1 g) were washed for 24 hours in 200 ml of 10 wt/vol % NaCl in order to leach free sulphate (Kampschulte et al., 2001), then rinsed and filtered, prior to isotope analysis. Total S measured on NaCl-washed residues was compared with the total S of untreated powders, yielding an estimate for the sulphate S (S_{sul}) fraction, after correction for the mass loss assuming leaching of pure $CaSO_4$ (Eq. 1).

$$S_{sul}\,[\text{wt. \%}] = -\frac{\sqrt{d^2y^2 + 200df(y-2z) + 10000f^2} - dy + 100f}{2df} \qquad [\mathbf{1}]$$

where:

$$d = -1\ [\text{constant}]$$

$$y = \text{Untreated TS}\ [\text{wt. \%}]$$

$$f = 0.308098084\ [S/CaSO_4\ \text{mol. ratio, constant}]$$

$$z = \text{Residue (NaCl treated) TS}\ [\text{wt. \%}]$$

In most cases, estimated S_{sul} was within or close to ± 0.08 wt. % of the total (untreated) S (i.e., the long-term analytical precision). Therefore S_{sul} is negligible for most samples. Elemental S is typically a trace component of the sedimentary S pool (e.g., Mossmann et al., 1991) and was therefore assumed to be negligible (*sensu.* Tribovillard et al.. 2001).

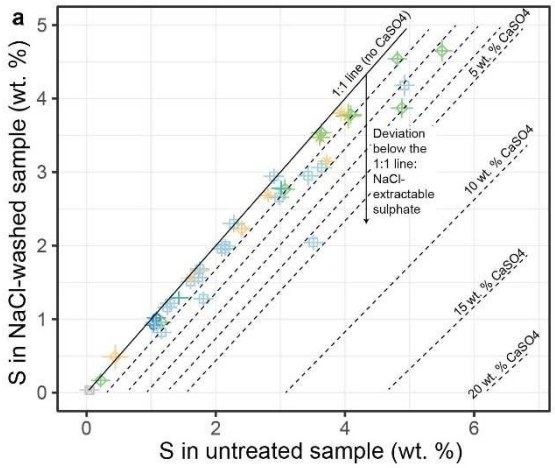

Fig. B-1. Comparison of total sulphur (S) measured in untreated and NaCl-washed samples. See main

text for key to sedimentary facies. The sulphate S (S_{sul}) pool was estimated using these data and inputs for Equ.1.

S_{org} was estimated by subtraction of S_{py} (Fe_{py}*1.15) and S_{sul} (Eq. 2).

$$S_{org} = TS - S_{py} - S_{sul} \quad [\mathbf{2}]$$

Propagating the precision of total S (TS), S_{py} and S_{sul} in quadrature yields a precision estimate of ± 0.12 % S_{org}.

Table B-5. Selected Rock-Eval Pyrolysis Data.

Sample	Location	Facies	Depth	Job	Analysis	Quantity [mg]	KFID	Tmax [°C]	TOC [%]	HI	MINC(%)
SSK60768	MHD4	A	10.80	20151203	02.R00	58.98	1461	435	2.66	281	6.78
SSK60776	MHD4	A	13.44	20151203	07.R00	59.25	1461	438	0.42	188	11.41
SSK60778	MHD4	A	13.90	20151203	09.R00	58.35	1461	440	0.50	182	11.38
SSK60783	MHD4	A	15.48	20151203	13.R00	59.95	1461	435	0.65	329	10.99
HC02_20	HC	A	21.80	20151123	09.R00	59.65	1461	439	1.12	138	9.43
HC02_2	HC	B	0.68	20151123	04.R00	59.83	1461	442	3.43	218	3.09
HC02_13	HC	B	11.60	20151123	06.R00	60.08	1461	442	3.31	203	2.03
HC02_14	HC	B	12.90	20151123	07.R00	59.55	1461	441	2.95	173	3.66
SSK60774	MHD4	B	12.90	20151203	05.R00	58.97	1461	435	4.87	319	5.51
SSK60775	MHD4	B	13.25	20151203	06.R00	59.74	1461	435	2.73	334	5.18
SSK60777	MHD4	B	13.87	20151203	08.R00	59.04	1461	435	3.19	298	3.93
SSK60782	MHD4	B	15.40	20151203	11.R00	59.08	1461	437	5.43	337	2.53
SSK60785	MHD4	B	15.64	20151203	14.R00	59.04	1461	435	4.60	300	1.59
HC02_16	HC	B	16.40	20151123	08.R00	60.31	1461	442	3.55	234	3.65
SSK60787	MHD4	B	16.55	20151203	15.R00	59.93	1461	435	5.20	372	5.09
SSK60788	MHD4	B	16.99	20151203	16.R00	59.34	1461	428	4.09	288	4.92
SSK60791	MHD4	B	17.60	20151203	17.R00	59.74	1461	435	3.38	166	0.75
SSK60794	MHD4	B	18.97	20151203	18.R00	59.79	1461	428	5.33	225	1.09
SSK60795	MHD4	B	19.60	20151203	19.R00	58.77	1461	428	3.55	175	3.41
SSK60797	MHD4	B	19.80	20151203	20.R00	58.43	1461	434	5.70	251	0.60
SSK60798	MHD4	B	20.18	20151203	21.R00	60.17	1461	430	4.54	222	2.41
SSK60800	MHD4	B	21.06	20151203	22.R00	60.75	1461	428	4.79	172	0.76
SSK60801	MHD4	B	21.75	20151203	24.R00	58.28	1461	417	2.32	28	0.35
HC02_21	HC	B	22.02	20151123	10.R00	59.84	1461	439	3.22	210	2.71
HC02_22	HC	B	22.27	20170912	06.r00	60.51	1615	441	2.92	268	0.00
SSK60804	MHD4	B	22.35	20151203	25.R00	58.14	1461	427	3.98	209	2.58
HC02_23	HC	B	22.58	20151123	11.R00	60.31	1461	437	3.51	251	2.26
HC02_24	HC	B	23.15	20151123	12.R00	58.69	1461	439	3.87	236	2.89
HC02_25	HC	B	23.32	20151123	13.R00	57.97	1461	436	4.40	209	0.16
SSK60806	MHD4	B	23.57	20151203	26.R00	60.02	1461	432	4.01	251	2.47
HC02_26	HC	B	23.60	20170912	07.r00	60.29	1615	435	4.23	234	2.21
SSK60807	MHD4	B	23.66	20151203	27.R00	58.42	1461	437	4.36	317	3.60
HC02_27	HC	B	24.16	20151127	02.R00	59.04	1461	437	3.12	232	1.98
SSK60808	MHD4	B	24.30	20151203	28.R00	60.7	1461	436	3.62	322	2.68
HC02_29	HC	B	24.68	20170912	08.r00	59.84	1615	441	3.65	243	1.16
HC02_30	HC	B	25.00	20170912	09.r00	59.15	1615	443	3.38	252	2.99
SSK60809	MHD4	B	25.10	20151203	29.R00	59.01	1461	437	3.39	301	2.61
SSK60812	MHD4	B	26.44	20151203	30.R00	58.67	1461	433	3.22	282	5.58
HC02_35	HC	B	27.80	20170912	11.r00	60.92	1615	440	3.18	214	0.12
HC02_50	HC	B	35.60	20170912	23.r00	59.70	1440	434	5.05	211	2.00

Sample	Location	Facies	Depth	Job	Analysis	Quantity [mg]	KFID	Tmax [°C]	TOC [%]	HI	MINC(%)
SSK61400	C-S9	B	38.47	20151214	13.R00	59.27	1461	443	3.31	135	1.72
SSK61404	C-S9	B	40.72	20151214	14.R00	60.29	1461	445	3.42	144	1.63
SSK61408	C-S9	B	43.28	20151214	15.R00	58.90	1461	444	3.12	143	1.70
SSK61412	C-S9	B	45.72	20151214	16.R00	58.73	1461	437	3.79	160	1.43
SSK61416	C-S9	B	47.91	20151214	17.R00	61.38	1461	441	2.59	90	0.39
SSK61424	C-S9	B	53.55	20151214	20.R00	60.26	1461	455	2.58	58	0.73
HC02_122	HC	B	62.00	20170915	40.r00	59.36	1440	433	4.70	128	0.21
HC02_123	HC	B	62.10	20170915	41.r00	60.09	1440	443	1.63	139	1.72
HC02_127	HC	B	62.78	20151127	30.R00	58.85	1461	433	4.92	196	0.21
HC02_135	HC	B	65.40	20170919	06.r00	60.21	1440	436	3.12	112	1.98
HC02_136	HC	B	66.30	20170919	07.r00	59.12	1440	437	3.24	111	1.04
HC02_151	HC	B	69.00	20170921	06.r00	60.32	1440	436	3.78	149	1.11
HC02_150	HC	B	69.16	20170921	05.r00	59.48	1440	437	3.86	145	1.43
HC02_156	HC	B	69.88	20170921	09.r00	60.47	1440	437	3.29	120	1.05
HC02_157	HC	B	70.10	20170921	10.r00	59.81	1440	438	3.35	116	0.69
HC02_159	HC	B	70.34	20170921	13.r00	60.79	1440	437	3.30	146	0.72
HC02_161	HC	B	70.68	20170921	15.r00	60.76	1440	443	1.51	91	1.94
HC02_163	HC	B	71.00	20170921	16.r00	59.37	1440	440	1.86	106	1.30
HC02_172	HC	B	75.00	20151127	33.R00	61.50	1461	433	3.84	229	4.42
HC02_173	HC	B	75.60	20151127	35.R00	61.21	1461	434	4.69	217	1.39
HC02_174	HC	B	76.10	20151127	36.R00	59.23	1461	432	4.46	194	1.47
HC02_175	HC	B	77.10	20170921	21.r00	59.84	1440	434	3.51	174	0.00
HC02_177	HC	B	77.15	20151127	37.R00	59.22	1461	432	4.16	168	0.99
HC02_178	HC	B	77.67	20151127	38.R00	59.02	1461	434	3.85	209	0.77
SSK60770	MHD4	C	11.75	20151203	03.R00	59.74	1461	436	3.77	281	3.96
SSK60772	MHD4	C	12.06	20151203	04.R00	59.74	1461	427	3.68	211	3.81
SSK60781	MHD4	C	14.80	20151203	10.R00	60.33	1461	435	3.56	325	3.28
HC02_31	HC	C	25.52	20151127	04.R00	59.42	1461	441	4.33	242	0.82
HC02_32	HC	C	26.20	20151127	05r.R00	60.24	1461	433	4.05	211	1.07
HC02_34	HC	C	27.30	20170912	10.r00	59.83	1615	429	2.29	91	0.16
HC02_64	HC	C	43.50	20170912	15.r00	60.97	1615	440	2.48	216	1.35
HC02_66	HC	C	44.25	20170912	18.r00	60.61	1374	442	1.94	168	1.24
HC02_124	HC	C	62.35	20170915	42.r00	59.58	1440	436	5.82	212	0.56
HC02_126	HC	C	62.70	20170915	43.r00	59.25	1440	440	0.65	231	2.36
HC02_11	HC	D	5.90	20151123	05.R00	59.93	1461	436	2.18	143	4.04
HC02_49A	HC	D	35.37	20151127	11.R00	60.13	1461	433	1.64	151	7.60
HC02_58	HC	D	39.50	20151127	16.R00	59.79	1461	433	2.23	138	0.84
HC02_63	HC	D	43.00	20151127	20.R00	61.41	1461	439	2.69	215	0.91
HC02_80	HC	D	49.95	20170915	04.r00	59.41	1440	437	2.79	186	0.77
HC02_81	HC	D	50.35	20170915	05.r00	60.93	1440	439	2.40	160	0.71
HC02_102	HC	D	55.02	20170915	22.r00	59.89	1440	444	1.28	172	2.92

Sample	Location	Facies	Depth	Job	Analysis	Quantity [mg]	KFID	Tmax [°C]	TOC [%]	HI	MINC(%)
HC02_110	HC	D	57.37	20170915	28.r00	59.82	1440	441	1.88	137	1.22
HC02_117	HC	D	59.37	20170915	36.r00	59.51	1440	435	0.78	73	5.11
HC02_118	HC	D	59.87	20170915	37.r00	59.58	1440	442	1.68	135	3.60
HC02_121	HC	D	61.69	20170915	39.r00	60.96	1440	435	2.27	104	0.13
HC02_125	HC	D	62.44	20151127	29.R00	61.02	1461	437	1.59	181	3.19
HC02_141	HC	D	67.15	20170919	11.r00	59.70	1440	438	3.28	148	2.37
HC02_142	HC	D	67.21	20170919	13.r00	59.05	1440	443	1.34	139	1.47
HC02_143	HC	D	67.28	20170919	14.r00	59.97	1440	437	3.01	139	1.12
HC02_144	HC	D	67.45	20170919	15.r00	60.88	1440	440	3.86	147	0.66
HC02_145	HC	D	67.66	20170919	16.r00	59.84	1440	444	1.45	134	2.41
HC02_146	HC	D	68.10	20170919	17.r00	59.80	1440	438	3.40	155	0.93
HC02_149	HC	D	68.70	20170921	04.r00	59.88	1440	439	2.25	126	1.17
HC02_155	HC	D	69.60	20170921	08.r00	59.91	1440	445	1.31	122	2.75
HC02_67	HC	E	44.77	20151127	21.R00	58.80	1461	431	2.27	152	1.57
HC02_69	HC	E	46.30	20170912	20.r00	59.88	1440	441	2.12	162	1.68
HC02_71	HC	E	46.53	20170912	21.r00	60.31	1440	440	2.06	146	0.44
HC02_72	HC	E	47.60	20170912	24.r00	60.82	1440	441	1.35	174	5.36
HC02_75	HC	E	48.82	20151127	24.R00	59.56	1461	442	1.71	153	1.13
HC02_76	HC	E	49.20	20170912	26.r00	60.00	1440	441	1.54	182	1.57
HC02_77	HC	E	49.40	20170912	27.r00	59.28	1440	442	1.54	158	1.83
HC02_78	HC	E	49.64	20170915	02.r00	60.93	1440	443	1.47	129	2.17
HC02_82	HC	E	50.72	20170915	06.r00	59.55	1440	443	1.78	153	0.95
HC02_86	HC	E	51.58	20170915	09.r00	60.49	1440	437	2.09	180	2.17
HC02_87	HC	E	51.86	20151127	25.R00	58.92	1461	435	3.77	185	1.21
HC02_88	HC	E	51.96	20170915	10.r00	60.39	1440	441	1.46	168	1.31
HC02_89	HC	E	52.17	20170915	11.r00	60.28	1440	445	1.27	156	2.67
HC02_91	HC	E	52.50	20170915	14.r00	59.07	1440	440	2.31	162	2.26
HC02_93	HC	E	52.79	20170915	15.r00	60.02	1440	442	2.35	158	1.47
HC02_95	HC	E	53.32	20170915	17.r00	59.67	1440	442	1.80	119	0.20
HC02_96	HC	E	53.57	20170915	18.r00	60.33	1440	444	1.50	157	1.92
HC02_99	HC	E	54.50	20170915	20.r00	60.07	1440	442	2.15	160	0.67
HC02_101	HC	E	54.70	20151127	26.R00	59.45	1461	439	2.43	191	0.38
HC02_103	HC	E	55.29	20170915	29.r00	59.23	1440	446	1.21	141	1.80
HC02_106	HC	E	56.35	20151127	27.R00	59.73	1461	439	3.45	173	1.71
HC02_111	HC	E	58.12	20170915	30.r00	59.73	1440	442	1.94	135	1.77
HC02_112	HC	E	58.35	20170915	31.r00	60.91	1440	440	2.05	107	3.34
HC02_114	HC	E	58.80	20170915	33.r00	60.18	1440	439	1.61	99	0.73
HC02_131	HC	E	63.80	20170919	03r.r00	61.16	1440	443	1.08	130	4.17
HC02_133	HC	E	64.60	20170919	04.r00	60.05	1440	436	3.44	135	0.60
HC02_134	HC	E	64.80	20170919	05.r00	59.35	1440	441	0.83	90	9.74
HC02_137	HC	E	66.36	20170919	08.r00	59.21	1440	443	1.48	120	1.15

Sample	Location	Facies	Depth	Job	Analysis	Quantity [mg]	KFID	Tmax [°C]	TOC [%]	HI	MINC(%)
HC02_138	HC	E	66.90	20170919	09.r00	60.74	1440	443	1.40	119	1.87
HC02_139	HC	E	66.97	20170919	10.r00	59.22	1440	436	3.93	133	1.26
HC02_147	HC	E	68.32	20170921	02.r00	60.77	1440	443	0.99	105	3.19
HC02_153	HC	E	69.24	20170921	07.r00	59.88	1440	444	1.37	141	1.11
HC02_160	HC	E	70.61	20170921	14.r00	59.91	1440	436	3.94	161	1.36
HC02_65	HC	Em	44.00	20170912	17.r00	60.39	1615	442	2.37	170	0.07
HC02_68	HC	Em	45.30	20170912	19r.r00	60.15	1440	440	2.24	183	1.34
HC02_73	HC	Em	48.14	20151127	22.R00	59.73	1461	440	2.19	163	1.14
HC02_74	HC	Em	48.70	20170912	25.r00	60.62	1440	431	4.28	129	0.17
HC02_79	HC	Em	49.83	20170915	03.r00	60.18	1440	430	4.15	114	0.16
HC02_83	HC	Em	50.95	20170915	07.r00	59.13	1440	439	1.95	157	1.15
HC02_84	HC	Em	51.20	20170915	08.r00	59.54	1440	442	2.15	120	0.06
HC02_90	HC	Em	52.31	20170915	13.r00	59.05	1440	433	3.90	110	0.16
HC02_94	HC	Em	52.92	20170915	16.r00	59.10	1440	432	4.48	125	0.13
HC02_97	HC	Em	53.98	20170915	19.r00	60.53	1440	441	4.32	150	0.16
HC02_100	HC	Em	54.56	20170915	21.r00	59.96	1440	432	3.88	95	0.15
HC02_105	HC	Em	55.50	20170915	25.r00	59.14	1440	440	2.07	117	0.67
HC02_104	HC	Em	55.80	20170915	24.r00	60.45	1440	443	4.40	241	0.14
HC02_107	HC	Em	56.80	20170915	26.r00	59.77	1440	439	2.97	127	1.96
HC02_109	HC	Em	57.33	20170915	27.r00	60.50	1440	432	3.54	97	0.18
HC02_113	HC	Em	58.60	20170915	32.r00	60.84	1440	436	3.40	102	0.27
HC02_116	HC	Em	59.32	20170915	35.r00	59.64	1440	438	3.00	88	0.11
HC02_119	HC	Em	59.90	20170915	38.r00	59.83	1440	437	3.27	92	0.10
HC02_120	HC	Em	61.60	20151127	28r.R00	59.03	1461	437	1.61	162	0.08
HC02_130	HC	Em	63.24	20170915	44.r00	60.05	1440	430	4.53	126	0.17
HC02_148	HC	Em	68.65	20170921	03.r00	59.86	1440	435	3.90	78	0.19
HC02_158	HC	Em	70.16	20170921	11.r00	60.61	1440	440	1.81	118	0.79
HC02_164	HC	Em	71.05	20170921	17.r00	59.78	1440	444	1.39	103	1.62
HC02_28	HC	F	24.55	20151127	03.R00	58.40	1461	431	2.99	122	0.19
HC02_33	HC	F	26.83	20151127	06r.R00	59.83	1461	430	3.04	130	0.17
HC02_37	HC	F	28.70	20151127	07.R00	59.29	1461	440	3.75	196	0.17
HC02_40	HC	F	30.30	20151127	08.R00	58.67	1461	441	3.36	188	0.17
HC02_42	HC	F	31.30	20170912	12.r00	60.74	1615	434	3.59	145	0.00
HC02_43	HC	F	32.10	20151127	09.R00	59.57	1461	439	2.77	156	0.14
HC01_14B	HC	F	33.00	20150618	08.R00	60.18	1483	436	3.37	100	0.11
HC01_13B	HC	F	33.38	20150618	07.R00	60.34	1483	426	3.64	133	0.06
HC01_11B	HC	F	33.42	20150618	05.R00	58.66	1483	438	3.23	144	0.11
HC01_10B	HC	F	33.58	20150618	04.R00	59.25	1483	432	4.11	152	0.10
HC01_09B	HC	F	33.95	20150519	14.R00	60.85	1483	432	3.56	148	0.15
HC02_47	HC	F	34.10	20151127	10.R00	59.83	1461	428	3.17	106	0.18
HC02_49	HC	F	35.10	20170912	13.r00	59.67	1615	434	3.36	130	0.00

Sample	Location	Facies	Depth	Job	Analysis	Quantity [mg]	KFID	Tmax [°C]	TOC [%]	HI	MINC(%)
HC02_51	HC	F	36.10	20151127	13.R00	59.86	1461	428	3.50	105	0.19
HC01_04A	HC	F	37.37	20170921	22.r00	59.80	1440	428	3.79	89	0.00
HC01_04B	HC	F	37.37	20150519	08.R00	59.63	1483	432	3.87	141	0.09
HC02_54	HC	F	37.90	20151127	14.R00	59.58	1461	427	4.98	131	0.20
HC01_01B	HC	F	38.22	20150519	05.R00	60.83	1483	427	4.10	145	0.07
HC01_05AB	HC	F	38.30	20150618	35.R00	60.49	1483	426	4.71	151	0.05
HC01_05BB	HC	F	38.30	20150519	10.R00	60.23	1483	427	4.39	164	0.07
HC02_57	HC	F	39.00	20151127	15.R00	59.80	1461	426	4.87	124	0.18
HC02_59	HC	F	40.00	20151127	17.R00	59.13	1461	429	3.89	118	0.19
HC02_61	HC	F	40.95	20151127	18.R00	59.66	1461	432	4.26	144	0.19
HC02_62	HC	F	41.50	20151127	19.R00	59.08	1461	438	3.16	176	0.10
SSK61420	C-S9	F	49.74	20151214	19.R00	59.19	1461	443	1.95	39	0.12
HC02_166	HC	F	72.02	20151127	31.R00	59.56	1461	433	3.51	130	0.15
HC02_167	HC	F	72.56	20170921	18.r00	59.98	1440	435	4.19	124	0.00
HC02_168	HC	F	73.10	20151127	32.R00	59.51	1461	431	3.51	91	0.20
HC02_169	HC	F	73.66	20170921	19.r00	60.15	1440	444	5.10	360	0.00
HC02_170	HC	F	74.21	20170921	20.r00	59.97	1440	442	9.61	472	0.00
HC02_181	HC	F	79.31	20151127	39.R00	59.14	1461	432	3.15	104	0.26
HC02_184	HC	F	80.83	20151127	40.R00	58.42	1461	432	4.09	135	0.19
HC02_198	HC	(F)	114.00	20151127	43.R00	57.97	1461	433	3.14	135	0.18
HC02_188	HC	G	83.60	20151127	41.R00	59.80	1461	440	3.31	232	0.16
HC02_191	HC	G	85.70	20151127	42.R00	58.74	1461	440	2.68	169	0.15
SSK61376	C-S9	H	22.62	20151214	06.R00	59.32	1461	458	1.92	57	0.80
SSK61380	C-S9	H	25.66	20151214	07.R00	60.39	1461	453	1.91	57	0.17
SSK60813	MHD4	(H)	26.72	20151203	31.R00	59.34	1461	424	2.23	41	0.32
SSK61392	C-S9	H	33.28	20151214	10.R00	59.73	1461	456	3.26	76	0.28
SSK61396	C-S9	H	36.18	20151214	11.R00	60.60	1461	442	2.67	99	0.44
SSK61428	C-S9	H	57.36	20151214	21.R00	58.05	1461	448	2.07	34	0.16
SSK61432	C-S9	H	59.71	20151214	22.R00	58.84	1461	455	2.12	95	0.75
SSK61440	C-S9	H	64.37	20151214	24.R00	61.96	1461	453	2.15	66	0.45
SSK61352	C-S9	I	11.90	20151203	32.R00	58.69	1461	457	2.17	59	0.30
SSK61356	C-S9	I	13.32	20151203	33.R00	60.47	1461	458	1.74	59	0.32
SSK61360	C-S9	I	14.69	20151214	02.R00	60.84	1461	456	2.36	51	0.52
SSK61364	C-S9	I	16.13	20151214	03.R00	60.69	1461	458	2.61	49	0.50
SSK61368	C-S9	I	18.47	20151214	04.R00	60.53	1461	457	2.40	49	0.60
SSK61372	C-S9	I	20.09	20151214	05.R00	60.35	1461	456	2.55	52	0.49
SSK61384	C-S9	I	28.86	20151214	08.R00	59.62	1461	456	2.51	59	0.45
SSK61388	C-S9	I	31.06	20151214	09.R00	59.50	1461	456	2.74	71	0.62
SSK61436	C-S9	I	62.03	20151214	23.R00	61.09	1461	452	2.26	110	0.34
SSK61444	C-S9	I	66.69	20151214	25.R00	61.16	1461	453	2.66	105	0.55

References

Emmings, J., 2018. Controls on UK Lower Namurian Shale Gas Prospectivity: Understanding the Spatial and Temporal Distribution of Organic Matter in Siliciclastic Mudstones. PhD Thesis, University of Leicester.

Kampschulte, A., Bruckschen, P., Strauss, H., 2001. The sulphur isotopic composition of trace sulphates in Carboniferous brachiopods: implications for coeval seawater, correlation with other geochemical cycles and isotope stratigraphy. Chemical Geology, 175(1): 149-173.

Mossmann, J.-R., Aplin, A.C., Curtis, C.D., Coleman, M.L., 1991. Geochemistry of inorganic and organic sulphur in organic-rich sediments from the Peru Margin. Geochimica et Cosmochimica Acta, 55(12): 3581-3595.

Tribovillard, N., Bialkowski, A., Tyson, R.V., Lallier-Vergès, E., Deconinck, J.F., 2001. Organic facies variation in the late Kimmeridgian of the Boulonnais area (northernmost France). Marine and Petroleum Geology, 18(3): 371-389.